

---

**MODELING AND EXPERIMENTAL STUDY  
OF CARBON DIOXIDE ABSORPTION  
IN A MEMBRANE CONTACTOR**

---

**BY**

**Karl Anders Hoff**

*Thesis submitted for the Degree of Dr. Ing.*

Norwegian University of Science and Technology  
Department of Chemical Engineering

March 2003

---



---

## *Abstract*

---

Membrane gas absorption is a new way of contacting gas and liquid for industrial scale gas purification and offers significant advantages compared to conventional absorption towers. Due to the separation of the phases by a microporous membrane the contactor may be operated without limitations caused by flooding, foaming, channeling and liquid entrainment. Very compact hollow fiber membrane units can be made resulting in significant savings in weight and space required.

This dissertation deals with membrane gas absorption in the application of CO<sub>2</sub> removal by aqueous alkanolamines, using microporous PTFE hollow fiber membranes. A new lab-scale apparatus was constructed and an extensive experimental study executed to determine the performance of the membrane gas absorber, with aqueous solutions of monoethanolamine (MEA) and methyldiethanolamine (MDEA) as absorbents. The important operation parameters CO<sub>2</sub> partial pressure, gas velocity, liquid velocity, temperature and liquid CO<sub>2</sub> loading were systematically varied within the range typically experienced in a process for exhaust gas CO<sub>2</sub>-removal.

The results clearly show the change in the absorption rate and the overall mass transfer coefficient related to each of the variables. An important conclusion from the experimental study is that the contribution from the gas phase in the overall mass transfer resistance is negligible for the conditions studied. Membrane mass transfer resistance corresponds to less than 12% of the total, leaving the liquid side as the totally dominating resistance term. It is found that the liquid side mass transfer is limited by component diffusivities except at low partial pressures, where the chemical reaction may be rate-limiting.

A comprehensive model for the simulation of the membrane gas absorber was developed. The model explicitly accounts for the rates of mass transfer through

---

the membrane, diffusion and chemical reaction in the liquid phase and the corresponding heat transfer model. The important effect of radial viscosity gradients on the liquid diffusivities was also included. An equilibrium model was developed to calculate liquid speciation and equilibrium partial pressures in the chemical systems CO<sub>2</sub>/MEA/water and CO<sub>2</sub>/MDEA/water.

The membrane gas absorber model calculates temperature profiles and concentration profiles of all components through the length of a single membrane tube. The total absorption rate in a membrane module is calculated from a mass balance of the gas and the liquid phase. It was observed that the diffusional transport of chemically bound CO<sub>2</sub> and other ionic reaction products is an important rate limiting step. This led to the requirement of new correlations for these component diffusivities, developed from parameter regression on selected experiments. Model predictions of absorption rates and the effects of individual variables agree well with experimental data, with maximum deviations within  $\pm 15\%$ . In the range of operation for an industrial contactor with CO<sub>2</sub> absorbing in aqueous MEA, the average model deviation is 2.8%.

The possibility of utilizing a lab-scale membrane gas absorber as a tool in measuring the kinetics of CO<sub>2</sub>-alkanolamine reactions is discussed. It has been shown that the sensitivity to reaction kinetics can be significantly improved by reducing the contact time beyond what is possible in the present experimental set-up. This may be achieved in a membrane module with 1-5 cm tube length and a high number of tubes so that absorption fluxes can still be measured with a high level of accuracy. To verify this procedure, experiments were performed in a range with a reasonably good sensitivity to reaction kinetics in the MDEA-system. The second order rate constant of the CO<sub>2</sub>-MDEA reaction was regressed from the experimental data resulting in an Arrhenius expression comparable to literature values.

---

## *Acknowledgements*

---

I would like to express my appreciation to all those people who have contributed to make this work possible through their help and support along the way.

My work in the field of CO<sub>2</sub>-absorption started with a diploma on equilibrium measurements and continued as a research assistant, both supervised by professor (now emeritus) Olav Erga. I would like to thank him for his good mood and encouragements through all these years.

My deepest gratitude goes to my supervisor professor Hallvard Svendsen for giving me the possibility to do this interesting job and for his trustworthy advice and support through all the phases of the project. Senior scientist Olav Juliussen at SINTEF has been of invaluable importance as an adviser and a partner of discussion for the experimental part. I would also like to thank the mechanics Jan-Morten Roel and Odd Ivar Hovin for building the experimental apparatus and the diploma students Hanne Bakstad and Roger Nilsen for performing parts of the experiments.

The contact with Kvaerner made it possible to keep in touch with the practical implications of the Ph.D., which necessarily has to focus on a smaller scale of the process. I would like to thank project manager Olav Falk-Pedersen of Kvaerner Process Systems for initiating this project and for an encouraging enthusiasm throughout its development. The collaboration with senior engineer Marianne Grønvold is appreciated. Thanks also to Howard Meyer and the Gas Technology Institute for a financial contribution. I wish to thank Richard Witzko and W.L. Gore & Associates for developing the membranes and offering the modules used for testing in this work.

Above all, I would like to give special thanks to my mother and father for their care and support, and to my wife Bodil for always being there.

---

This work has been financed by the Norwegian Research Council, through the Klimatek programme, by Kvaerner Process Systems, and by a contribution from the Gas Technology Institute. The financial support is gratefully acknowledged and appreciated.

---

# *Contents*

---

<b>Abstract</b> .....	<b>iii</b>
<b>Acknowledgements</b> .....	<b>v</b>
<b>Symbols</b> .....	<b>xi</b>
<b>CHAPTER 1 Introduction</b> .....	<b>1</b>
1.1 Background .....	<b>1</b>
1.1.1 The absorption process .....	<b>1</b>
1.1.2 Absorption liquids .....	<b>3</b>
1.1.3 Tower design and operation .....	<b>4</b>
1.2 Membranes for gas separation .....	<b>5</b>
1.3 Membrane Gas Absorption .....	<b>6</b>
1.3.1 Principle .....	<b>6</b>
1.3.2 Breakthrough pressure .....	<b>8</b>
1.3.3 Membrane materials .....	<b>10</b>
1.3.4 The Kvaerner/Gore membrane contactor .....	<b>10</b>
1.4 Purpose .....	<b>12</b>
1.4.1 Scope of this work .....	<b>12</b>
1.4.2 Problem formulation .....	<b>13</b>
1.4.3 Thesis outline .....	<b>14</b>
<b>CHAPTER 2 Literature review of membrane gas absorption</b> .....	<b>15</b>
2.1 Studies focusing on the mass transfer performance of membrane gas absorbers ..	<b>15</b>
2.2 Work including rate-based modeling .....	<b>19</b>
2.3 Conclusions from literature review .....	<b>21</b>
<b>CHAPTER 3 Chemistry of carbon dioxide absorption in aqueous alkanolamine solutions</b> .....	<b>23</b>
3.1 Introduction .....	<b>23</b>
3.2 Reactions in aqueous solution .....	<b>24</b>
3.3 Alkanolamine reactions .....	<b>26</b>
3.3.1 Mechanism of tertiary alkanolamines .....	<b>26</b>

---

3.3.2	Mechanism of primary and secondary alkanolamines.....	28
3.3.3	Alkylcarbonate formation .....	33
3.4	The rate of reaction in the absorber model .....	34
<b>CHAPTER 4</b>	<b>Modeling of equilibria in aqueous CO<sub>2</sub>-alkanolamine systems .....</b>	<b>37</b>
4.1	Introduction .....	37
4.2	Non-ideal behavior.....	39
4.2.1	Phase equilibria .....	40
4.2.2	The alkanolamine/water system .....	42
4.3	Literature review of corrections for non-idealities in the liquid phase .....	44
4.3.1	Models using the apparent equilibrium constant approach.....	44
4.3.2	Rigorous thermodynamic models for the liquid phase .....	47
4.3.3	Discussion and implications for this work.....	51
4.4	Equilibrium model for the membrane absorption simulator .....	54
4.4.1	Chemical equilibria .....	54
4.4.2	The Astarita representation of chemical equilibria .....	56
4.4.3	The CO <sub>2</sub> equilibrium partial pressure .....	62
4.5	The correction for non-ideality .....	63
4.5.1	The salting out effect.....	63
4.5.2	The apparent equilibrium constants.....	65
4.5.3	Tuning the model to experimental data .....	68
4.5.4	Equilibrium curves and model performance .....	70
4.6	Summary and conclusions .....	72
<b>CHAPTER 5</b>	<b>Experimental study of membrane gas absorption.....</b>	<b>83</b>
5.1	Introduction .....	83
5.1.1	Scale up and design of a membrane gas absorber.....	83
5.2	Apparatus assembly .....	84
5.2.1	The liquid system.....	88
5.2.2	The gas system .....	89
5.2.3	Control and interface.....	90
5.3	Operating procedures.....	91
5.3.1	Calibration .....	91
5.3.2	Chemicals .....	91
5.3.3	Experiments with circulating gas phase .....	92
5.3.4	Experiments with pure CO <sub>2</sub> and stagnant gas phase.....	94



---

5.4	Calculation of absorption rate .....	95
5.5	The mass transfer coefficient.....	97
5.6	Liquid sample analysis.....	99
5.6.1	CO <sub>2</sub> -analysis .....	99
5.6.2	Analysis of amine in the liquid phase .....	100
<b>CHAPTER 6 Results and discussion of the absorption experiments .</b>		<b>103</b>
6.1	Introduction .....	103
6.2	The individual mass transfer coefficients.....	104
6.2.1	Mass transfer correlations for the shell and the tube side .....	105
6.2.2	The enhancement factor.....	106
6.2.3	Mass transfer in the membrane .....	109
6.3	Results .....	110
6.4	Discussion .....	115
6.4.1	Implications of the mass transfer coefficient.....	115
6.4.2	The possibility of measuring diffusivities and rates of reaction .....	118
<b>CHAPTER 7 Modeling of the membrane gas absorber .....</b>		<b>125</b>
7.1	Introduction .....	125
7.2	Description of the model equations .....	126
7.2.1	The flow structure .....	126
7.2.2	Flux across the membrane.....	128
7.2.3	Balance equations for the gas phase .....	129
7.2.4	Transport model for the liquid phase.....	131
7.3	Physical properties.....	133
7.3.1	Liquid viscosity and density .....	134
7.3.2	Specific heat of liquid .....	134
7.3.3	Diffusivities in the gas phase.....	136
7.3.4	Diffusivities of CO <sub>2</sub> and amine in the liquid phase .....	136
7.3.5	Diffusivity of the reaction products.....	138
7.3.6	Further discussion of the problem of electrolyte diffusion .....	146
7.4	Model implementation.....	148
7.5	Model verification and validation .....	151
7.5.1	Concentration, temperature and viscosity profiles .....	151
7.5.2	Effect of viscosity and density gradients.....	155
7.5.3	The effect of partial penetration into the membrane .....	156
7.5.4	Porosity and effective interfacial area .....	157

---

7.6 Comparison of the model performance with experimental data . . . . .	159
<b>CHAPTER 8 Measurement of kinetics for carbon dioxide absorption</b>	<b>165</b>
8.1 Measurement of rate constants. . . . .	165
8.2 Sensitivity analysis on the membrane model. . . . .	168
8.3 Kinetics measurement . . . . .	172
8.4 Driving force effects . . . . .	174
<b>CHAPTER 9 Conclusions . . . . .</b>	<b>179</b>
9.1 Summary . . . . .	179
9.2 Conclusions . . . . .	180
9.3 Future work . . . . .	181
<b>References . . . . .</b>	<b>185</b>
<b>APPENDIX 1 Solution in terms of the extent of reaction . . . . .</b>	<b>199</b>
<b>APPENDIX 2 Correlations for the equilibrium model. . . . .</b>	<b>201</b>
A2.1 Equilibrium Constants. . . . .	201
A2.2 The Henry's law constants . . . . .	203
A2.3 Salting-out coefficients . . . . .	204
A2.4 Solvent vapor pressure . . . . .	205
<b>APPENDIX 3 Accuracy of the measurements. . . . .</b>	<b>207</b>
A3.1 Error analysis . . . . .	207
A3.2 Accuracy of the absorption rates. . . . .	208
A3.3 Accuracy of the liquid sample analysis. . . . .	209

---

# Symbols

---

## Uppercase latin symbols

<i>Symbol</i>	<b>Meaning</b>	<b>Unit</b>
$A_g$	Free cross section of the gas phase	$m^2$
$C$	Electrical charge	C
$D_i$	Diffusivity of component $i$ in the liquid phase	$m^2/s$
$\tilde{D}_{cb}$	Apparent diffusivity of chemically bound $CO_2$	$m^2/s$
$D_{i,g}$	Diffusivity of component $i$ in the gas phase	$m^2/s$
$E$	Enhancement factor	
$E_i$	Enhancement factor of an infinitely fast reaction	
$F$	Faraday constant	C/mol
$Ha$	Hatta modulus	
$H_i$	Henry's law constant for component $i$	$(kPa\ m^3)/mol$
$\Delta H_{vap}$	Heat of vaporisation	J/mol
$\Delta H_r$	Heat of reaction	J/mol
$I$	Ionic strength	mol/l
$K$	Equilibrium constant, activity based	
$K_\gamma$	Equilibrium constant in terms of the activity coefficients	
$K_c$	Equilibrium constant, concentration based	
$K_G$	Overall, gas film based mass transfer coefficient	$mol/(m^2\ s\ kPa)$
$L$	Length of membrane tube	m
$N_{CO_2}$	Molar flux of component $i$ across the membrane	$mol/(m^2\ s)$
$N_w$	Flux of water	$mol/(m^2\ s)$
$P$	Total pressure	kPa
$P_i^s$	Vapor pressure of pure liquid solvent	kPa
$Q$	Heat flux	$W/m^2$

---

$Q_i$	Flowrate of gas component $i$ at Normal conditions	Nl/min
$Q_L$	Volumetric flowrate of liquid	$m^3/s$
$Re$	Reynolds number ( $dvp/\mu$ )	
$R$	Gas constant (8.314 J/(K mol))	
$R_i$	Molar rate of absorption of component $i$	mol/s
$R_i$	Inner membrane tube radius	m
$R_o$	Outer membrane tube radius	m
$R_m^{rel}$	Relative membrane mass transfer resistance	
$Sc$	Schmidts number ( $\mu/(\rho D)$ )	
$Sh$	Sherwoods number ( $kl/D$ )	
$T$	Temperature	K
$T_g$	Gas temperature	K
$T_l$	Liquid temperature	K

### Lowercase latin symbols

---

Symbol	Meaning	Unit
$a$	Specific inner surface area of membrane module	$m^2/m^3$
$a_i$	Activity of component $i$	$mol/m^3$
$a_m$	Inner surface area of the membrane module	$m^2$
$c_i$	Molar concentration of component $i$ ( $cb=$ bound $CO_2$ )	$mol/m^3$
$c_p$	Specific heat	J/(K mol)
$d_i$	Inner tube diameter	m
$g_i$	Equilibrium model correction factor	
$h_g$	Heat transfer coefficient of the gas phase	$W/m^2$
$h_i$	Salting out coefficient for component $i$	
$h_m$	Heat transfer coefficient of the membrane	$W/m^2$
$k_2$	Second order reaction rate constant	$m^3/(mol\ s)$
$k_3$	Third order reaction rate constant	$m^6/(mol^2\ s)$
$k'_g$	Gas film coefficient	m/s
$k_g$	Gas film coefficient	$mol/(m^2\ s\ kPa)$

---

---

$k_m'$	Mass transfer coefficient of the membrane	m/s
$k_m$	Mass transfer coefficient of the membrane	mol/(m <sup>2</sup> s kPa)
$k_l^0$	Liquid physical mass transfer coefficient	m/s
$l$	Film thickness	m
$m$	Amine molarity	mol/m <sup>3</sup>
$n_i$	Molar convective flux of component $i$ in the gas phase	mol/(m <sup>2</sup> s)
$n_{tot}$	Total molar convective flux of the gas phase	mol/(m <sup>2</sup> s)
$p_i$	Partial pressure of component $i$	kPa
$p_{vap}$	Vapor pressure	kPa
$p^*$	Liquid bulk equilibrium pressure	kPa
$\Delta p_{lm}$	Logarithmic mean driving force	kPa
$p_i^*$	Equilibrium back-pressure of component $i$	
$r$	Radial position	m
$r_i$	Rate of chemical reaction in terms of component $i$	mol/(m <sup>3</sup> s)
$v_g$	Gas velocity	m/s
$v_l$	Liquid velocity	m/s
$v_z$	Velocity in axial direction	m/s
$v_i$	Molar volume of component $i$	m <sup>3</sup> /mol
$v_i^\infty$	Molar volume of solute $i$ at infinite dilution	m <sup>3</sup> /mol
$v_m^0$	Molar volume at Normal conditions (22.41 Nl/mol)	
$w_i$	Weight fraction of component $i$	
$x_i$	Mole fraction of component $i$	
$x_i$	Liquid mole fraction of component $i$	
$y$	CO <sub>2</sub> loading, $c_{CO_2, tot}/m$	mol/mol
$\bar{y}$	CO <sub>2</sub> loading corresponding the chemically bound CO <sub>2</sub>	mol/mol
$y_i$	Mole fraction of component $i$ in the gas phase	
$z$	Axial position	m
$z_i$	Valence of ion $i$	

---

---

## Greek symbols

Symbol	Meaning	Unit
$\tau$	Membrane tortuosity	
$\varepsilon$	Membrane porosity	
$\varepsilon_g$	Fraction of total flow area available for gas flow	
$\nu$	Stoichiometric coefficient	
$\lambda$	Thermal conductivity	W/(m K)
$\mu_l$	Liquid viscosity	Pa s
$\rho_l$	Liquid density	kg/m <sup>3</sup>
$\gamma_l$	Surface tension of liquid	N/m
$\gamma_i$	Activity coefficient of component i, infinite dilution reference state	
$\hat{\gamma}_i$	Activity coefficient of component i, pure component reference state	
$\xi$	Molar extent of reaction	mol/m <sup>3</sup>
$\phi_i$	Fugacity coefficient of component i	
$\phi$	Electric potential	V
$\theta$	Contact angle	

## Abbreviations

Abbrev.	Meaning
AMP	2-amino-2-methyl-1-propanol
DEA	Diethanolamine
MDEA	Methyldiethanolamine
MEA	Ethanolamine
MGA	Membrane Gas Absorption
NTNU	Norwegian University of Science and Technology
PTFE	Polytetrafluorethylene
SINTEF	The Foundation for Scientific and Industrial Research at the Norwegian Institute of Technology
TEA	Triethanolamine

## **1.1 Background**

### **1.1.1 The absorption process**

The large scale removal of carbon dioxide from a gas stream is an important industrial operation, which has traditionally been motivated by technical and economical reasons. Carbon dioxide (CO<sub>2</sub>) present in natural gas will reduce the heating value of the gas. In addition, it is desirable to remove the CO<sub>2</sub> before pipeline transport to avoid pumping any extra volume of gas. Being an acidic gas, CO<sub>2</sub> also has the potential of enhancing corrosion on process equipment. The sales gas specification for natural gas typically requires the CO<sub>2</sub> content to be less than 1-2%, which normally makes a removal efficiency of 80-90% sufficient. The traditional approach to cope with this is by means of an absorption process where the gas is contacted by a liquid with an affinity to the acid gas species.

In processes like ammonia and LNG manufacture, the CO<sub>2</sub> content must be reduced to a level of 10-100 ppm to avoid catalyst poisoning. In these cases the

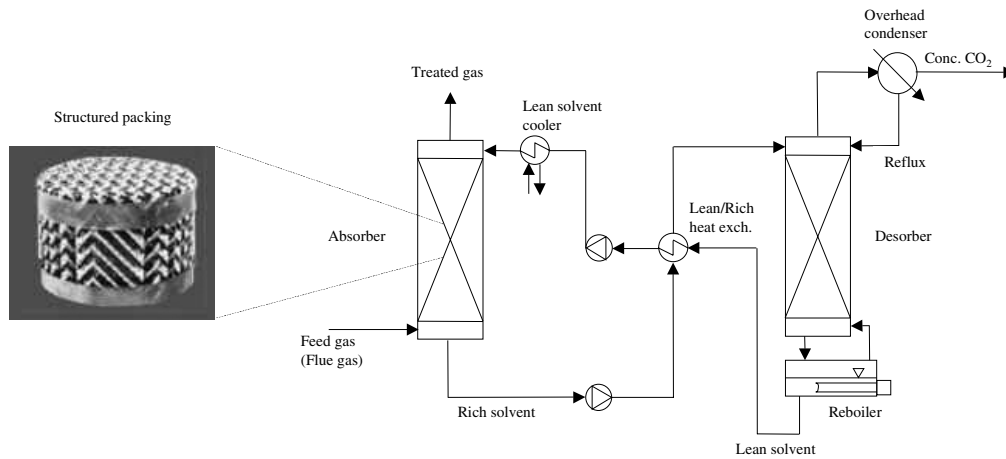


**FIGURE 1.1: Schematic view of a conventional gas absorption/desorption process, with Mellapak 250.Y structured packing (Sulzer Chemtech).**

absorption process must normally be combined with features like adsorption or irreversible chemical conversion (Astarita, 1983), which is termed final or trace purification as opposed to the bulk removal achieved in the absorption processes.

In the traditional absorption process, normally the contact between gas and liquid is achieved in an absorption tower where the liquid flows downwards on the surface of a packing material countercurrently to the upflowing gas. The packing material may be a traditional dumped packing like Raschig rings, or a structured packing like Mellapak, as illustrated in figure 1.1. In some situations, plate towers are preferred (Kohl and Nielsen, 1997).

The absorption process must in general be regenerative in the sense that the liquid is circulating in the process. The liquid regeneration is achieved by raising the temperature and desorbing the carbon dioxide from the liquid by means of countercurrent contact with steam generated in a reboiler (fig. 1.1). If the absorber pressure is elevated as in natural gas  $\text{CO}_2$  removal, one or more flash stages would be utilized before the desorber (stripper). After condensation of



vapor on top of the stripping tower a pure CO<sub>2</sub> gas results which in principle could be released to the atmosphere.

However, the increased attention given to global warming and increasing concentration of atmospheric CO<sub>2</sub> has motivated an intensive research on CO<sub>2</sub> capture and storage. This may be achieved by storage in aquifers, by deepwater storage or by injection into oil wells for enhanced oil recovery, which are all subjects of current research. The technical/economical and environmental aspects of CO<sub>2</sub> removal are combined in the offshore processing platform on the Statoil “Sleipner” gas field, which is a unique example. Here the well stream CO<sub>2</sub> content of 9% is brought down to 2% by a chemical absorption process before pipeline transport to the European market. The separated pure CO<sub>2</sub> is further compressed and injected into an aquifer. This corresponds to an annual amount of 2 mill. tons of CO<sub>2</sub>.

For similar environmental reasons the possibility of CO<sub>2</sub> removal from large scale fossil fuel combustion (coal fired or natural gas fired power plants) has gained increased attention during the last years. In this case, the exhaust feed gas will be of atmospheric pressure and typically contain 3-4% CO<sub>2</sub> if the fuel is natural gas and 10-12% from a coal fired process. In order to make this an economically acceptable operation it is of crucial importance that the energy penalty caused by CO<sub>2</sub> removal is minimized. The process of post-combustion decarbonization by chemical absorption is still considered a promising technology to achieve this goal (Bolland and Undrum, 2002).

### **1.1.2 Absorption liquids**

The absorption liquid may be a physical or a chemical solvent. Chemical solvents in general have a higher absorption capacity which makes for a reduced volume of liquid to be pumped through the process. The chemical equilibria provide a high driving force for absorption and enable low CO<sub>2</sub> levels in the exit gas to be achieved. The ideal chemical solvent would be one with fast reaction kinetics and close to irreversible reaction, but which may be cyclically reversed

e.g. upon heating. In any case the major draw-back with chemical solvents is the high energy requirement to regenerate the solvent. For flue gas CO<sub>2</sub> removal, however, a chemical solvent is the only considerable option.

The *alkanolamines* have been found to possess many of the desirable properties as the reactive component in an aqueous absorbent solution. Approximately 90% of all acid gas (CO<sub>2</sub> and H<sub>2</sub>S) treating processes in operation today use alkanolamine solvents. Bottoms (1930) introduced triethanolamine (TEA), which was used in the early gas treating plants. Today monoethanolamine (MEA) and promoted methyldiethanolamine (MDEA) in aqueous solution are the most important solvent systems for CO<sub>2</sub> absorption. Promoted potassium carbonate solution and potassium salts of amino acid however still has a market share. Some “hybrid” solvents are also in use comprised of alkanolamines in organic physical solvents like methanol.

### 1.1.3 Tower design and operation

The design and operation of absorption towers are limited by constraints regarding the gas and liquid flow and the coupling between them. The packing material is designed in order to provide as high specific surface area (m<sup>2</sup>/m<sup>3</sup>) as possible. In low pressure operations it is especially important that the pressure drop through the packed bed is minimized in order to reduce the energy requirement of the gas blowers. The distribution of liquid over the packing cross section is important to avoid channeling, by-passing and unstable operation of the process.

The lower constraint of the liquid flow is the one that gives a complete wetting of the packing surface. An upper constraint exist where liquid “bridges” form, which serve to reduce the area available for mass transfer. When increasing the gas velocity at a given liquid load, the “loading point” is eventually reached where the liquid is held back by the upflowing gas. The pressure drop over the bed then starts to increase rapidly until the flooding point, when liquid is forced upwards by the gas. To minimize the required tower cross section it is desirable

to operate as close to the flooding limit as possible. The design limit in terms of gas velocity is therefore typically at 70% of flooding.

## 1.2 Membranes for gas separation

Membrane technology is a rapidly emerging field and has since the 1980's been applied in a number of fields for large scale gas purification. Reliable and selective polymer membranes have been developed for a number of applications. In this process the selectivity is provided by the membrane due to differences in solubility, diffusivity and/or size of the molecules to be separated. With a selective membrane, no chemicals are needed for the separation, and in principle a compact and robust process may be designed.

The driving force for this separation is given by differences in partial pressures of the components between the feed side and the permeate side of the membrane. This may be provided by a difference in total pressure or by making use of a sweep gas on the permeate side. If the permeate is a desired product, a vacuum is required in order to capture the separated component in highly concentrated form. This will have to be the case in large scale CO<sub>2</sub> capture from flue gas, where the CO<sub>2</sub> is subsequently compressed to the subsea injection pressure.

Present research on polymer membranes with fixed site carriers and supported liquid membranes show promising results on a laboratory scale. There is however a number of challenges to overcome, especially in terms of membrane stability. Microporous membranes made of carbon or inorganic materials have shown excellent selectivity but are very sensitive to humidity in the gas. This is a problem since the exhaust gas normally contains around 7% water. For flue gas CO<sub>2</sub> removal the challenge still remains to develop a membrane with a combined high selectivity and permeability. According to a study referred to by Feron et al. (1992), a two stage system was required for a flue gas CO<sub>2</sub> removal operation using commercially available gas separation membranes. The cost was found to be at least twice the cost of a conventional MEA absorption process, mostly due to the high energy requirements for gas compression. The low

partial pressure of CO<sub>2</sub> in the power plant flue gas is a final limitation as the driving force will always be small. Feron and Jansen (2002) claimed that it is doubtful whether gas separation membranes present a viable option for this application.

Morimoto et al. (2002) compared the costs of CO<sub>2</sub> capture from combustion gas of a coal fired power plant (13% CO<sub>2</sub>) with a conventional MEA absorption process and a polymer membrane. They found that the membrane process was 30% more expensive with a produced CO<sub>2</sub> of 59% purity compared to the 99.9% purity produced in the absorption process. 80% of the energy requirement was found in the vacuum pump. The cost of a membrane process was significantly reduced when studying removal from a more concentrated blast furnace gas of 27% CO<sub>2</sub>. They thus concluded that in cases with a high CO<sub>2</sub> concentration in the flue gas, membrane separation can be feasible in the near future.

## 1.3 Membrane Gas Absorption

### 1.3.1 Principle

Membrane gas absorption is a new separation technique under rapid development. It may be considered a hybrid of a gas absorption technology and membrane technology. In this operation the gas phase is separated from the liquid phase by a microporous membrane not wetted by the absorption liquid. The membrane works only as a barrier between the phases, while the selectivity for separation is provided by the absorption liquid, which may be of similar type as in conventional gas absorption, e.g. an aqueous solution of alkanolamines. The fundamental difference between membrane gas absorption and conventional membranes for gas separation is illustrated in figure 1.2.

In membrane gas absorption the advantages of absorption technology and membrane technology are combined. The membrane gas absorber acts as a different way of contacting the gas and the liquid phase and gives a number of advantages

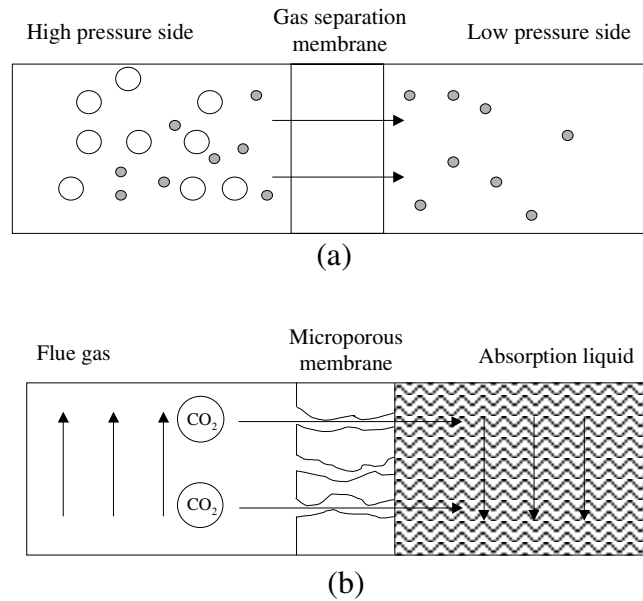


**FIGURE 1.2: Principle of gas separation membrane (a) and membrane gas absorption (b)**

compared to conventional absorption towers, which may be considered dispersed phase contactors. The decoupling of the gas and liquid phase prevents any momentum transfer from occurring across the phase boundary. As a consequence, the operation problems and constraints like foaming, channeling, entrainment and flooding are eliminated. The presence of the membrane will also serve to reduce the interfacial contact and mass-transfer of undesirable gas phase components like oxygen and nitrous oxide that may operate as degradation agents to the alkanolamine in solution. The possible disadvantage from an extra resistance layer between the gas and the liquid phase may be minimized by proper membrane design and choice of materials.

By forming the membrane as hollow fibers stacked in membrane modules, very compact units can be made, as illustrated in figure 1.3. The possibility of a specific surface area 30 times higher than conventional absorption towers has been reported (Qi and Cussler, 1985a/1985b). However, in practice this is limited by pressure drop considerations and the level of gas pretreatment in order to

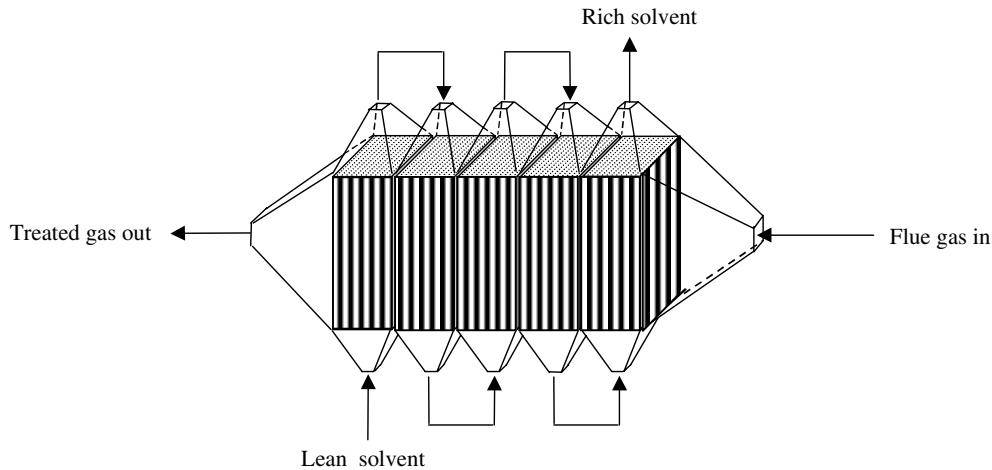


**FIGURE 1.3: Module design of a hollow fiber membrane contactor for flue gas CO<sub>2</sub> removal**

remove particles, dust and liquid droplets, that may lead to clogging of the membrane module.

Membrane contactors have a number of possible applications in both gas absorption and liquid/liquid extraction (Gabelman and Hwang, 1999). In some situations where gas side resistance is dominating, it may be desirable to operate the membrane in wetted mode i.e. with liquid filled pores. When operated as a liquid-liquid contactor the pores should be wetted by the phase with the lowest resistance to mass transfer. A dense polymer or gel layer may be added on either side of the porous membrane in order to invoke selectivity in the membrane.

### 1.3.2 Breakthrough pressure

As most systems applied in CO<sub>2</sub> absorption are controlled by liquid side mass transfer resistance, it is of utmost importance to prevent any penetration of liquid into the pores of the membrane. This is dependent on the trans-membrane pressure and the wettability of the membrane material. The membrane breakthrough pressure may be described by the Young-Laplace equation as:

$$\Delta P_{br} = -\gamma_l \cos \theta \left( \frac{1}{r_1} + \frac{1}{r_2} \right) \quad (1.1)$$

where  $\gamma_l$  is the liquid surface tension,  $\theta$  is the contact angle between liquid and solid (the membrane material).  $r_1$  and  $r_2$  are the two characteristic radii of an elliptic shaped pore. For a circular pore the equation is simplified to:

$$\Delta P_{br} = \frac{-2\gamma_l \cos \theta}{r} \quad (1.2)$$

with  $\Delta P$  defined as:

$$\Delta P = P_{liquid} - P_{gas} \quad (1.3)$$

The requirement is that the liquid does not wet the membrane material. This does not spontaneously occur if  $\theta > 90^\circ$ . Liquid penetration into the pores will then occur only if  $\Delta P > \Delta P_{br}$ . If  $\Delta P_{br} > \Delta P > 0$  the gas/liquid interface will be “immobilized” at the liquid side pore opening as illustrated in figure 1.2b. This is the desired situation when it comes to the application of the membrane in a CO<sub>2</sub>/alkanolamine contactor. If  $\Delta P < 0$  the gas will penetrate as bubbles into the liquid phase.

In order to design a robust industrial process it is desirable to use a membrane with as high  $\Delta P_{br}$  as possible. From eq. (1.1) it is seen that this may be obtained by a small pore radius and by using a liquid with a high surface tension. A lower limit exist for the pore radius when the contribution from Knudsen diffusion becomes significant, thus reducing the effective diffusivity through the membrane. This limits the pore radius to be higher than the mean free path of the CO<sub>2</sub>-molecules, which is around 0.07  $\mu\text{m}$ , depending on temperature. The use of aqueous solutions assure that the surface tension is relatively high. However, the surface tension is decreasing considerably upon increasing alkanolamine concentration (Vásquez et al., 1997; Alvarez et al., 1998). This effect is counteracted by a slight increase with CO<sub>2</sub>-concentration (Kumar et al., 2002). These aspects should always be considered in a conservative design.

### 1.3.3 Membrane materials

In table 1–1, the surface energy of a number of polymers that may be used in microporous membranes is given. Wetting of the polymer by the liquid solution is generally favored by high surface energy. It is seen that polytetrafluorethylene (PTFE) has the desirable property in terms of a significantly lower surface energy than the other polymers. Important additional advantages of PTFE are the chemical stability and inertness that prevent the polymer from changing its properties over time. Tests with CO<sub>2</sub> absorption into alkanolamine using polyethylene and polypropylene membranes have shown that the resistance to liquid penetration breaks down after a period of long term operation, probably due to a combination of surface wetting and swelling of the polymer with the elapse of time (Kreulen et al., 1993; Nishikawa et al. 1995).

**TABLE 1–1: Surface energy of some polymers (Mulder, 1991)**

Polymer	Surface energy (10 <sup>3</sup> N/m)
polytetrafluorethylene	19.1
polypropylene	30.0
polyethylene	33.2
polyvinylchloride	36.7

### 1.3.4 The Kvaerner/Gore membrane contactor

Kvaerner Process Systems, in collaboration with W.L Gore & Associates, has for a number of years worked on the development of membrane contactors based upon microporous PTFE hollow fiber membranes. The aim has been the application in CO<sub>2</sub> removal with aqueous alkanolamines, both from exhaust gas and natural gas (Falk-Pedersen, et al., 2000). The technology has also been developed for natural gas dehydration (King et al., 2002).

The membrane modules essentially consist of layers formed as microporous tubes interconnected by impermeable bridges. The tube layers are separated by a spacer that serves to prevent adjacent layers from coming into direct contact,



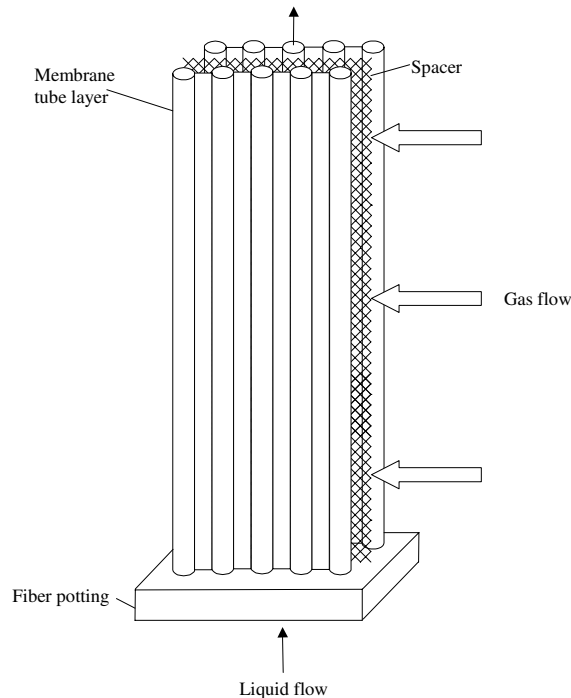


**FIGURE 1.4: Principle of the interconnected tube membrane design, with spacer between the tube layers. The fiber ends are potted with a thermosetting resin.**

---

as illustrated in figure 1.4. The gas flow is thus regularly distributed on the available cross-section. The spacer additionally serves to provide a thorough mixing of the gas phase in order to minimize the presence of gas phase mass transfer resistance.

Membrane tubes will in these contactors typically have diameters from 0.5-1.5 mm and the specific area of the units range from 500-1500 m<sup>2</sup>/m<sup>3</sup>. Based upon testing performed on a pilot scale the important advantages of this technology have been verified (Falk-Pedersen et al., 2000). These may be summarized as:

- 60-75% reduction in size and weight compared to a conventional tower
- Footprint requirement reduced by 40% compared to conventional case
- The contactor is insensitive to motion

- No foaming, channeling, entrainment or flooding
- Significant reduction of corrosion problems
- Operating cost savings of 38-42%
- Capital cost savings by 35-40%

## 1.4 Purpose

### 1.4.1 Scope of this work

The Norwegian climate technology programme Klimatek is aimed at development and verification of new cost-effective technologies which can capture and sequester CO<sub>2</sub> from gas fired power generation. Within this programme the project contracted by Kvaerner Process Systems is focusing on the development of a membrane gas/liquid contactor for CO<sub>2</sub>-removal using amine absorption. Important objectives within this project are the reduction of weight, volume and energy requirements for the CO<sub>2</sub> removal operation. The technology is demonstrated in a pilot plant at Statoils gas processing plant at Kårstø, Norway and in a smaller test rig, erected at SINTEF/NTNU in Trondheim, Norway.

The purpose of this work has been to develop a fundamental understanding of the mechanisms involved in the operation of a membrane gas absorber through a lab-scale experimental study, a theoretical study and mathematical modeling of the process. Being a fundamental study, the work has been limited to the performance of straight tube membranes. Other new membrane designs, where liquid mixing points have been implemented are not studied. Proprietary experimental data show that these new membranes lead to a significant increase in mass transfer coefficients. The values of mass transfer coefficients presented in this study are thus not representative of what may be realized in a technical process using the Kvaerner/Gore membrane gas absorbers.

### 1.4.2 Problem formulation

Membrane gas absorption may still be considered an immature technology, and the major objective of this work has been to achieve an increased understanding of the mechanisms involved in the operation. This has been limited to the application as a contactor for CO<sub>2</sub>-absorption in aqueous alkanolamines. The solvent systems used are the aqueous solutions of MEA and MDEA. These are the most common alkanolamine solvents in use and they also represent two extremes regarding chemistry and range of operation. MEA is the most common component for application in exhaust gas CO<sub>2</sub> removal, while MDEA has a similar position in natural gas operation. The main focus has been on the following fields:

- Investigate the effect of operating variables like CO<sub>2</sub> partial pressure, liquid CO<sub>2</sub> loading, liquid velocity, gas velocity and temperature. All in the range of operation expected from a technical process applied in exhaust gas CO<sub>2</sub> removal. This has required the design and establishment of a new lab-scale apparatus which is a major part of this work.
- Establish a simulation tool by rigorous modeling of the membrane gas absorption process explicitly accounting for the rate of diffusion and chemical reaction in the liquid phase including gas bulk and membrane transport. The model should include thermal effects and the effect of water evaporation caused by contact with an unsaturated gas. This requires the establishment of an equilibrium model in order to capture the effects of reaction reversibility both in the CO<sub>2</sub>/MEA/water and CO<sub>2</sub>/MDEA/water systems.
- Investigate the possibility of utilizing a lab-scale membrane gas absorber as a tool to obtain fundamental mass transfer data like diffusivities and reaction rate constants in alkanolamine systems. This includes a sensitivity analysis in order to map the reaction regimes that may be realized.

### 1.4.3 Thesis outline

In chapter 2, a literature survey of membrane gas absorption (MGA) is given. The review is limited to microporous membranes focusing on CO<sub>2</sub> as the transferable component. Chapter 3 gives an overview of the chemistry involved in the absorption of CO<sub>2</sub> into aqueous alkanolamine solutions. This include chemical reactions, rate expressions and a discussion of possible reaction mechanisms. In chapter 4 the problems involved in developing an equilibrium model for CO<sub>2</sub>/alkanolamine/water systems are discussed. A review is given regarding different approaches to the subject. The non-iterative equilibrium model used in the MGA simulator model is developed and discussed.

The experimental setup and operation of the lab-scale apparatus are presented in chapter 5 along with the sampling and analysis procedures. The procedure for calculation of CO<sub>2</sub> absorption rates from experimental raw data is shown. Results from the absorption experiments are shown and discussed in chapter 6 in terms of the overall mass transfer coefficients and relative enhancement factors.

The different parts of the MGA simulator model are outlined in chapter 7, including the gas and liquid flow model and the model describing mass and heat transport in the gas phase, membrane and liquid phase. The effect of important physical properties are discussed along with the coupling phenomena between the effect of increased viscosity due to CO<sub>2</sub> absorption and the component diffusivities. The importance of correct values for the bound CO<sub>2</sub> diffusivities are discussed and new correlations are developed from parameter regression on selected experiments from the lab-scale apparatus. The comparison of model predictions with experimental data is shown and discussed.

The possibility of using a lab-scale membrane gas absorber for the purpose of measuring reaction kinetics is further discussed in chapter 8, including a sensitivity analysis on the developed model. New experiments are presented and used in the regression of the second order rate constant for the CO<sub>2</sub>-MDEA reaction. In chapter 9, conclusions and recommendations for further work are presented.

*Literature review of  
membrane gas  
absorption*

---

The literature review given here will have the emphasis on membrane gas absorption using microporous, hydrophobic membranes with CO<sub>2</sub> removal as the main application. Microporous membrane gas absorption in general has been reviewed by Sirkar (1992).

**2.1 Studies focusing on the mass transfer performance of membrane gas absorbers**

The first known application of a microporous membrane as a gas-liquid contacting device was for oxygenation of blood using hydrophobic flat Gore-Tex membranes (Esato and Eiseman, 1975). The possibility of an industrial application of hollow fibre membranes as gas/liquid contactors was first studied by Qi and Cussler (1985a, 1985b). Seeing the potential in terms of a larger area per volume compared to conventional absorption towers, they investigated possible negative effects of the additional membrane resistance. They used a microporous hydrophobic polypropylene hollow fiber membrane for absorption of carbon dioxide in aqueous sodium hydroxide.

Their experimental results verified that the correlation by Sieder and Tate (1936) is appropriate for the liquid side mass transfer coefficient and found that the mass transfer area of the membrane module is unaltered even at very low liquid flow. Investigating different chemical systems, they concluded that the membrane resistance was dominant for gas absorption in strong acid and base ( $\text{NH}_3$  in  $\text{H}_2\text{SO}_4$ ,  $\text{H}_2\text{S}$  and  $\text{SO}_2$  in  $\text{NaOH}$ ), which is not surprising since these are the systems that normally would be gas-film controlled. Absorption of  $\text{CO}_2$  in  $\text{NaOH}$  was found to be less dominated by membrane resistance, due to the slower chemical reaction. Experiments done with absorption of  $\text{CO}_2$  in a number of common alkanolamine solutions showed that liquid side resistance is dominant in these cases, thus concluding that selectivities can be obtained which are comparable to those of packed towers.

Comparing their results with the performance of packed towers in terms of the volumetric overall mass transfer coefficient,  $K_G a$ , they found the values to be possibly thirty times greater for their membrane modules. They also recognized the independency of gas and liquid flows as an important advantage in favour of the membrane contactor. These conclusions were further investigated by Yang and Cussler (1986), who studied gas-liquid mass transfer by desorbing  $\text{O}_2$  from water, and determined the influence of liquid velocity on the mass-transfer coefficient. Wang and Cussler (1993) and Cussler (1994) showed that liquid side mass transfer may be significantly improved if the liquid flows on the shell side and perpendicular to the fibers. This is a consequence of better mixing on the liquid side. New module designs were presented that partially combined the advantages of countercurrent flow in terms of driving force and the advantage of cross-flow in terms of mass transfer. This was basically achieved by using baffles on the shell side.

To verify that the Graetz-Leveque solution for heat transfer is applicable for the tube side mass transfer, Kreulen et al. (1993a) studied the physical absorption of  $\text{CO}_2$  into water/glycerol. By varying the glycerol fraction, the liquid viscosity could be varied and experimental results were found to follow the solution calculated from the correlation. The membranes were microporous polypropylene

and polysulfone. The effect of membrane porosity on the effective mass transfer area was investigated by absorption experiments of pure CO<sub>2</sub> in water with two membranes of 70% and 3% porosity. With liquid flowing through the fibers they found very good agreement between theoretical and experimental values of the mass transfer coefficient when the mass transfer area was taken as the surface area of the fibers and not just the pores themselves. This was true for both membranes, thus supporting the common assumption that the active mass transfer area is given by the total membrane surface area and is independent of porosity.

Referring to studies of analogous problems (e.g. Wakeham and Mason, 1979), the results could be explained by considering the liquid to be instantaneously saturated along the membrane wall compared to saturation in the radial direction. This may result from the extremely short distance between pores compared to the distance from the fiber wall to the center of the fiber. The boundary layer adjacent to the fibre can be considered homogeneously saturated and from this layer the diffusion into the flowing liquid is taking place.

The TNO group in the Netherlands has been studying the application of a hydrophobic (polypropylene) membrane contactor for CO<sub>2</sub> removal from flue gases (Feron and Jansen, 2002). They proposed a transversal flow membrane module design using a reactive solvent. They estimated the equipment cost to be 30% lower than that of a process using packed towers. Furthermore, the estimated gas side pressure drop for the membrane contactor was half of that of a conventional absorber, which will lead to a significant reduction in energy cost.

Experiencing problems with wetting of the polypropylene/polyethylene membranes using conventional alkanolamine-based solvents, the TNO group has developed a new class of solvents, having a higher surface tension and thus reducing the tendency of leakage from the liquid phase through the membrane. This may be achieved by addition of a water soluble carbonate salt to the alkanolamine solution or by using alkaline salts of amino acids as the active component of the absorbent liquid (Jansen and Feron, 1998; Kumar et al., 2002).

Mitsubishi Heavy Industries and Tokyo Electric Power Company have published a series of articles related to their work on CO<sub>2</sub> removal from thermal power plant flue gas by a hollow fiber gas/liquid contactor. They have developed a method whereby a membrane module is installed inside the flue gas duct, proposing conventional steam desorption as the method for regenerating the MEA-water solvent applied. (Matsumoto et al. 1995; Nishikawa et al., 1995). Their experimental results indicated that the microporous membranes are suitable for the CO<sub>2</sub>-MEA/water system due to the high value of the volumetric mass transfer coefficient (five times that of a packed bed) when there is no wetting of the microporous membrane. PTFE was found to be an excellent membrane material as it was not subject to wetting during a long term continuous testing period of 6600 hours. The polyethylene membranes tested showed a gradual decrease in the overall mass transfer coefficient with time, probably due to wetting of the membrane. By surface treatment with a fluorocarbonic material the durability of the PE-membranes was improved.

Matsumoto et al. (1995) apparently found the overall mass transfer coefficient to be strongly dependent on membrane porosity upon absorption of CO<sub>2</sub> in chemical solvents, while practically no effect of porosity was found with pure water as absorbent. This resulted from testing of a series of membranes made of PTFE, PE and PP with porosities ranging from 40 to 80%. The chemical solvents were a 30wt% aqueous MEA-solution and a 1 M aqueous NaOH-solution. Matsumoto et al. (1995) explained the effect by considering the concentration boundary layer thickness in the two cases. This was found to be significantly lower in the chemical system due to the rapid chemical reaction, and comparable to the apparent distance between adjacent pores, based upon the assumption that the pores are open with a staggered arrangement.

These results would indicate the effective mass transfer area to be related to the area represented by the pore openings in the case of chemical absorption. However, a closer look at the data given by Matsumoto et al. (1995) reveal that the experiments were done with decreasing membrane wall thickness, pore diameter and membrane tube diameter in addition to increasing membrane porosity.



The effects observed can thus partially be explained by considering the variations in membrane resistance vs. the total resistance.

Rangwala (1996) published results from experiments with absorption of carbon dioxide in water, sodium hydroxide and DEA solution using polypropylene microporous hollow fibers. He compared the results with those calculated by the use of correlations for gas, membrane and liquid mass transfer coefficients. Rangwala found a lower value for the membrane mass transfer coefficient than expected and attributed this to partial liquid penetration into the pores.

Li and Teo, (1998) studied the removal of carbon dioxide from a gas mixture using hollow fibre membranes with both permeation and absorption methods. Their two types of membranes were made of homogeneous silicon rubber and polyethersulphone with a dense skin layer at the outer edge of the fibre. The use of dense membranes for gas absorption inevitably increases the mass transfer resistance, but eliminates the wetting problems commonly encountered in microporous membranes. Another advantage is the flexibility in operation with a high gas side pressure without bubble formation. This was tested with a gas pressure 200 kPa higher than the liquid pressure, and may to some degree compensate the disadvantage of higher membrane resistance due to the possibility of a higher driving force for absorption. Membrane gas absorption using nonporous membranes was also investigated by Nii and Takeuchi, (1994) who named the process “permabsorption”.

## **2.2 Work including rate-based modeling**

The majority of the publications so far mentioned use simplified methods for the theoretical mass transfer analysis making use of individual film (gas, membrane and liquid) and overall mass transfer coefficients. These may be considered lumped-parameter models compared to the use of transport equations for the chemical components explicitly accounting for the rates of diffusion and chemical reaction.

Karoor and Sirkar (1993) were among the first to study membrane gas absorption in terms of a diffusion-reaction model. They assumed isothermal conditions and thereby neglected the heat of absorption and heat transfer between the phases. They used the Method of Lines combined with a finite difference scheme to solve the problem numerically. They explored the separation of carbon dioxide and sulphur dioxide from nitrogen using pure water and an aqueous amine solution as absorbent. Experiments were also done with pure carbon dioxide and pure sulphur dioxide in order to eliminate gas and membrane mass transfer resistance. The membranes were microporous commercial polypropylene hollow fibers.

For the case of absorption with chemical reaction, Kreulen et al. (1993b) calculated the concentration profiles in the liquid by solution of the differential mass balances. Solutions for different values of the reaction rate constant served to illustrate the effect of chemical reaction vs. diffusion. Similar sensitivity analysis were done for the external (gas bulk and membrane) resistance. The experimental study served to explain the effect of fibre length and diameter. For low liquid velocities the highest fluxes were measured in the membrane with the lowest diameter. At higher liquid velocities, the highest diameter gave the highest flux which could be explained when considering that the transition to turbulent flow (at  $Re = 2100$ ) is depending on the product of liquid velocity and tube diameter.

Kim et al. (2000) studied the separation of carbon dioxide - nitrogen mixtures with microporous PTFE membranes. Aqueous solutions of MEA, AMP and MDEA were tested as absorbents. Absorption rates were measured at varying temperature and liquid flow rate. The experimental study was accompanied by a theoretical model similar to Karoor and Sirkar (1993).

Chun and Lee (1997) and Lee et al. (2001) carried out a numerical analysis of the performance of a hollow fibre membrane contactor for the removal of carbon dioxide with aqueous potassium carbonate as the absorbent. They were studying the radial and axial concentration profiles in the hollow fiber from

their solution of the transport equations for CO<sub>2</sub> and bicarbonate also taking into account the reversibility of the reaction.

## 2.3 Conclusions from literature review

The following conclusions may be drawn from the review of the existing literature of membrane gas absorption:

- The advantages of membrane gas absorption compared to conventional contacting equipment have been recognized by several authors and research groups.
- The operation is sensitive to membrane resistance which is minimized by using microporous membranes.
- For liquid side controlled mass transfer, the performance is sensitive to membrane wetting/liquid penetration which will dramatically increase the mass transfer resistance of the membrane.
- Most studies are performed using microporous membranes made of polypropylene.
- Of the authors considering chemical absorption, few have done experiments with solvents of “technical” composition as would be the choice in a large scale regenerative process. Most experimental studies are done with sodium hydroxide or low concentrated carbonates or alkanolamines.
- Only a few authors have modelled the process with a rigorous transport model. Most authors have used an approach with mass transfer coefficients.
- No authors have included the effect of increased liquid viscosity vs. CO<sub>2</sub> loading and the effect of viscosity gradients on the molecular transport.
- No authors have included a rigorous equilibrium model in order to study effects of the reversible chemical reactions involved.

- The assumption of isothermal operation is made by all authors, thus not considering the temperature increase due to heat of absorption and heat exchange between the gas and liquid side of the membrane.
- No authors have included water as a transferable component between the gas and the liquid phase.

No commercial CO<sub>2</sub>-removal process using this technology is presently in operation. It is expected that membrane gas absorbers have the potential of significantly improving the performance of gas/liquid contactors in a number of applications. The characteristics given above show that there is still much to be done in order to map the performance and operation of membrane gas absorbers with a view to an industrial application.

---

*Chemistry of carbon dioxide absorption in aqueous alkanolamine solutions*

---

### **3.1 Introduction**

Alkanolamines have achieved a special position within the field of acid gas absorption, i.e. removal of CO<sub>2</sub> and H<sub>2</sub>S from process gas. Alkanolamines may be distinguished as primary, secondary or tertiary, depending on the number of carbon containing groups attached to the nitrogen atom. The amines that have been of principal commercial interest for gas purification are monoethanolamine (MEA), diethanolamine (DEA) and methyldiethanolamine (MDEA) (Kohl and Nielsen, 1997). The structural formulas are shown in figure 3.1. MEA is the preferred component for gas streams containing relatively low concentrations of CO<sub>2</sub>, while MDEA is more suitable for higher CO<sub>2</sub> contents. The relatively low rate of absorption in MDEA solvents may be increased by addition of relatively low concentrations of primary or secondary amines or diamines as piperazine.

The effectiveness of any amine for the absorption of acid gas is due primarily to the alkalinity, although a number of chemical reactions may occur in solution.

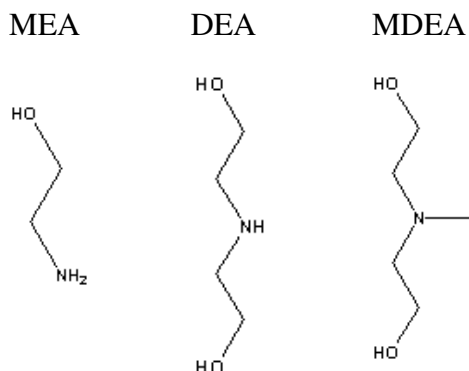


**FIGURE 3.1: Structural formulas of common alkanolamines**

---

The presence of the alcohol group provides the high water solubility and the low volatility that is important to minimize evaporation losses of the solvent. Other problems involved in the operation of amine absorbers include solvent degradation, which leads to the requirement of regularly replacing the solvent and corrosion of process equipment facilitated by chemically “aggressive” components of the liquid phase (Kohl and Nilsen, 1997). Research is aimed at finding chemically stable and less corrosive components with high rates of absorption and low heats of reaction in order to minimize energy requirements for regeneration of the solvent.

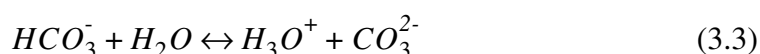
The purpose of this chapter is to present and review the important chemical reactions occurring upon absorption of CO<sub>2</sub> in an aqueous alkanolamine solutions. The different kinetic mechanisms and rate expressions are discussed in order to explicitly account for the rate of reaction in an absorber model.

## 3.2 Reactions in aqueous solution

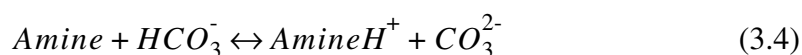
When CO<sub>2</sub> is dissolved in water it may undergo the hydration reaction to form carbonic acid. CO<sub>2</sub> may be considered a Lewis acid in aqueous solution.



The amount of CO<sub>2</sub> that undergoes the hydration reaction is much less than the amount remaining in the physically dissolved state, corresponding to approximately 99%. The carbonic acid may dissociate according to:



The distribution of CO<sub>2</sub> between HCO<sub>3</sub><sup>-</sup> and CO<sub>3</sub><sup>2-</sup> is pH-dependent, which is important when considering an alkanolamine system. The *pK<sub>a</sub>* values of carbonic acid at 25 °C are 6.37 for step 1 and 10.25 for step 2 (Lide, 1991). It follows that at a pH of 10.25 the amount of HCO<sub>3</sub><sup>-</sup> and CO<sub>3</sub><sup>2-</sup> will be equal and that CO<sub>3</sub><sup>2-</sup> may not be neglected until the pH is less than about 9. Looking at the *pK<sub>a</sub>*-values for common alkanolamines (Astarita et al., 1983) it can be concluded that the pH operating region for aqueous alkanolamine solutions may be both below and above this limit. The *pK<sub>a</sub>* of MEA and MDEA at 25 °C is 9.6 and 8.5, respectively. It follows that the carbonate ion is a stronger base than both these alkanolamines. The equilibrium



will thus be shifted to the left hand side. This is a common argument to disregard carbonate formation in equilibrium modeling of alkanolamine systems. However, the pH- dependent equilibrium (3.3) must also be considered.

In general it can be said that the carbonate formation may be neglected in MEA-solutions despite the fact that the *pK<sub>a</sub>* is relatively high and the possibility of a pH approaching 12 in CO<sub>2</sub>-free solution exists. The reason for this is the existence of the *carbamate formation* reaction, which is the totally dominating mechanism except at CO<sub>2</sub>-loadings (mol CO<sub>2</sub>/mol amine) close to and higher than 0.5, where bicarbonate formation is taking over as the main reaction. Then the pH-value is so low that carbonate formation may be neglected. However, in MDEA-solutions the bicarbonate is the only species formed, and at low CO<sub>2</sub>-loadings a considerable amount may further deprotonize to carbonate. As will

be shown later, the reaction kinetics of CO<sub>2</sub> absorption is denominated by other reactions, since the HCO<sub>3</sub><sup>-</sup>/CO<sub>3</sub><sup>2-</sup> shift may be considered instantaneous. The mechanisms of bicarbonate and carbamate formation in aqueous amines are further described below.

Recognizing the basicity of alkanolamine solutions the direct reaction with hydroxide must also be considered.



The low concentration of OH<sup>-</sup> limits the importance of this reaction to the lowest loadings of CO<sub>2</sub>/the highest pH-values. This is the region where kinetic constants of the reaction between CO<sub>2</sub> and alkanolamines preferably are measured, and in this respect the OH<sup>-</sup> reaction may be very important, especially in tertiary amines.

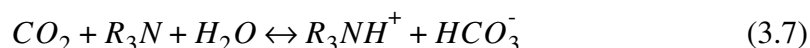
### 3.3 Alkanolamine reactions

#### 3.3.1 Mechanism of tertiary alkanolamines

The reaction mechanism when CO<sub>2</sub> is absorbed into an aqueous solution of a tertiary alkanolamine like MDEA was first thought of being as simple as the MDEA acting as a base for CO<sub>2</sub> to react with hydroxide ions in solution (Barth et al., 1981).



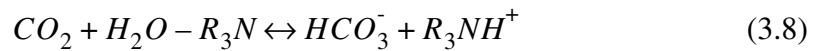
The base protonation followed by reaction (3.5) give the bicarbonate formation overall:



However, the observed reaction rates could not be explained by such a route alone. This has led to the conclusion that the tertiary amine is taking part in the



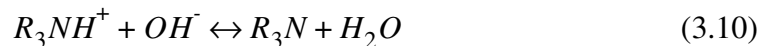
rate limiting step in what is called the base-catalyzed hydration of  $\text{CO}_2$ , as first suggested by Donaldson and Nguyen (1980). The base catalysis effect is now generally accepted but there is still some controversy regarding the actual reaction mechanism. The most accepted mechanism goes through the formation of a hydrogen bond between the tertiary amine and water, thus weakening the O-H bond in water and increasing the reactivity towards  $\text{CO}_2$ .



Barth et al. (1981) and Yu et al. (1985) proposed a possible zwitterion mechanism to account for the catalytic effect although structural considerations showed this to be relatively unlikely. Both reaction mechanisms result in a reaction order of one in the amine, which also is the conclusion from most experimental studies performed. The rate expression for the reversible reaction will thus be:

$$r_{\text{CO}_2} = k_2[\text{CO}_2][\text{R}_3\text{N}] - k_{-2}[\text{R}_3\text{NH}^+][\text{HCO}_3^-] \quad (3.9)$$

where  $k_2$  and  $k_{-2}$  are the forward and reverse rate constants of reaction (3.8). This rate equation can be simplified by introducing the equilibrium concentration of  $\text{CO}_2$ ,  $[\text{CO}_2]_e$ , in equilibrium with the local concentration of free amine ( $[\text{R}_3\text{N}]_e$ ). It is important to note that the protonated alkanolamine can revert back to the unprotonated form by reacting with the hydroxide ion:



This reaction is considered to be at equilibrium because it involves only a proton transfer, thus  $[\text{R}_3\text{N}] = [\text{R}_3\text{N}]_e$ . Considering this, the following rate expression results:

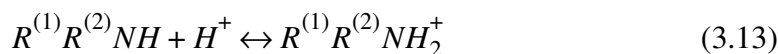
$$r_{\text{CO}_2} = k_2[\text{R}_3\text{N}]( [\text{CO}_2] - [\text{CO}_2]_e ) \quad (3.11)$$

In this form, the driving force for the chemical reaction is explicitly given by the difference ( $[\text{CO}_2] - [\text{CO}_2]_e$ ), making the rate of reaction zero at equilibrium.

The bicarbonate reaction can take place for all amines, but the lack of competing reactions makes it vital in solutions of tertiary alkanolamines.

### 3.3.2 Mechanism of primary and secondary alkanolamines

For primary and secondary alkanolamines, the possibility of carbamate formation leads to a different reaction scheme. A mechanism for this reaction was proposed by Danckwerts et al. (1967) and is shown here for a primary or secondary alkanolamine  $R^{(1)}R^{(2)}NH$  ( $-R^{(2)} = -H$  for a primary alkanolamine).



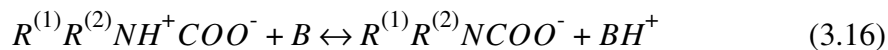
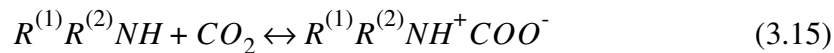
Overall:



Carbon dioxide, according to this mechanism, reacts directly with the primary or secondary amine to form a carbamic acid. The hydrogen formed by the acid is subsequently neutralized by a second molecule of amine. The second step must be regarded as instantaneous, and the overall reaction is then of second order. The stoichiometry of this overall reaction explained why the  $CO_2$  loading of MEA-solutions is limited to around 0.5 mol/mol.

Experimental studies of reaction kinetics in secondary alkanolamines like DEA have by several authors been found not consistent with the early mechanism. The overall reaction order was found to be 3 and by some authors between 2 and 3. This is also the case for experiments with non-aqueous MEA-solutions in systems like MEA/ethanol and MEA/ethylene glycol (see the review article by Versteeg et al., 1996), where a second order dependence in MEA-concentration has been found. This lead to the need for a modification of the early mechanism.

The *zwitterion-mechanism* was first presented by Caplow (1968). In this mechanism the direct reaction between  $\text{CO}_2$  and the alkanolamine results in a zwitterion intermediate which is subsequently deprotonated by a base B:



Any base present in the solution can contribute to the zwitterion deprotonation, depending on its strength and concentration. In lean aqueous solutions the species water and  $\text{OH}^-$  can act as deprotonation bases in addition to the free alkanolamine itself, which is by far the dominating one.

Blauwhoff et al. (1984) showed that much of the data so far reported in the literature could be explained following this mechanism. Johnson and Morrison (1971) concluded that the lifetime of the zwitterion is very small based upon kinetic studies of decarboxylation of a series of substituted N-arylcarbamates. Ohno et al. (1999) verified the overall reactions for both secondary and tertiary amines using a combination of Raman spectroscopy and ab-initio calculations on aqueous alkanolamine solutions loaded with  $\text{CO}_2$ . The zwitterion, although not observed in solution at equilibrium, was examined with regards to stability and the results indicated that the zwitterion should essentially be very unstable, and is most probably a transition species.

The rate expression for this mechanism including reaction reversibility can be derived using the assumption of pseudo steady-state for the zwitterion concentration (Glasscock, 1990).

$$r_{\text{CO}_2} = \frac{k_2[\text{CO}_2][R^{(1)}R^{(2)}NH] - k_{-1}[R^{(1)}R^{(2)}NCOO^-] \frac{\sum k_{-bi}[BH^+]}{\sum k_{bi}[B]}}{1 + \frac{k_{-1}}{\sum k_{bi}[B]}} \quad (3.17)$$

where  $k_2$  and  $k_{-1}$  are the forward and reverse rate constants of reaction (3.15).  $k_{bi}$  and  $k_{-bi}$  are the forward and reverse rate constants of reaction (3.16).

This equation can be simplified by introducing the equilibrium concentration of  $\text{CO}_2$ ,  $[\text{CO}_2]_e$ .

$$r_{\text{CO}_2} = \frac{k_2[R^{(1)}R^{(2)}NH]([\text{CO}_2] - [\text{CO}_2]_e)}{1 + \frac{k_{-1}}{\sum k_{bi}[B]}} \quad (3.18)$$

The rate expression can be further simplified by looking at two asymptotic situations as described by Versteeg et al. (1996).

1. The second term in the denominator is  $\ll 1$ , the zwitterion formation reaction is rate limiting and the rate expression reduces to that of a simple second-order reaction.

$$r_{\text{CO}_2} = k_2[R^{(1)}R^{(2)}NH]([\text{CO}_2] - [\text{CO}_2]_e) \quad (3.19)$$

This has been found to be the case for MEA in aqueous solutions.

2. When the second term in the denominator is  $\gg 1$ , indicating that the zwitterion deprotonation is rate-limiting, a rate expression results that shows the possibility for an overall reaction order of three.

$$r_{\text{CO}_2} = \frac{k_2 \sum k_{bi}[B]}{k_{-1}} [R^{(1)}R^{(2)}NH]([\text{CO}_2] - [\text{CO}_2]_e) \quad (3.20)$$

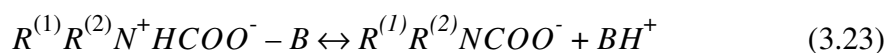
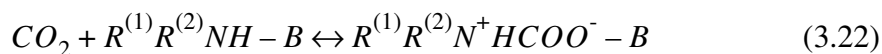
With the alkanolamine as the only deprotonation base, the equation reduces to:

$$r_{\text{CO}_2} = \frac{k_2 k_{R^{(1)}R^{(2)}NH}}{k_{-1}} [R^{(1)}R^{(2)}NH]^2 ([\text{CO}_2] - [\text{CO}_2]_e) \quad (3.21)$$

Between the two asymptotic cases, a transition region exists, where the overall order is changing from two to three, and the shifting reaction orders found in several systems can thus be explained.

However, as pointed out by Astarita et al. (1983) and Bishnoi (2000), it is still not completely understood how a proton transfer such as the zwitterion deprotonation can be rate limiting. As long as no other mechanism is able to reconcile the data, the zwitterion mechanism is still used universally to explain the observed kinetic relations. Crooks and Donnellan (1989) presented a single step termolecular reaction mechanism, which will result in a rate expression similar to eq. (3.20). This mechanism is generally questioned by other authors (e.g. Versteeg et al., 1996). However, the idea that a base is involved in the zwitterion formation and not just in the deprotonation step may offer a way of resolving the observed behavior without forcing the deprotonation to be rate-limiting. This is in fact in line with the original mechanism proposed by Caplow (1968), where the amine group is partially hydrated *before* zwitterion formation (Bishnoi, 2000).

Silva (2003), using ab initio calculations, concludes that the presence of a second amine molecule or a water molecule may be necessary for the zwitterion to form. The charge displacement in the zwitterion is partially stabilized by the approaching base, thus reducing the energy barrier for zwitterion formation. The Crooks and Donnellan mechanism is however found to be unlikely in the sense that the transition state energy for the *simultaneous* bond-braking and formation is too high. The suggested reaction mechanism may be written as:



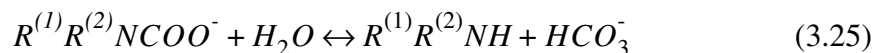
*-B* here indicates hydrogen bonding to the base. The third order reaction (3.22) will in this mechanism always be rate limiting. The study of reaction energy barriers following this route shows that in the MEA-case water is the most favorable base, while in the DEA-case another DEA-molecule is required for

zwitterion stabilization. If only the alkanolamine and the solvent are considered as bases, the following rate expression results:

$$r_{CO_2} = (k_3^{am}[R^{(1)}R^{(2)}NH] + k_3^{sol}[Hsol])[R^{(1)}R^{(2)}NH][CO_2] \quad (3.24)$$

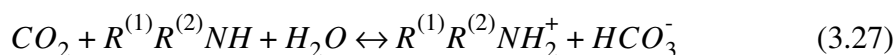
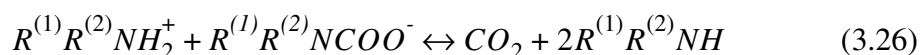
where “Hsol” denotes a general amphiprotic solvent like water, alcohols or glycols, which all have the ability to act as both acids and bases in solution. The observed fractional orders in the amine may thus be explained by the extent of which the amphiprotic solvent (which is always in excess) may act as a base in reaction (3.22). This is reflected by the solvent autoprotolysis constant, as discussed by e.g. Eimer (1994).

From eq. (3.14) it can be seen that the maximum CO<sub>2</sub>-loading is 0.5 if the only form of chemically bound CO<sub>2</sub> is the carbamate ion. However the reaction of carbamate reversion permits higher loadings to be achieved:



The bound CO<sub>2</sub> is here transferred to the bicarbonate form releasing one molecule of free amine which can react with additional CO<sub>2</sub>. For amines like MEA with reaction (3.14) highly displaced to the right, carbamate formation at  $y < 0.5$  and carbamate reversion at  $y > 0.5$  are the only important reactions, with a smooth transition between the two regimes. Although the overall reaction is a carbamate hydrolysis, the mechanism and rate of this reaction has not been studied extensively in the literature except in some early work (e.g. Emmert and Pigford, 1962).

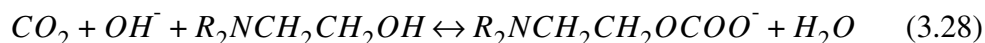
The direct reaction between carbamate and water does however not seem possible (Silva, 2003) and it is suggested that the carbamate reversion is simply a result of the competing mechanisms of carbamate formation and the bicarbonate formation. It is easily seen that the sum of the reverse carbamate formation (3.26) and the bicarbonate formation (3.27) gives the carbamate reversion (3.25) overall.



The reaction of carbamate reversion may be important for the absorption rate prediction at loadings close to and higher than 0.5, although this is outside the range of operation for an MEA-absorption process. An equilibrium calculation would in this range suggest the presence of free amine that can react through reaction (3.14) but the rate is actually limited by the base catalyzed CO<sub>2</sub> hydration.

### 3.3.3 Alkylcarbonate formation

In spite of the general conception that tertiary amines do not react with CO<sub>2</sub> directly, Jørgensen and Faurholt (1954) concluded that a monoalkylcarbonate was formed from studying the reaction with TEA at high pH-values of around 13. The expected reaction mechanism involves a deprotonation of the hydroxyl group of the alcohol substituent and subsequent addition of CO<sub>2</sub>, leading to the following overall reaction:



The reaction is found to be strongly pH-dependent and will also occur in solutions of primary and secondary amines at high pH. The alkylcarbonate formation reaction has not been studied extensively in the literature and most authors consider its contribution to be negligible. The only temperatures studied are 0 and 18°C in the work by Jørgensen and Faurholt (1954) and Jørgensen (1956) and only the alkanolamines DEA and TEA.

The third order rate constant for the reaction with TEA was extrapolated by Donaldson and Nguyen (1980) from the data presented by Jørgensen and Faurholt (1954) and Jørgensen (1956), leading to a value of  $k_3 = 1.53 \times 10^{-2}$  (m<sup>6</sup>/mol<sup>2</sup>s) at 25°C. Emmert and Pigford (1962) estimated the rate constant in MEA-solution as  $k_3 = 3.00 \times 10^{-2}$  (m<sup>6</sup>/mol<sup>2</sup>s) at 25°C based upon the value

published by Jørgensen (1956) for the analogous reaction with DEA. The contribution from monalkylcarbonate formation together with the direct reaction with hydroxide was found to be only about 1% of the rate of carbon dioxide removal due to the carbamate formation reaction (Thomas, 1966). Blauwhoff et al. (1984) concluded that the alkylcarbonate reaction contributes negligibly to the CO<sub>2</sub> absorption rate for MEA and DEA at pH<12.

Versteeg et al. (1988), studying the kinetics of carbon dioxide absorption in tertiary amines claimed that alkylcarbonate formation could be neglected at pH<11. As the kinetics of absorption is required at temperatures up to 80°C, and as rate-determining experiments are normally done in highly concentrated amine solutions at zero loading of CO<sub>2</sub>, the relative importance of alkylcarbonate formation should receive further attention in future work. This is especially the case for tertiary amines like MDEA, where no studies have been performed.

### 3.4 The rate of reaction in the absorber model

The total rate of disappearance of CO<sub>2</sub> when reacting in an aqueous alkanolamine solution is given by be the sum of the parallel reactions with water (3.1), hydroxide ion (3.5) and the alkanolamine itself (3.8)/(3.14).

$$r_{CO_2} = r_{CO_2, OH^-} + r_{CO_2, H_2O} + r_{CO_2, am} \quad (3.29)$$

The rate of reaction with water to form carbonic acid is normally negligible compared to the hydroxide and alkanolamine reaction. The hydroxide reaction (3.5) may be taken as irreversible when considering the high value of the equilibrium constant, being about  $6 \times 10^4$  m<sup>3</sup>/mol at ambient temperature (Pohorecki and Moniuk, 1988). The following rate expression then results for the total rate of CO<sub>2</sub> consumption due to chemical reaction:

$$r_{CO_2} = k_{2, OH^-} c_{CO_2} c_{OH^-} + k_{2, am} c_{am} (c_{CO_2} - c_{CO_2, e}) \quad (3.30)$$

In the MEA-system the stoichiometry of reaction (3.14) give the corresponding rate of free MEA-consumption:



$$r_{MEA} = 2r_{CO_2, MEA} \quad (3.31)$$

The rate of formation of bound  $CO_2$  in the form of carbamate, bicarbonate or carbonate is equal to the rate of  $CO_2$ -consumption. Following the discussion in 3.2, the carbonate is neglected in the MEA-system.

$$r_{MEACOO^-/HCO_3^-} = -r_{CO_2} \quad (3.32)$$

The corresponding relations for the MDEA-system can be seen from the stoichiometry of eq. (3.8) and (3.3):

$$r_{MDEA} = r_{CO_2, MDEA} \quad (3.33)$$

$$r_{CO_3^{2-}/HCO_3^-} = -r_{CO_2} \quad (3.34)$$

The second order rate constant of the hydroxide reaction is given by Pinsent et al. (1956):

$$k_{2, OH^-} = 4.3 \times 10^{10} \exp\left(\frac{-6668}{T}\right) \quad (3.35)$$

The rate behavior of the reaction between  $CO_2$  and alkanolamines has been a subject of intensive research throughout the years. An overview of reported rate constant relations for different alkanolamine systems is given by Versteeg et al. (1996). For MEA, the discrepancy between values reported from different sources is relatively low, and the overall reaction order of two in aqueous solution is well established. Versteeg et al. (1996) recommend the following rate expression:

$$k_{2, MEA} = 4.4 \times 10^8 \exp\left(\frac{-5400}{T}\right) \quad (3.36)$$

MDEA is a relatively new alkanolamine compared to MEA. The overall order of reaction (see eq. (3.8)) is found to have a value of two. However, the reported second order rate constant from different researchers has a relatively large vari-

ation, with extreme values deviating by a factor of three (Glasscock, 1990). The core of the reported values has a relatively low variation, and Versteeg (2000) recommends the relation reported by Tomcej and Otto (1989):

$$k_{2, MDEA} = 1.62 \times 10^5 \exp\left(\frac{-5134}{T}\right) \quad (3.37)$$

---

*Modeling of equilibria  
in aqueous CO<sub>2</sub>-  
alkanolamine systems*

---

## **4.1 Introduction**

When CO<sub>2</sub> is absorbed into an alkanolamine solution, the chemical reactions reviewed in chapter 3 result in a complex mixture of nonvolatile or moderately volatile molecular species and nonvolatile ionic species. The coupling between physical and chemical equilibria is illustrated in figure 4.1.

The traditional approaches to absorber/stripper design, either the equilibrium stage method or the “height of transfer unit” (HTU) method both depend on a model that relates the partial pressure of CO<sub>2</sub> in the gas to the total amount of CO<sub>2</sub> absorbed in the solvent at equilibrium. This enables a determination of the maximum concentration of CO<sub>2</sub> in the liquid outlet and the maximum concentration of the acid gases which can be left in the regenerated solution in order to meet the product gas specification.

The rate-based or non-equilibrium models have now taken over as the standard approach in general reactor modeling and so also in gas absorber design

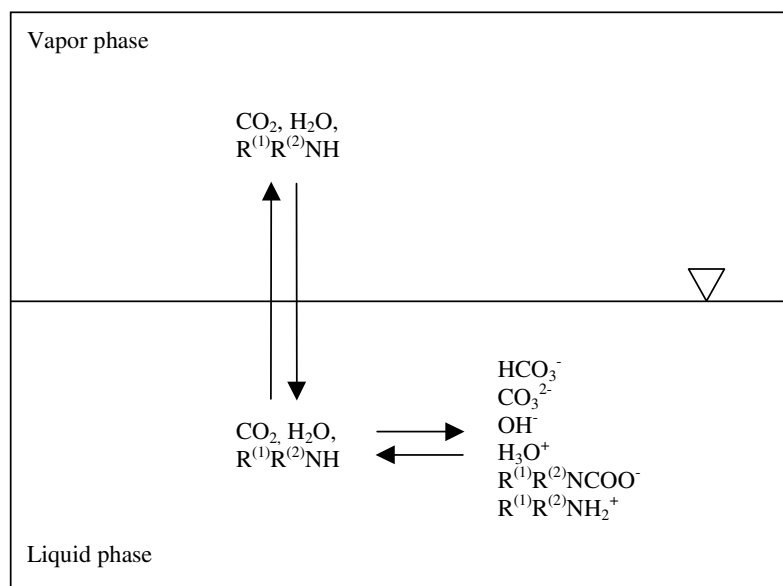


**FIGURE 4.1: Equilibria and species in the system CO<sub>2</sub>/H<sub>2</sub>O/alkanolamine**

(Chakravarty et al., 1985; Kohl and Nielsen, 1997). These models account explicitly for the finite rates of mass and heat transfer and the chemical reactions. This has led to the requirement that the equilibrium model should provide the “speciation” of the liquid phase, meaning the concentration of all molecular and ionic species in liquid, and not just the total CO<sub>2</sub> concentration at a given partial pressure. The equilibrium model comes into play as a physical equilibrium is assumed to exist for molecular components at the gas-liquid interface, and as the bulk liquid solution is assumed to be in a state of chemical equilibrium. Looking at the chemical reaction term, the equilibrium model is needed in order to specify the actual driving force for the reaction, as can be seen from eq. (3.30). The physical and chemical equilibria serve to provide the initial and boundary conditions for the transport equations and are therefore a most important part of a diffusion-reaction model.

The purpose of this chapter is to review the different approaches to equilibrium modeling of CO<sub>2</sub>/alkanolamine/water systems, and to develop an efficient non-iterative equilibrium model suitable for implementation in the membrane gas absorber model, described in chapter 7.

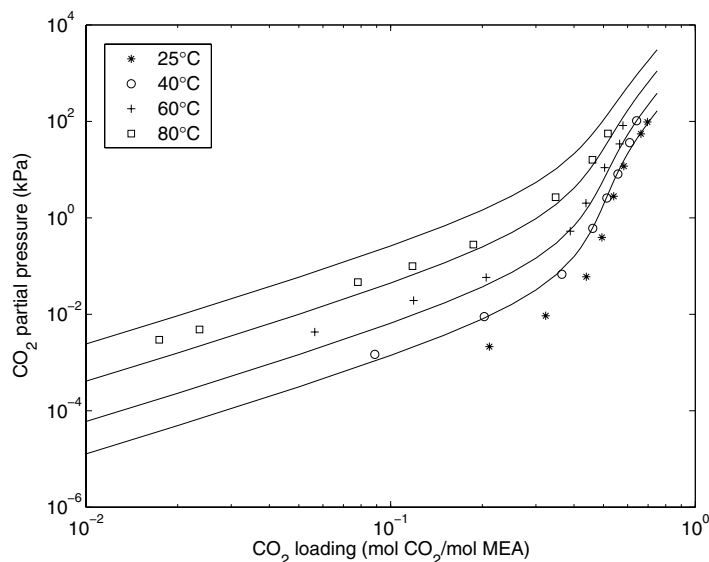


**FIGURE 4.2: Experimental equilibrium data points from Jou et al. (1994) for 30% aqueous MEA and calculated curves from direct use of published equilibrium constants**

## 4.2 Non-ideal behavior

Both acid gases and alkanolamines may be considered weak electrolytes in solution, thus they dissociate only moderately in a binary aqueous system. However, in a mixture the chemical reactions, all forming ionic species as products, may lead to a high degree of dissociation resulting in a high ionic strength of the solution. The high molar concentrations and high ionic strengths lead to an expected non-ideal behavior of the liquid phase resulting from long-range ionic interactions and short range molecular interactions between species in solution.

If published values for ionization (equilibrium) constants and Henry's coefficients are used directly in an equilibrium model of a  $\text{CO}_2$ /alkanolamine/water system, the  $\text{CO}_2$  equilibrium partial pressures calculated will not be in agreement with measured values. This is illustrated in figure 4.2, where literature values of all the equilibrium constants are used to predict the equilibrium for  $\text{CO}_2$  in a 30% MEA solution as if the system was ideal. Even if the number of data

points is limited, the graph indicates that the “ideal” model is approaching the measured values at the lowest loadings, where the ionic strength is low and thereby ionic interactions are at a minimum.

### 4.2.1 Phase equilibria

The general equation of phase equilibria (the vertical equilibria of figure (4.1)) may be written as outlined in the following for the distribution of components between the gas and the liquid phase (Prausnitz et al., 1999). For a liquid solvent the following relation applies, assuming incompressibility of the liquid phase:

$$\phi_i y_i P = \hat{\gamma}_i x_i P_i^s \phi_i^s \exp\left(\frac{v_i(P - P_i^s)}{RT}\right) \quad (4.1)$$

were  $\phi_i$  and  $\hat{\gamma}_i$  are the gas phase fugacity coefficient and the liquid phase activity coefficient of component  $i$ . The fugacity coefficient  $\phi_i^s$  corrects for deviations of the saturated vapor from ideal gas behavior. The exponential term, often called the Poynting correction, takes into account that the liquid is at a pressure  $P$  different from  $P_i^s$ , the solvent vapor pressure.

The conditions encountered in this work allow a number of simplifications to be made. According to Prausnitz et al (1999) the correction  $\phi_i^s$  is very close to unity when the temperature is significantly lower than the solvent critical temperature, say  $T_r < 0.6$ , which for water corresponds to a temperature of 115°C. The Poynting correction is generally small at low pressure, reflecting the fact that activity coefficients are weak functions of pressure (but strong function of temperature and liquid phase composition). For a pressure less than 5 bar higher than the saturation pressure, the Poynting correction may be considered negligible. The gas phase may be treated as ideal when considering a mixture of non-polar or moderately polar gases at pressures lower than 5 bar. Equation (4.1) is then reduced to:

$$y_i P = \hat{\gamma}_i x_i P_i^s \quad (4.2)$$

The pure solvent at system temperature is taken as the solvent reference state, giving:

$$\hat{\gamma}_i \rightarrow 1 \quad \text{as} \quad x_i \rightarrow 1 \quad (4.3)$$

This results in the well-known Raoult's law for the vapor pressure of the solvent at high dilution of the solutes. Introduction of the gas phase partial pressure,  $p_i$ , gives:

$$p_i = x_i P_i^s \quad (4.4)$$

For a molecular solute, the phase equilibrium equation is given as follows when considering the liquid phase as incompressible:

$$\phi_i y_i P = \gamma_i x_i H_i P_{ref} \exp\left(\frac{v_i^\infty (P - P_{ref})}{RT}\right) \quad (4.5)$$

The Henry's law constant,  $H_i$ , is equal to the reference fugacity at infinite dilution of component  $i$ , most often evaluated at a reference pressure of 1 atm. The exponential Poynting factor corrects the Henry's law constant if the pressure is far different from the reference pressure. For the conditions encountered in this work this factor may be taken as unity. Treating the gas phase as ideal, the following expression results:

$$p_i = \gamma_i x_i H_i \quad (4.6)$$

For molecular solutes in aqueous solution, infinite dilution in water is normally taken as the reference state, leading to:

$$\gamma_i \rightarrow 1 \quad \text{as} \quad x_i \rightarrow 0 \quad (4.7)$$

This situation corresponds to the well known Henry's law:

$$p_i = x_i H_i \quad (4.8)$$

The same standard state is adopted for ionic solutes, although any presence in the gas phase can be neglected, corresponding to an infinitely small Henry's law constant.

### 4.2.2 The alkanolamine/water system

The solution vapor pressure may be calculated as the sum of the contributions from the alkanolamine and water.

$$P_{vap} = \hat{\gamma}_{am} x_{am} P_{am}^s + \hat{\gamma}_w x_w P_w^s \quad (4.9)$$

The mole fractions of alkanolamines in the mixed solvent of alkanolamine and water, as applied in the absorption processes, will normally be low. E.g. for a 30wt% MEA aqueous solution, the MEA fraction is 0.11, and for a 48.8% MDEA, the mole fraction is 0.13. For the alkanolamine, when treated as a solvent, the actual mole fraction is far from what corresponds to ideality according to eq. (4.3). This results in an activity coefficient significantly different from unity, as illustrated in figure 4.3 for the MEA/water system at 298 K (Austgen, 1989). It may therefore be considered erroneous to apply Raoult's law in calculating the amine vapor pressure over the mixture. The water mole fraction is however close to the pure water reference value, and as can be seen from figure 4.3, it may be considered a reasonable assumption to state the water activity coefficient is equal to 1 in the alkanolamine/water mixture.

Most alkanolamines in practical use are considerably less volatile than water. Correlations for calculating the pure component vapor pressures are given by Austgen (1989). At 40°C the water vapor pressure is 7 kPa, while the vapor pressure of pure MEA is 0.16 kPa. The pure MDEA vapor pressure is not correlated at temperatures lower than 120°C, where it is 0.9 kPa. The extrapolated value at 40°C is less than 0.01 kPa. The amine is thus most conveniently disregarded in the vapor phase. Eq. (4.9) is then reduced to:



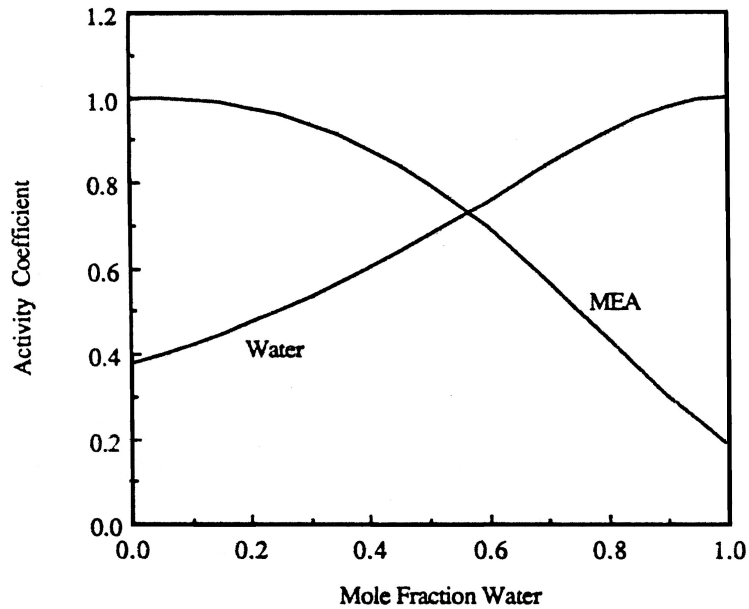


**FIGURE 4.3:** Component activity coefficients in an MEA-water mixture at 298 K, calculated with the NRTL equation, with pure solvent standard state for both components (Austgen, 1989).

$$p_{vap} = x_w P_w^s \quad (4.10)$$

with the pure water vapor pressure,  $P_w^s$ , calculated from the correlation given in appendix 2.

The calculation of solvent vapor pressure by Raoult's law is a common assumption in the analysis of experimental equilibrium data (e.g. Jou et al., 1995). Liu et al. (1999), using a thermodynamically rigorous model for the CO<sub>2</sub>/MEA/water system, showed that the error introduced by doing this is negligible, except at loadings higher than 0.5, which is outside the range considered in this work.

As the mole fractions of the alkanolamines in the aqueous solvent are relatively low, and as the published values of the chemical equilibrium constants are measured at concentrations corresponding to a high degree of dilution, it is often

more convenient to treat the alkanolamine as a solute. The activity coefficients according to a solute reference state and a solvent reference state are related by:

$$\gamma_i = \frac{\hat{\gamma}_i}{\hat{\gamma}_i^\infty} \quad (4.11)$$

where  $\hat{\gamma}_i^\infty$  is the activity coefficient from a pure solvent reference state, extrapolated to infinite dilution. For MEA at 298 K,  $\hat{\gamma}_i^\infty \approx 0.2$ , as can be seen from figure 4.3 when  $x_{water} \rightarrow 1$ . From figure 4.3 and eq. (4.11), it can also be seen that activity coefficient of MEA when treated as a solute will be around 1.5 in a 5 mol/l (30wt%) CO<sub>2</sub>- free aqueous solution, corresponding to a water mole fraction of 0.9.

### 4.3 Literature review of corrections for non-idealities in the liquid phase

Following the discussion above, it is clear that the non-ideal behavior of the liquid solution has to be taken into account when modeling the equilibrium behavior of CO<sub>2</sub>/alkanolamine/water systems. As the gas phase in this work is treated as ideal, the following review of equilibrium models for CO<sub>2</sub>/alkanolamine/water systems considers only the treatment of non-idealities in the liquid phase. The fugacity coefficients correcting the gas phase for eventual non-ideality may be calculated straightforward from a suitable equation of state e.g. Soave-Redlich-Kwong or Peng-Robinson (see Prausnitz et al., 1999).

#### 4.3.1 Models using the apparent equilibrium constant approach

Early speciation models were based on apparent equilibrium constants, thus setting all activity coefficients to unity, which is by convention (infinite dilution reference state for all species except water) only true at infinite dilution. For a chemical reaction such as



the condition for chemical equilibrium is expressed in terms of the activities of the components:

$$K = \frac{a_{B_2}}{a_{B_1} a_A} \quad (4.13)$$

The true thermodynamic equilibrium constant  $K$  will only be a function of temperature, and it will equal the value of the concentration based equilibrium constant,  $K_c^\infty$ , at infinite dilution. This is the value of the published equilibrium constants, as a normal procedure will be to do measurements on varying concentration at high level of dilution and then extrapolate the results to infinite dilution (see e.g. Kamps and Maurer, 1996).

As the activity of each component equals the product of the activity coefficient and the concentration, one may introduce the *apparent* equilibrium constant,  $K_c^{app}$ :

$$K = \frac{[B_2]}{[B_1][A]} \cdot \frac{\gamma_{B_2}}{\gamma_{B_1}\gamma_A} = K_c^{app} \cdot K_\gamma \quad (4.14)$$

$$K_c^{app} = \frac{K}{K_\gamma} \quad (4.15)$$

The apparent equilibrium constants will be a function of composition through the variation of  $K_\gamma$  in addition to the expected temperature dependence of  $K$ . For electrolyte systems the ionic strength may be chosen as a yardstick to correlate this composition dependence as it is related to the degree of ionic interactions in solution. The ionic strength is defined as follows, by summing over all ionic species in solution:

$$I = \frac{1}{2} \sum_i c_i z_i^2 \quad (4.16)$$

where  $z_i$  is the valency of the ion.

Van Krevelen et al. (1949) were the first to use an approach like this on an acid gas system. They regressed the equilibrium and Henry's constants to functions of ionic strength and temperature for the aqueous solution of CO<sub>2</sub>, H<sub>2</sub>S and NH<sub>3</sub>. The same method was used by Danckwerts and McNeil (1967) to calculate vapor and liquid composition in amine-CO<sub>2</sub>-H<sub>2</sub>O systems.

Kent and Eisenberg (1976) modified the Danckwerts/McNeil approach by tuning two of the equilibrium constants in order to make a fit to published vapor pressure data for CO<sub>2</sub>/H<sub>2</sub>S/amine/water systems for the amines MEA and DEA. No ionic strength dependence was considered and the value of the amine protonation constant and the carbamate reversion constant was instead treated as adjustable parameters fitted to functions only of temperature. All other equilibrium constants were used at their infinite dilution value as reported in the literature.

The Kent & Eisenberg model has been adopted by several other authors due to its simplicity and reasonably good ability to correlate experimental data. Jou et al. (1982) adjusted the value of the amine protonation constant and included a dependence of acid gas loading and amine molarity to fit their experimental data for the system CO<sub>2</sub>/H<sub>2</sub>S/MDEA/H<sub>2</sub>O. Hu and Chakma (1990) used a similar procedure to correlate their VLE data for CO<sub>2</sub>/AMP/H<sub>2</sub>O. Li and Shen (1993) successfully correlated their data for the mixed system of MEA and MDEA by the same method.

Kritpiphat and Tontiwachwuthikul (1996) developed a modified Kent-Eisenberg model for CO<sub>2</sub> in aqueous solutions of AMP. They performed a sensitivity analysis and identified the apparent constants of amine protonation, dissociation and physical dissolution of CO<sub>2</sub> to be the significant parameters in the system. These were fitted to functions of temperature and amine strength. According to the authors the resulting model was capable of accurately predicting concentrations of the important chemical species in addition to CO<sub>2</sub> partial pressures and loadings.

The model proposed by Atwood et al. (1957) made use of a “mean ionic activity coefficient” which was assumed equal for all ionic species. This single activity coefficient was correlated to ionic strength. The model was used for the calculation of equilibria in the H<sub>2</sub>S/amine/H<sub>2</sub>O system. Klyamer and Kolesnikova (1972) developed the Atwood model for the CO<sub>2</sub>/amine/H<sub>2</sub>O system and a generalized model for the CO<sub>2</sub>/H<sub>2</sub>S/amine/H<sub>2</sub>O system was given by Klyamer et al. (1973).

According to Austgen et al. (1989), this generalized model is essentially equivalent to the apparent equilibrium constant model of Van Krevelen et al. (1949), where effects of solution non-ideality is lumped directly into the equilibrium constant. In this case, however, the non-ideality effects are separated into an empirical parameter which is used to adjust the model predictions to experimental data. The assumption of equal ionic activity coefficients is reasonable if only one cation and one anion are present in significant amounts. This is normally the case for single acid gas/single alkanolamine systems.

### 4.3.2 Rigorous thermodynamic models for the liquid phase

Based upon further development of the theory of strong electrolyte solutions, a new generation of rigorous equilibrium models have been developed during the recent years. The work has been facilitated by increased attention given to mixed alkanolamine solutions and a continuous growth in the accessibility of experimental data for the systems under consideration. The rapid growth of computational power also makes implementation of more rigorous models into absorber simulators possible. In these models a major effort is put in the excess Gibbs energy model, which is directly related to the species activity coefficient by:

$$RT \ln \gamma_i = \left( \frac{\partial G^E}{\partial n_i} \right)_{T, P, n_j} \quad (4.17)$$

where the term on the right hand side is the partial molar Gibbs free energy of component  $i$ . Equation (4.17) forms the basis for a thermodynamically consistent treatment of species activity coefficients, in line with the Gibbs-Duhem equation. The model expression for Gibbs free energy usually contain a number of empirical parameters related to interaction between constituent species in the solution (Austgen, 1989). These interaction parameters may be estimated from fitting the model to binary alkanolamine-water VLE data and ternary data including CO<sub>2</sub>. A mixed alkanolamine solvent can thus in principle be modelled based upon data for the constituent sub-systems. This reduces the experimental effort required and ideally allows the model to be extrapolated beyond the range of existing experimental data.

The historically most important  $G^E$ -models developed for electrolyte systems can basically be divided in two groups. These are those based upon direct extensions of the Debye-Hückel limiting law for weak electrolytes and those arising from a combination of a long range term derived from Debye-Hückel theory with a short range term arising from local composition models originally developed for molecular systems (i.e the Wilson, UNIQUAC and NRTL models). In the following, a short review is given to gain an insight into the development and present status of these more elaborate, however still semi-empirical, models applied to the CO<sub>2</sub>/alkanolamine/water systems.

The first attempt to treat the absorption equilibria in a thermodynamically rigorous manner was made by Edwards et al. (1975). They developed a molecular thermodynamic framework to calculate vapor and liquid equilibrium composition for a dilute aqueous system containing weak electrolytes, such as CO<sub>2</sub> and NH<sub>3</sub>. The activity coefficients were calculated using an extended Guggenheim equation (Guggenheim, 1935). The model was related to binary interaction parameters for the long range ion-ion interactions and short range ion-ion, ion-molecule and molecule-molecule interactions. These parameters were estimated or fitted to experimental data. The validity was limited to weak electrolyte concentrations of less than 2 molal, but was later extended by making use of the Pitzer model (Edwards, 1978).

The model by Desmukh and Mather (1981) is based upon the Guggenheim equation for all activity coefficients except water. The temperature dependence of the alkanolamine protonation and the carbamate reversion was adjusted to experimental data, and the model was then able to represent VLE-data for MEA-CO<sub>2</sub>-H<sub>2</sub>O to ionic strengths approaching 5 mol/l. Weiland et al. (1993) provided values for the interaction parameters of the model for most of the commercially important amine systems and implemented this in the commercial code ProTreat (Optimized Gas Treating, Inc.).

The ion-interaction model by Pitzer (1973) is one of the most widely used activity coefficient models for electrolyte solutions. It is in principle an elaborate extension of the Debye-Hückel equation resulting from addition of a virial expansion in composition. The Pitzer model has recently been applied for the solubility and speciation modeling of aqueous systems of CO<sub>2</sub> and alkanolamines (Li and Mather, 1994; Silkenbäumer et al., 1998; Kamps et al., 2001).

Austgen et al. (1989) proposed a thermodynamically rigorous model based on the electrolyte-NRTL model of Chen and Evans (1986). The activity coefficients of the liquid phase were represented treating both long range ion-ion interactions and short range interactions between all true species in the liquid phase. For the CO<sub>2</sub>/MEA/H<sub>2</sub>O system Austgen fitted 11 parameters for the temperature dependent interaction parameters. Some parameters, believed to have less importance were set to default values. Furthermore the equilibrium constant for carbamate reversion was treated as an adjustable parameter. This work has received considerable attention in the literature, and forms the basis for the Ratefrac gas absorption model of Aspen Tech.

Kaewschian et al. (2001) used a similar approach based upon the electrolyte-UNIQUAC model (Sander et al., 1986) to predict the solubility of CO<sub>2</sub> and H<sub>2</sub>S in aqueous solution of MEA and MDEA. They adopted the concept of interaction between ion-pairs instead of between individual ions. This resulted in a simplification of the activity coefficient expressions compared to electrolyte-NRTL model, and required fewer interaction parameters.

Recently a few models following a different approach than those considered above have been applied. These models basically arise from the rapid development in the application of statistical mechanics.

The ElecGC-model by Lee (1996) combines the mean spherical approach (MSA) from ionic solution theory of statistical mechanics with the UNIFAC group contribution (GC) method of Wu and Sandler (1991) for polar solvents. The MSA model is considered capable of describing ionic solutions up to a molality of 19 molal (Wu and Lee, 1992), which is considerably higher than most expressions arising from simple Debye-Hückel theory. By introducing the group contribution approach, the alkanolamine molecules may be considered as composed of a subset of identifiable groups that are common in wide classes of amines. From considering the interaction between the groups instead of the molecules a general expression with fewer parameters arises. The consequence is a model easily applied to other amines and amine blends composed of similar groups, even if no experimental data are available. The ElecGC-model was successfully applied in modeling the VLE involving the amines MDEA, DEA and MEA including their blends covering wide range of conditions (Lee, 1996).

Poplsteinova et al. (2002) adopted the approach of Lee (1996). In their work the group contribution method UNIFAC was combined with a simpler electrolyte activity coefficient model based on the Debye-Hückel theory following the approach by Deshmukh and Mather (1981). A relatively simple model was obtained and proved to give satisfactory representation of the VLE for CO<sub>2</sub> in 50% MDEA in the temperature range 25 to 140 °C and the loading range from 0.001 to 1 mol CO<sub>2</sub>/mol MDEA.

A few authors have modelled the VLE of CO<sub>2</sub>/alkanolamine/water using an equation of state (EOS) for the liquid phase. Kuranov et al. (1997) modelled the VLE for CO<sub>2</sub> and H<sub>2</sub>S in aqueous solutions of MDEA using an equation of state based on a lattice theory. They recommended a further work following the EOS approach and including an MSA model to account for the long-range electrostatic interactions. Fürst and Renon (1959) used a simplified form of the MSA-model in their equation of state model. This approach, using an electrolyte



equation of state, was applied in the modeling of VLE for CO<sub>2</sub> and H<sub>2</sub>S in aqueous solutions of DEA by Vallée et al. (1999) and in aqueous solutions of MDEA by Chunxi and Fürst (2000). Button and Gubbins (1999) used the Statistical Associating Fluid Theory (SAFT) equation of state to model the VLE of carbon dioxide in aqueous MEA and DEA. The SAFT equation of state consist of terms for repulsion, dispersion, chain formation and association. It does not require any knowledge of the chemical reactions in the liquid phase, as these are incorporated in the association term by allocation of association sites to the molecules.

### **4.3.3 Discussion and implications for this work**

The prediction of acid gas partial pressures over a solution loaded with CO<sub>2</sub> is reasonably good from the simple models using apparent equilibrium constants. The liquid phase speciation is more uncertain but can be expected to give a good approximation to the true liquid phase composition. The most important drawback of these models is that they must be used with great caution outside the range of temperatures and concentrations of which they have been tested and fitted to experimental data. To be able to broaden the range where such models could be applied, in principle all equilibrium constants should be expressed as functions of ionic strength and temperature. For systems of mixed acid gases and mixed alkanolamine systems, the high number of ionic reaction products leads to the need for a more rigorous treatment of the interaction forces and ionic activity coefficients cannot in general be taken to be equal.

The thermodynamically rigorous models use real equilibria involving activities, not concentration and should in principle provide the true liquid speciation. The more general approach should also enable the possibility of extrapolating the model beyond the range of experimental data. However, it has been pointed out that the more rigorous models does not give predictions that fit experimental data better than the simpler ones (Hu and Chakma, 1990). The large spread in experimental VLE data from different sources complicates the problem further, as these data are the basis for regression of the interaction parameters. Thus, the

choice of experimental data for parameter regression may be considered more important than the model itself.

The majority of experimental data from various workers in terms of the equilibrium CO<sub>2</sub> partial pressure typically differ from each other by about 50% (Weiland et al., 1993), although 16% of the data investigated considering the amines MEA, DEA, DGA and MDEA differ by an order of 300-400% or more. There are basically two ways of dealing with this large discrepancy. One way is to perform a detailed statistical analysis based upon all available data for a given system, as done by e.g. Austgen et al. (1989) and Weiland et al (1993). It may be stated about this approach that the resulting averaged equilibrium curves are definitively in error, as there is no guarantee that the unique, true equilibrium may result from an average of data spanning a difference several orders of magnitude. Another approach is to select a single data source to trust, preferably as new as possible, covering the range of interest. Data from a single source may at least be considered to be consistent and to give correct predictions of temperature and amine strength dependence.

The activity coefficient models result in a high number of nonlinear equations leading to a requirement of substantial computing times for the equilibrium model. Failure to provide good initial guesses may cause convergence problems and numerical instabilities. One way of reducing these problems is to generate tables of the speciation and activity coefficients covering the range of interest and use an efficient interpolation routine. For the purpose of including the equilibrium model in an absorber simulation program, the computational simplicity may still be a major reason to choose an approach of the Kent-Eisenberg type.

It appears that there is a tendency that the researchers working on acid gas absorption with alkanolamines may be divided in two main groups. Those working on kinetics measurements basically seem to ignore the concept of non-ideality as opposed to those working solely on modeling and measurements of equilibria. The rate constants of CO<sub>2</sub>-alkanolamine reaction published in the literature are generally apparent rate constants, measured at high concentration of the alkanolamine (Versteeg et al., 1996). Tomcej and Otto (1987) measured the

reaction rate constant for CO<sub>2</sub> absorption in MDEA solution of 20 and 40 wt% and used them in the development of an absorber simulator package, making use of plate efficiencies. Rinker et al. (1995) developed a diffusion-reaction model based on Higbie's penetration theory. The liquid speciation was solved from including all significant reaction equilibria and balance equations, using equilibrium constants as published in literature without any correction for non-ideality. This model was used in the estimation of the reaction rate constant for CO<sub>2</sub>-MDEA from experimental absorption data with 10-30 wt% MDEA. The resulting rate constant showed a linear dependence in amine concentration.

From studying the literature it appears that, except in the works by Glasscock (1990) and Bishnoi (2000), no attempts have been made to include activity coefficients when treating the CO<sub>2</sub>-amine reaction kinetics. Neither has anyone attempted to include an ionic strength dependence in the CO<sub>2</sub>-amine reaction rate constant, which would be the next best thing. Glasscock (1990) provides an enlightening discussion on the consistency between chemical kinetics and reaction equilibria.

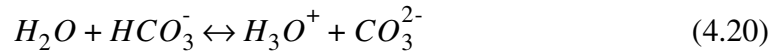
The conclusion from the preceding discussion is that a rigorous thermodynamic model will temporarily not be included. It is considered outside the scope of this work, which is to develop a simulation program able to reproduce the experiments done in the membrane absorber while keeping down the time required for computation. However, the advantages of activity-based models makes it desirable to include such a model in the future. This will be done following the work of Poplsteinova et al. (2002). In the following paragraphs, the non-iterative, concentration-based equilibrium model used in this work is outlined.

## 4.4 Equilibrium model for the membrane absorption simulator

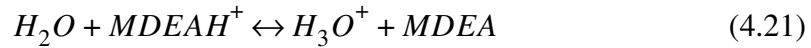
### 4.4.1 Chemical equilibria

The chemical equilibria describing the species distribution when CO<sub>2</sub> is absorbed in an aqueous solution of a single alkanolamine (MEA or MDEA) are given as follows. The notation is here simplified by introducing MEA and MDEA instead of  $R^{(2)}NH_2$  and  $R^{(1)}R^{(2)}N$ .

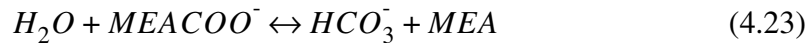
For water and carbon dioxide:



For MDEA, the deprotonation reaction:



For MEA the carbamate needs to be considered. This is done through the carbamate reversion reaction, similar to Austgen (1989). The carbamate formation reaction discussed in 3.3.2 may be obtained by combination of reactions (4.19), (4.22) and (4.23).



The set of reactions given above involve 7 species for the MDEA system and 8 species for the MEA system.

The corresponding apparent (concentration-based) equilibrium constants are given by:

$$K_1 = \frac{[H_3O^+][OH^-]}{[H_2O]^2} \quad (4.24)$$

$$K_2 = \frac{[H_3O^+][HCO_3^-]}{[H_2O]^2[CO_2]} \quad (4.25)$$

$$K_3 = \frac{[H_3O^+][CO_3^{2-}]}{[H_2O][HCO_3^-]} \quad (4.26)$$

$$K_4 = \frac{[H_3O^+][MDEA]}{[H_2O][MDEAH^+]} \quad (4.27)$$

$$K_5 = \frac{[H_3O^+][MEA]}{[H_2O][MEA H^+]} \quad (4.28)$$

$$K_6 = \frac{[HCO_3^-][MEA]}{[H_2O][MEACOO^-]} \quad (4.29)$$

The following additional relations between species concentrations may be written.

Overall alkanolamine balance:

MDEA:

$$[MDEA]_{tot} = [MDEA] + [MDEAH^+] \quad (4.30)$$

MEA:

$$[MEA]_{tot} = [MEA] + [MEA H^+] + [MEACOO^-] \quad (4.31)$$

Overall carbon (from CO<sub>2</sub>) balance:

MDEA:

$$[CO_2]_{tot} = [HCO_3^-] + [CO_3^{2-}] + [CO_2]_{molecular} \quad (4.32)$$

MEA:

$$[CO_2]_{tot} = [MEACOO^-] + [HCO_3^-] + [CO_3^{2-}] + [CO_2]_{molecular} \quad (4.33)$$

Electroneutrality:

MDEA:

$$[MDEAH^+] + [H_3O^+] = [HCO_3^-] + 2[CO_3^{2-}] \quad (4.34)$$

MEA:

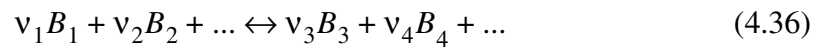
$$[MEAH^+] + [H_3O^+] = [MEACOO^-] + [HCO_3^-] + 2[CO_3^{2-}] \quad (4.35)$$

The relations given above form a closed system of equations for the species concentrations from the chemical equilibria in the liquid phase.

#### 4.4.2 The Astarita representation of chemical equilibria

The system of equations (4.24) to (4.35) may be solved by an appropriate numerical method like the Newton method or the Broyden method for sets of non-linear equations. However, this is a cumbersome problem involving very different orders of magnitude of the unknowns, leading to problems of convergence and numerical instability. In order to get convergence, initial guesses often has to be provided that are very close to the actual solution. For the membrane absorber model, as the equilibrium speciation has to be determined for every point in the computational grid of the liquid phase (chapter 7), an iterative procedure may lead to unacceptably high computation times.

Astarita et al. (1983) provide a discussion of the problem of solving the equilibrium speciation for acid gas/alkanolamine system describing how the model can be reformulated in order to produce the simplest possible mathematical problem. An important feature of the “Astarita representation” is the introduction of the *extent of reaction* in the model equations. The concept of extent of reaction may be illustrated by considering a general chemical reaction with stoichiometric coefficients  $\nu_j$  and species  $B_j$ .



If, by convention, stoichiometric coefficients are taken positive for reactants and negative for products eq. (4.36) can be written in the following form:

$$\sum \nu_j B_j = 0 \quad (4.37)$$

The condition for chemical equilibrium can be written as:

$$K = \prod_j [B]_j^{-\nu_j} \quad (j = 1, 2, \dots, M) \quad (4.38)$$

Following Astarita et al. (1983), from eq. (4.37) it can be seen that as long as the composition only changes as a result of the chemical reaction, the variation of the concentration of the individual components  $[B_j]$  are not independent of each other but are related by the following stoichiometric condition defining the reaction variable  $\xi$ , called the molar extent of reaction.

$$\xi = \frac{[B]_j - [B]_{j,0}}{\nu_j} \quad (4.39)$$

or

$$[B]_j = [B]_{j,0} - \nu_j \xi \quad (4.40)$$

An important characteristic of the variable  $\xi$  is that it has the same value for each molecular species involved in the reaction, and the complete progress of

the chemical reaction is thus given by the value of this single variable. Astarita et al. uses the term “admissible composition” to the initial molar concentrations indicating that any set of values  $[B]_{j,0}$  satisfying the restrictions given by the reaction stoichiometry may be used as starting point. Substitution of eq. (4.40) in (4.38) yields:

$$K = \prod_j ([B]_{j,0} - \nu_j \xi)^{-\nu_j} \quad (4.41)$$

which is a polynomial equation in  $\xi$ , subject to restrictions preventing any of the  $[B]_j$  from being negative. This defines the only real solution to eq. (4.41) that may be substituted into eq (4.40) in order to give the equilibrium composition of the system. Generalizing to a system where  $N$  independent chemical reactions are involved in the distribution of the  $M$  species yields:

$$[B]_j = [B]_{j,0} - \sum_k \nu_{jk} \xi_k \quad (4.42)$$

and

$$K_k = \prod_j ([B]_{j,0} - \sum_k \nu_{jk} \xi_k)^{-\nu_{jk}} \quad (k = 1, 2, \dots, N) \quad (4.43)$$

This gives a set of  $N$  polynomial equations for the  $N$  unknowns  $\xi_k$  to be solved for the unique set of values that when substituted in eq. (4.42) result in all negative values of  $[B]_j$ .

For a system like the acid gas/alkanolamine/water, what complicates the matter is that the liquid phase composition also may change due to acid gas absorption or desorption. Eq. (4.42) is thus not valid for all the components in the system. This may be coped with by formulating only one equilibrium relation involving the absorbing species and other relations describing the distribution between non-volatile species in solution (Astarita et al., 1983). The equilibrium problem is thus separated in two parts, as the distribution of non-volatile species may



then be calculated independent of the concentration of absorbing species, which is subsequently determined. For a system involving a single acid gas and a single alkanolamine, the solution is straightforward and the procedure is outlined here for the CO<sub>2</sub>/MEA/H<sub>2</sub>O-case.

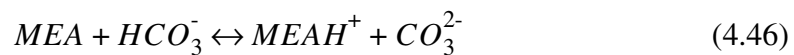
If the reactions (4.19), (4.22) and (4.23) are combined, this results in the reaction describing the combination of free CO<sub>2</sub> and MEA to form the carbamate.



with the equilibrium constant:

$$K_{\text{abs}} = \frac{K_2}{K_5 K_6} \quad (4.45)$$

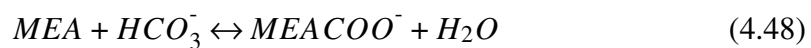
Two more equilibria are needed to describe how chemically combined CO<sub>2</sub> distribute between the three different forms of carbamate, bicarbonate and carbonate ion. By combining reaction (4.20) and (4.22) we get for the bicarbonate/carbonate equilibrium:



with the equilibrium constant:

$$K_{c1} = \frac{K_3}{K_5} \quad (4.47)$$

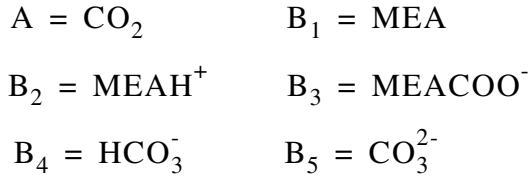
The reverse of reaction (4.23) gives the bicarbonate/carbamate equilibrium:



with the equilibrium constant:

$$K_{c2} = \frac{1}{K_6} \quad (4.49)$$

For convenience, the chemical species are now renamed as follows:



Eq. (4.31) and (4.33) can then be reformulated as:

$$m = [B_1] + [B_2] + [B_3] \quad (4.50)$$

$$\bar{y}m = ym - [A] = [B_3] + [B_4] + [B_5] \quad (4.51)$$

where  $m$  is the amine molarity,  $y$  is the total loading (mol CO<sub>2</sub>/mol amine) and  $\bar{y}$  is the loading in terms of the chemically bound CO<sub>2</sub>.

For the admissible composition,  $[B_j]^0$ , it is assumed that all chemically combined CO<sub>2</sub> is captured in the form of bicarbonate. This corresponds to reaction (4.46) and (4.48) totally shifted to the left. The admissible composition is determined by the equilibrium resulting from combining reaction (4.44) and the opposite of reaction (4.48), leading to the bicarbonate formation reaction as described in chapter 3.

$$[B_1]^0 = m(1 - \bar{y}) \quad (4.52)$$

$$[B_2]^0 = m\bar{y} \quad (4.53)$$

$$[B_3]^0 = 0 \quad (4.54)$$

$$[B_4]^0 = m\bar{y} \quad (4.55)$$

$$[B_5]^0 = 0 \quad (4.56)$$

We then allow reaction (4.46) and (4.48) to proceed to the right until equilibrium is reached, as described by the extents of reaction  $\xi_1$  and  $\xi_2$ . From eq. (4.42) we have:

$$[B_1] = m(1 - \bar{y}) - \xi_1 - \xi_2 \quad (4.57)$$

$$[B_2] = m\bar{y} + \xi_2 \quad (4.58)$$

$$[B_3] = \xi_2 \quad (4.59)$$

$$[B_4] = m\bar{y} - \xi_1 - \xi_2 \quad (4.60)$$

$$[B_5] = \xi_1 \quad (4.61)$$

Substitution into the equilibrium relations of reaction (4.46) and (4.48) give:

$$K_{c1} = \frac{(m\bar{y} + \xi_1)\xi_1}{[m(1 - \bar{y}) - \xi_1 - \xi_2](m\bar{y} - \xi_1 - \xi_2)} \quad (4.62)$$

$$K_{c2} = \frac{\xi_2}{[m(1 - \bar{y}) - \xi_1 - \xi_2](m\bar{y} - \xi_1 - \xi_2)} \quad (4.63)$$

The solution in terms of  $\xi_1$  and  $\xi_2$  are given as the roots of a fourth order polynomial, as shown in appendix 1. The true physical solution may be identified as the root satisfying the following constraints:

$$\xi_1 \geq 0 \quad (4.64)$$

$$\xi_2 \geq 0 \quad (4.65)$$

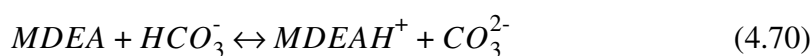
$$\xi_1 + \xi_2 \leq m\bar{y} \quad (4.66)$$

$$\xi_1 + \xi_2 \leq m(1 - \bar{y}) \quad (4.67)$$

The values of  $\xi_1$  and  $\xi_2$  are inserted in eq. (4.57)-(4.61) to calculate the concentration of the non-volatile components  $[B_i]$ . The final step is then to calculate the free CO<sub>2</sub>-concentration ( $[A]$ ) from the equilibrium condition of reaction (4.44):

$$[A] = \frac{[B_2][B_3]}{[B_1]^2 K_{abs}} \quad (4.68)$$

The solution for the MDEA-case is analogous and is given from considering only the bicarbonate formation and the bicarbonate/carbonate shift:



This corresponds to setting  $\xi_2 = 0$  in the equations above (as no carbamate can be formed) and results in a single second order polynomial equation in  $\xi_1$  (appendix 1). Correlations and literature reference for the equilibrium constants are given in appendix 2.

#### 4.4.3 The CO<sub>2</sub> equilibrium partial pressure

The distribution of species between the vapor and liquid phase is governed by phase equilibria, as described in 4.2.1 and 4.2.2. We choose in this work only to consider CO<sub>2</sub> and water in the gas phase, in the ideal case described by Henry's law (4.8) and Raoult's law (4.4). The Henry's law constant,  $H_{CO_2}$ , has to be determined from experimental solubility data. Contrary to what is the case for most mixed solvents, the physical solubility of CO<sub>2</sub> in alkanolamine/water systems has been studied significantly in the literature.

The difficulty of obtaining physical solubility measurements for a gas in a reacting solution may be circumvented by using a non-reacting gas with similar properties in terms of molecular size and electronic structure. The solubilities of reacting and non-reacting gas may thus be related at zero concentration of the reactants. N<sub>2</sub>O has been found suitable as measuring gas to mimic CO<sub>2</sub> in reacting solutions. The *N<sub>2</sub>O analogy* has been used successfully by a number of researchers (see Al-Ghawas et al., 1989) and is expressed in the following form.

$$\frac{H_{CO_2}^S}{H_{N_2O}^S} = \frac{H_{CO_2}^W}{H_{N_2O}^W} \quad (4.71)$$

where  $H_i^S$  and  $H_i^W$  are the Henry's law constants of the alkanolamine/water mixture and pure water, respectively. Haimour and Sandall (1984) confirmed the  $N_2O$  analogy by performing  $CO_2$  absorption experiments in aqueous MDEA with an apparatus offering extremely short exposure times, so that the effect of the chemical reaction was negligible.

The equilibrium partial pressure of  $CO_2$  over the amine/water mixture is given by:

$$p_{CO_2} = H_{CO_2}^S [CO_2] \quad (4.72)$$

where the Henry's law constant is correlated by the relations given in appendix 2. The "ideal" VLE-model is then completed by multiplying the free  $CO_2$ -concentration ( $[CO_2] = [A]$ ) from eq. (4.68) with the Henry's law constant, to calculate the partial pressure of  $CO_2$  in the gas phase at a given  $CO_2$  loading in the liquid phase. This is the model resulting in figure 4.2.

## 4.5 The correction for non-ideality

### 4.5.1 The salting out effect

It is generally observed that as the ionic strength of a solution increases, the physical solubility of molecular species decreases. This is termed the salting out effect and makes the free  $CO_2$  solubility a strong function of  $CO_2$  loading. The effect is obvious from the "like dissolves like" principle of basic chemistry as the  $CO_2$  molecule is overall non-polar. To correlate the Henry's law constant in terms of ionic strength, van Krevelen and Hoftijzer (1948) proposed the following equation:

$$\log\left(\frac{H_A}{H_A^s}\right) = h_A I \quad (4.73)$$

where  $H_A$  and  $H_A^s$  are the Henry constants for the electrolyte solution and the molecular solvent, at the same temperature. Since infinite dilution in the mixed alkanolamine/water solvent is adopted as reference state, we thus assume that the ionic strength of the CO<sub>2</sub>-free alkanolamine solution is negligible. This is reasonable as less than 2% of the alkanolamine dissociates in CO<sub>2</sub>-free aqueous solution. We can then make use of the experimentally correlated values for  $H_A^s$  and let the relation  $H_A/H_A^s$  denote the salting out due to absorption of CO<sub>2</sub> in the mixed solvent of alkanolamine and water.

The factor  $h_A$  of eq. (4.73) is the sum of contributions from the species of positive and negative ions present and the dissolving gas, referred to as the van Krevelen coefficients.

$$h_A = \sum_i h_{B_i^+} + \sum_i h_{B_i^-} + h_{Ag} \quad (4.74)$$

The coefficients  $h_{B_i^+}$ ,  $h_{B_i^-}$  (denoting any positively or negatively charged ion) and  $h_{Ag}$  (attributed to the dissolved gas) are independent of concentration and may be assumed independent of temperature (Browning and Weiland, 1994). They have been evaluated for a number of common ionic species and dissolved gases (Danckwerts, 1970). Browning and Weiland (1994) made solubility measurements on loaded amine (MEA, DEA and MDEA) solutions and calculated the van Krevelen coefficients for the protonated amines, MEA and DEA carbamates and bicarbonate ions.

For the system under consideration, we have the ionic species denoted by  $B_2$ ,  $B_3$ ,  $B_4$  and  $B_5$ , leading to:

$$h_A = h_{B_2} + h_{B_3} + h_{B_4} + h_{B_5} + h_{Ag} \quad (4.75)$$

For a neutral molecule in an electrolyte solution, the activity coefficient may be determined from the Debye-McAuley formula (Pohorecki and Moniuk, 1988):

$$\log \gamma_A = \beta_A I \quad (4.76)$$

By recognizing the salting-out effect as a direct measure of the deviation from ideal behavior for the dissolved molecular species and combination of eq. (4.73), (4.75) and (4.76):

$$\gamma_A = \frac{H_A}{H_A^s} = 10^{(h_{B_2} + h_{B_3} + h_{B_4} + h_{B_5} + h_A)I} \quad (4.77)$$

This gives an expression for the activity coefficient of CO<sub>2</sub>, closely related to experimental data of the Henry's law constant and the salting out coefficients, with values given in appendix 2.

The phase equilibrium determining the solubility of free CO<sub>2</sub> in the loaded solution is then given by:

$$p_{CO_2} = \gamma_{CO_2} H_{CO_2}^s [CO_2] \quad (4.78)$$

### 4.5.2 The apparent equilibrium constants

The equilibrium CO<sub>2</sub> partial pressure in the gas phase may be considered a function of the liquid phase equilibrium composition. A typical algorithm for the rigorous speciation models will be to start with an initial estimate of the component concentration and then to iterate on the composition in order to satisfy the equations given by the equilibrium constants, the component balance and the electroneutrality equation. This is combined with an outer iteration loop which is used in calculating the activity coefficients of all the species, depending on component concentrations through the ionic strength. Every new estimate of the set of activity coefficients is passed to the inner loop to calculate a

new estimate of the component concentrations. This is repeated until the concentration of all species does not change significantly on consecutive iterations (Austgen, 1989).

Following the objective of developing a non-iterative equilibrium model for the membrane absorber, the need for an inner loop is eliminated since the component concentrations are calculated analytically as outlined in 4.4.2. The model depend on three equilibrium relations, represented by (4.45), (4.47) and (4.49). For the MEA-system, a sensitivity analysis shows that  $\xi_1$  may be set to zero without loss of generality, thus saying that no carbonate is formed (see 3.2). This makes the model independent of  $K_{c1}$ , as shown in appendix 1.  $K_{c2}$  and  $K_{abs}$  are thus the only important equilibrium constants in the MEA-model. According to eq. (4.15) the corresponding *apparent* equilibrium constants are given by the following:

$$K_{c2}^{app} = \frac{\gamma_{B_1}\gamma_{B_4}}{\gamma_{H_2O}\gamma_{B_3}}K_{c2} \quad (4.79)$$

$$K_{abs}^{app} = \frac{\gamma_A\gamma_{B_1}^2}{\gamma_{B_2}\gamma_{B_3}}K_{abs} \quad (4.80)$$

The speciation in terms of the ionic species ( $B_2$ ,  $B_3$  and  $B_4$ ) is dependent only on  $K_{c2}$  and  $K_{abs}$  and is subsequently used in calculating the molecular CO<sub>2</sub>-concentration (eq. (4.68)). This enables the use of eq. (4.77) in calculating explicitly the ionic-strength dependent  $\gamma_A$ . In order to prevent the need for an “outer” loop, the groups  $\gamma_{B_1}\gamma_{B_4}/\gamma_{H_2O}\gamma_{B_3}$  and  $\gamma_{B_1}^2/\gamma_{B_2}\gamma_{B_3}$  can be fitted to functions of CO<sub>2</sub>-loading, since the ionic strength is not available when calculating  $K_{c2}^{app}$ . A temperature and amine strength dependence may be included if required. The structure of the non-iterative equilibrium model is illustrated in figure 4.4.

The approach is simplified by only considering the coefficient for the free alkanolamine,  $\gamma_{B_1}$ , giving the activity coefficient of the ionic species,  $B_2$ ,  $B_3$ ,  $B_4$  and  $H_2O$  a value of 1. The assumption in terms of water is well justified due to



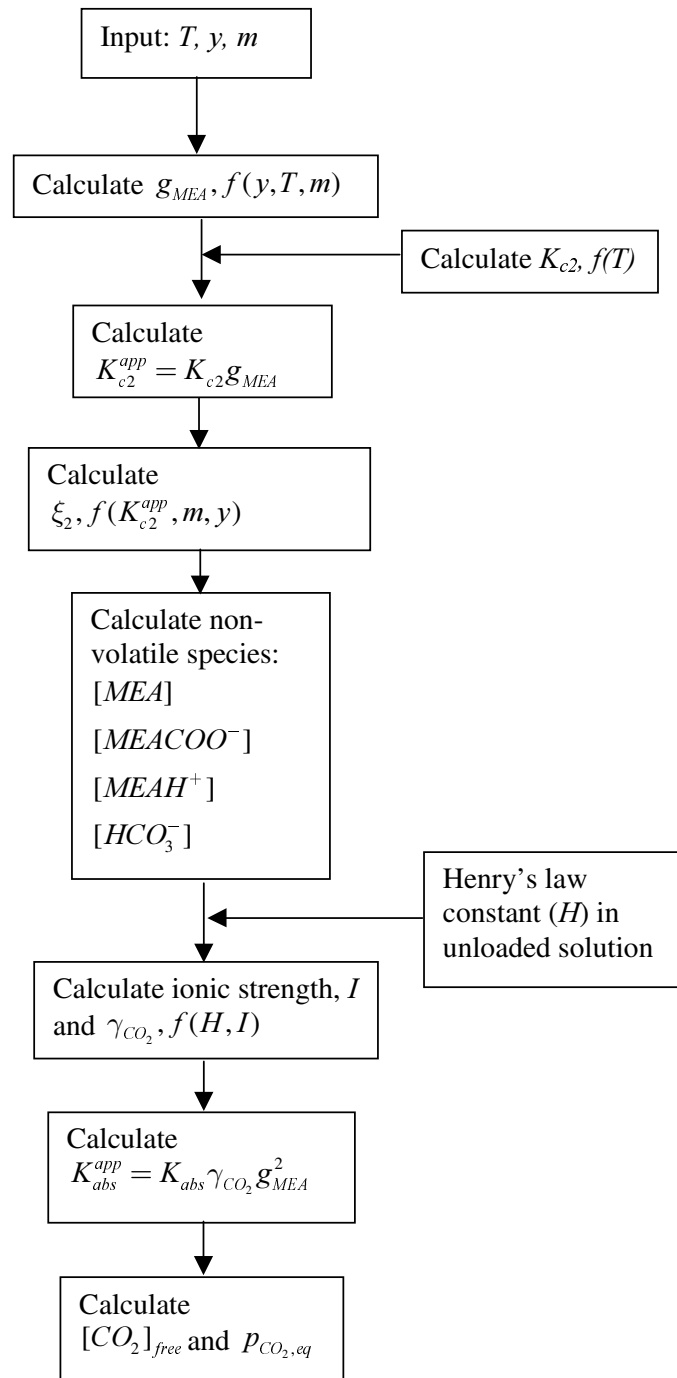


FIGURE 4.4: Block diagram of the equilibrium model (MEA-system)

the high mole fraction, which is close to the reference state value, as discussed in 4.2.1. However, this is in any case only a factor into which all remaining non-idealities are lumped. It works as a means of tuning the values of the apparent equilibrium constants to make the model fit experimental VLE-data. This formulation is mathematically similar to the approach of Atwood et al. (1957) and Kent and Eisenberg et al. (1976). The symbol  $g_{B_1}$  is chosen for this factor, as there is no justification to call it an activity coefficient.  $K_{c2}^{app}$  and  $K_{abs}^{app}$  are thus given by:

$$K_{c2}^{app} = K_{c2} g_{B_1} \quad (4.81)$$

$$K_{abs}^{app} = K_{abs} \gamma_A g_{B_1}^2 \quad (4.82)$$

The corresponding equations in the MDEA-system are derived from the equilibrium constants of reaction (4.69) and (4.70).

### 4.5.3 Tuning the model to experimental data

Any equilibrium model, rigorous or not, can after all never be better than the quality of the experimental data to which it is fitted. The large spread in experimental VLE-data from different sources makes this a final limitation in terms of comparing the results from different VLE-modeling approaches.

A review in terms of both MEA/water and MDEA/water has been done by Nilsen (2001), including an overview of amine concentrations, CO<sub>2</sub>-loadings and temperatures where experiments have been done. In the present work, considering only absorption, it is desirable that the equilibrium model covers the temperature range from 25 to at least 80°C and CO<sub>2</sub>-loadings from 0-0.5 and 0-1 for MEA and MDEA respectively. The amine concentration in industrial absorbers have gradually increased through the years. This is due to the introduction of efficient corrosion inhibitors and is reflected in the experimental VLE-data published. An MEA-concentration of 30wt% and an MDEA concentration of 48.8/50wt% may presently be considered base case values for these two alkanolamine/water systems. To include the effect of varying concentration

of the alkanolamine a second concentration of 15wt% in MEA and 23.5% in MDEA should preferably be included in the model tuning. Other alkanolamine concentrations than these have so far only sporadically been investigated in the MEA/water and MDEA/water cases.

Based upon these requirements, the VLE-data published by the group of Alan Mather at the University of Alberta, Canada points itself out as a natural source. This is partially motivated by the fact that no other groups apparently have a comparable experience in this kind of measurements and from the desire to avoid combining possibly inconsistent data from different sources in the model fitting. The references to the selected sources are given in table 4–1.

**TABLE 4–1: References to experimental VLE-data used in the model tuning**

Amine	Amine conc.	Temperatures	Source
MEA	30wt%	25, 40, 60, 80°C	Jou et al. (1995)
MEA	15wt%	25, 40, 60, 80°C	Lee et al. (1976)
MDEA	23.5 and 48.8wt%	25, 40, 70, 100°C	Jou et al. (1982)

The development of an equilibrium model for the MEA/water and MDEA/water-case is thus concluded by forcing a fit to the experimental data from tuning the value of  $g_{B_1}$ .  $g_{B_1}$  was in both systems treated as a smooth function of temperature, amine molarity and CO<sub>2</sub> loading. It was however found that no temperature dependence is required in the MEA/water case. The following simple relations resulted from the manual tuning:

$$g_{MEA}^{15} = 3(1 - y) \quad (4.83)$$

$$g_{MEA}^{30} = 1.6/(1 - y) \quad (4.84)$$

$$f = -4 \times 10^{-4} c_{MEA} + 2 \quad (4.85)$$

$$g_{MEA} = g_{MEA}^{15} f + (1 - f) g_{MEA}^{30} \quad (4.86)$$

Here,  $f$  is a weighting factor to account for amine concentrations in the range between 2500 mol/m<sup>3</sup> (15wt%) and 5000 mol/m<sup>3</sup> (30wt%). For the MDEA/water system the following relations resulted:

$$g_{MDEA}^{23.5} = 0.5(1 - y)^{-0.1}(1 + 10y^{0.5})(313/T)^2 \quad (4.87)$$

$$g_{MDEA}^{48.8} = 0.25(1 - y)^{-0.25}(1 + 10y^{0.2})(298/T)^{2.5} \quad (4.88)$$

$$f = -4 \times 10^{-4} c_{MDEA} + 1.88 \quad (4.89)$$

$$g_{MDEA} = g_{MDEA}^{23.5} f + (1 - f) g_{MDEA}^{48.8} \quad (4.90)$$

$f$  is here the weighting factor to account for amine concentrations in the range between 2000 mol/m<sup>3</sup> (23.5wt%) and 4280 mol/m<sup>3</sup> (48.8wt%).

#### 4.5.4 Equilibrium curves and model performance

In figure 4.5-4.12, the tuned model prediction is plotted together with the experimental data for the MEA and MDEA systems. The plots are given both in logarithmic and linear scale. Equilibrium curves for CO<sub>2</sub> in alkanolamine solutions are traditionally presented on a logarithmic scale, which however tend to give the data in the low loading range the highest attention. The slope of the equilibrium curve, and the model prediction vs. experimental data in the higher loading range is better illustrated on a linear scale. Besides, when implemented in an absorber simulation program, the one major goal of the equilibrium model is to account for the driving force for absorption through the *linear* relation  $P_{CO_2} - P_{CO_2}^{eq}$ .

The “asymptotic” behavior of the equilibrium curves for the MEA/water system is clearly seen from figure 4.6 and 4.8. For CO<sub>2</sub>-loadings higher than about 0.45, large deviations in the prediction of the equilibrium partial pressure are possible. The opposite problem, of calculating the saturation loading at a given partial pressure correspondingly has a low uncertainty. The deviation in this range may to a large extent be attributed to the uncertainty in the experimental

determination of CO<sub>2</sub>-loading, which, according to Jou et al. (1995), has an error of  $\pm 2-3\%$ . The MDEA-model in figure 4.9-4.12 shows a reasonably good fit to the data, except for loadings lower than 0.01.

The plot in figure 4.13 shows the MEA-model, tuned to the data of Jou et al. (1995) plotted together with the data from Shen and Li (1992). The poor agreement illustrates the problem of large deviations between different sources for experimental VLE-data. The MEA-system is, however, special due to the significant steepness of the equilibrium curves. The agreement between different sources considering the MDEA-system is better, at least in the loading range considered here. This is illustrated in figure 4.14, where the model prediction is plotted together with the experimental data of Austgen and Rochelle (1991) and Xu et al. (1992).

The example speciation plot for the MEA-system, given in figure 4.15, may be compared with the corresponding speciation from the thermodynamically consistent model of Liu et al. (1999) in figure 4.16. Liu et al. used the electrolyte-NRTL model similar to Austgen (1989) and refitted the important parameters. The difference between the model prediction from this work and the model by Liu et al. is relatively small. There is, however, no way of comparing the model predictions in terms of the free CO<sub>2</sub>-concentration, which is a very important part of the speciation, as it determines the driving force for the chemical reaction. This is a general problem, since the value of the free CO<sub>2</sub> concentration is usually not reported. In figure 4.17 an example speciation plot is given for the MDEA-system. There is apparently no comparative plot available from publications of rigorous models.

The “buffer-curves” given in figure 4.18 and 4.19 show an important characteristic of the alkanolamine solutions. The correct prediction of pH is very important as an indirect measure of the OH<sup>-</sup>-concentration. This is especially important when interpreting kinetic data performed at close to zero loading. The buffer curves may serve as a consistency check of the model as the pH-data were not used in the model tuning. The model seems to underpredict the pH at

higher loadings in the MEA-system, while the prediction in the MDEA system is apparently good in the whole loading range.

## 4.6 Summary and conclusions

An equilibrium model has been developed for the prediction of gas phase partial pressure and liquid phase speciation in the ternary systems CO<sub>2</sub>/MEA/water and CO<sub>2</sub>/MDEA/water. The chosen approach is strongly motivated by the desire to avoid any iterations during the equilibrium speciation. This is presently considered a requirement in order to keep the computational times of the membrane absorber simulator developed in this work at acceptable levels. An activity coefficient for the molecular CO<sub>2</sub> is calculated from a salting out-correlation, while remaining deviations from ideality is lumped into an apparent activity coefficient for the alkanolamine. This is used as a factor to tune the model prediction of the equilibrium partial pressure to experimental data. The speciation from the model gives similar results as a considerably more rigorous model, solving for the activity coefficient of all species in solution.

The model developed in this work is limited to the range where it is fitted to experimental data:

- MEA concentrations from 15 to 30wt% and MDEA concentrations from 23.5-48.8wt%
- Temperatures from 25-80/100°C
- CO<sub>2</sub> partial pressures from 0 to 100 kPa

A future improvement of the equilibrium model is desirable in order to extend the model to mixed alkanolamine systems and different alkanolamine concentrations, temperatures and CO<sub>2</sub>-loadings. To be able to predict the performance of the membrane gas absorber in natural gas CO<sub>2</sub> removal at total pressures from 80-200 bar, a calculation of gas phase fugacity coefficients needs to be included. A review shows that a number of thermodynamically rigorous models

#### *4.6 Summary and conclusions*

---

have been applied with success in the modeling of CO<sub>2</sub>/amine equilibria. Such a model is presently being developed in this group (Poplsteinova et al., 2002).

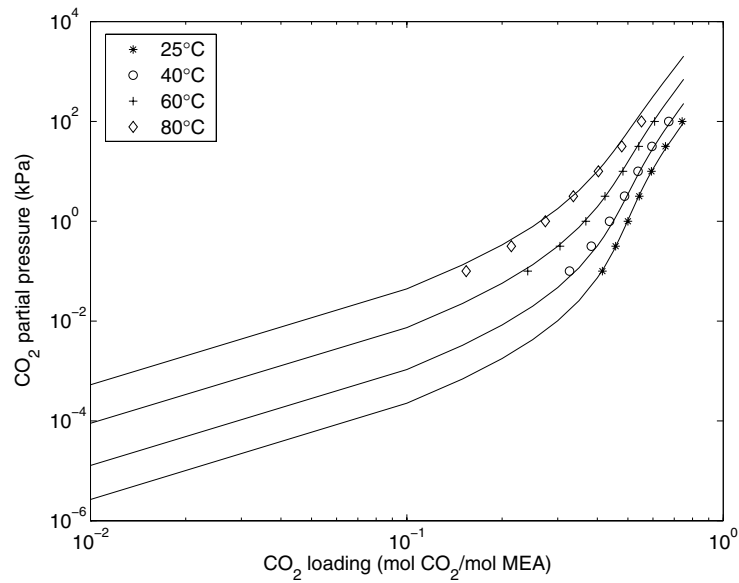


**FIGURE 4.5: CO<sub>2</sub> equilibrium for a 15wt% MEA solution. Model (solid line) and experimental data points from Lee et al. (1976).**

---

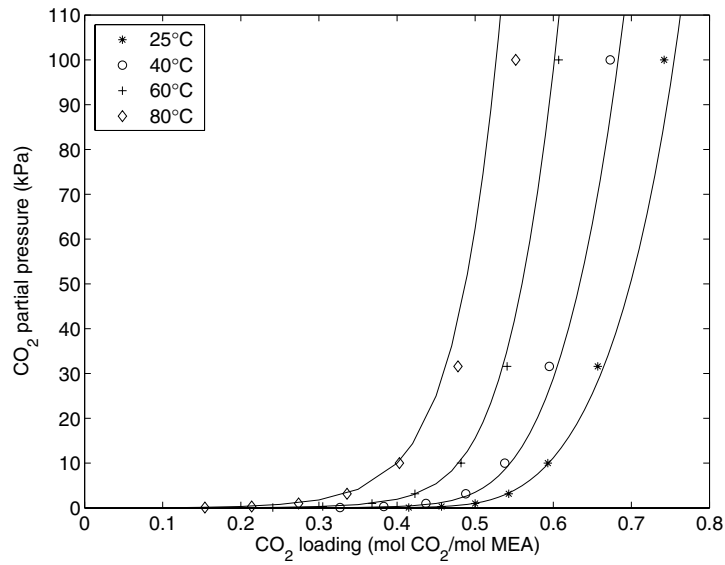


**FIGURE 4.6: CO<sub>2</sub> equilibrium for a 15wt% MEA solution. Model (solid line) and experimental data points from Lee et al. (1976).**

---



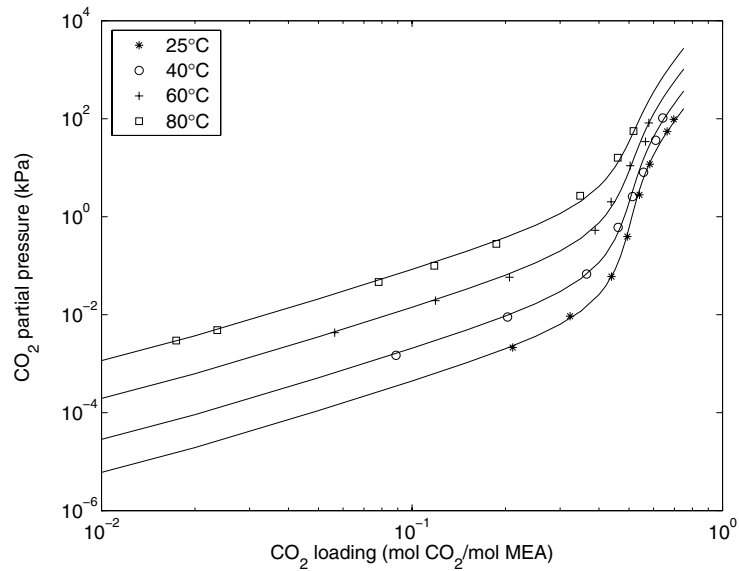


**FIGURE 4.7: CO<sub>2</sub> equilibrium for a 30wt% MEA solution. Model (solid line) and experimental data points from Jou et al. (1995).**

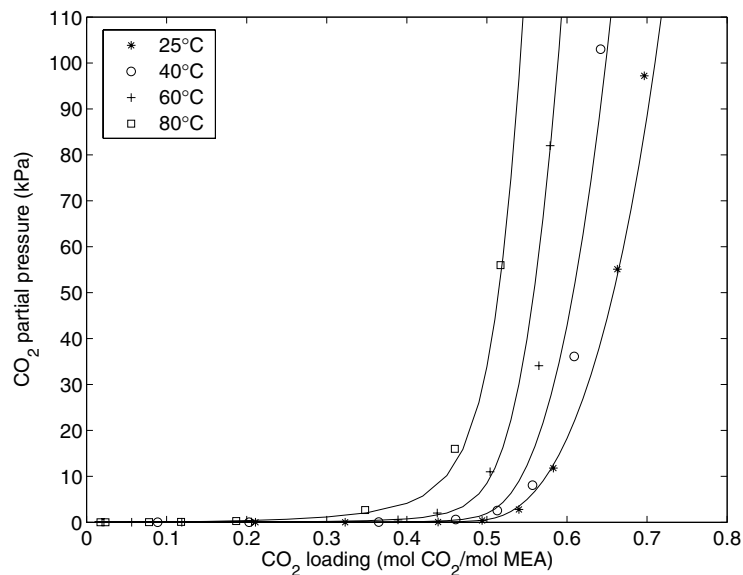


**FIGURE 4.8: CO<sub>2</sub> equilibrium for a 30wt% MEA solution. Model (solid line) and experimental data points from Jou et al. (1995).**

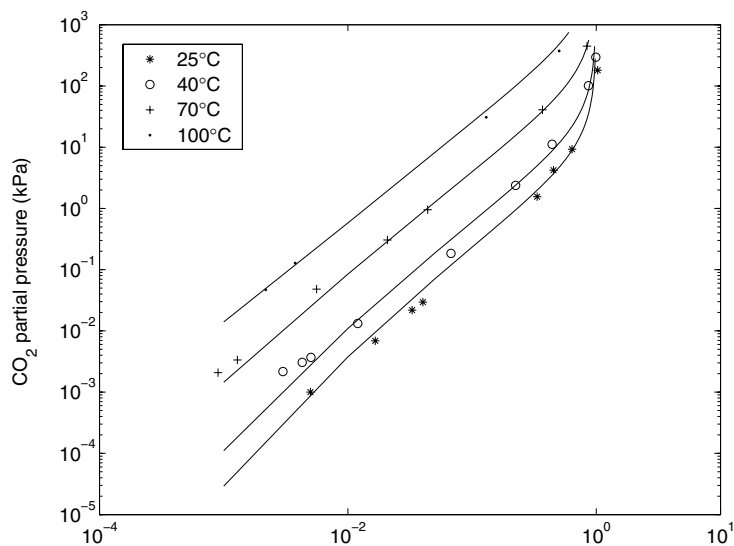


**FIGURE 4.9:** CO<sub>2</sub> equilibrium for a 23.5wt% MDEA solution. Model (solid line) and experimental data points from Jou et al. (1982).

---

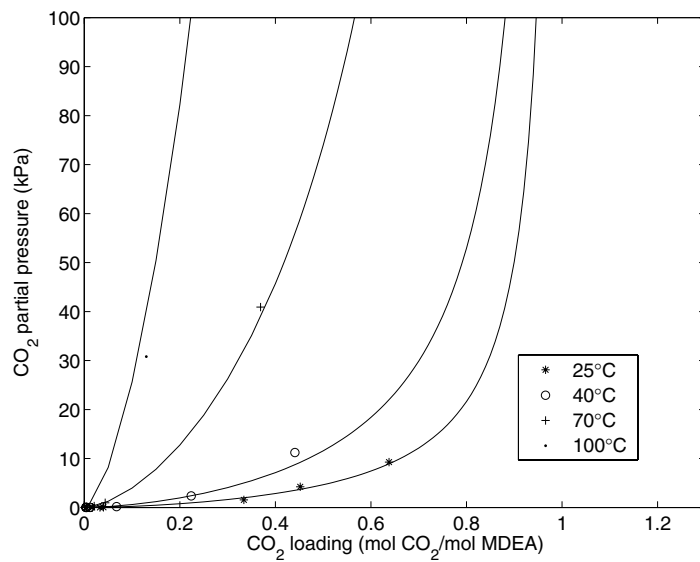


**FIGURE 4.10:** CO<sub>2</sub> equilibrium for a 23.5wt% MDEA solution. Model (solid line) and experimental data points from Jou et al. (1982).

---

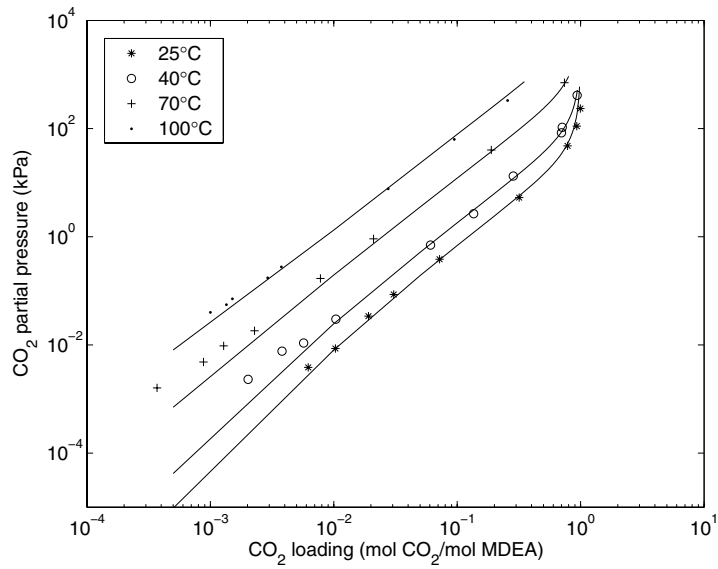


**FIGURE 4.11: CO<sub>2</sub> equilibrium for a 48.8wt% MDEA solution. Model (solid line) and experimental data points from Jou et al. (1982).**

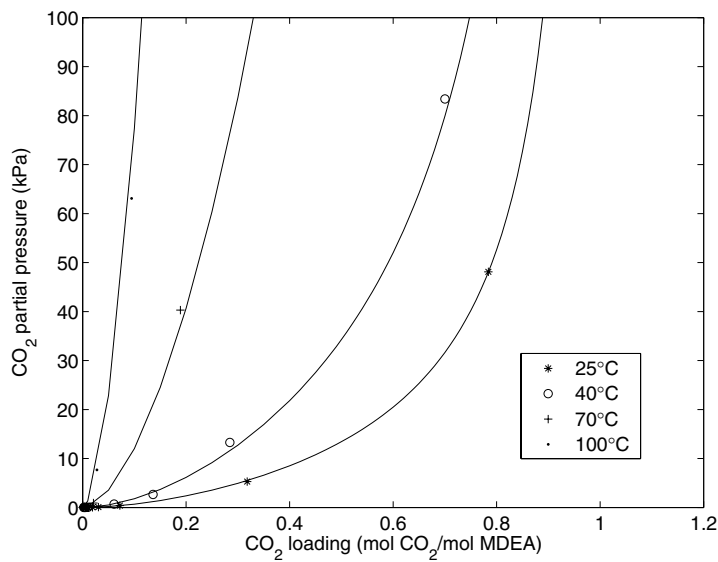


**FIGURE 4.12: CO<sub>2</sub> equilibrium for a 48.8wt% MDEA solution. Model (solid line) and experimental data points from Jou et al. (1982).**

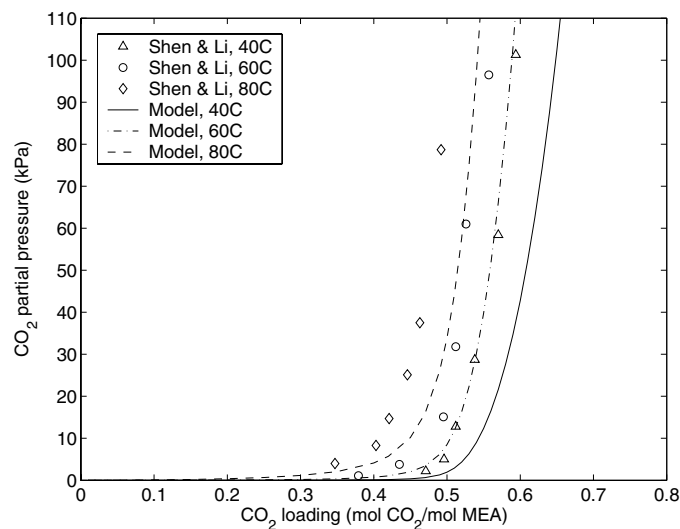


**FIGURE 4.13:** CO<sub>2</sub> equilibrium for a 30wt% MEA solution. Experimental data points from Shen and Li (1992) and the prediction of the model tuned to data from Jou et al. (1995).

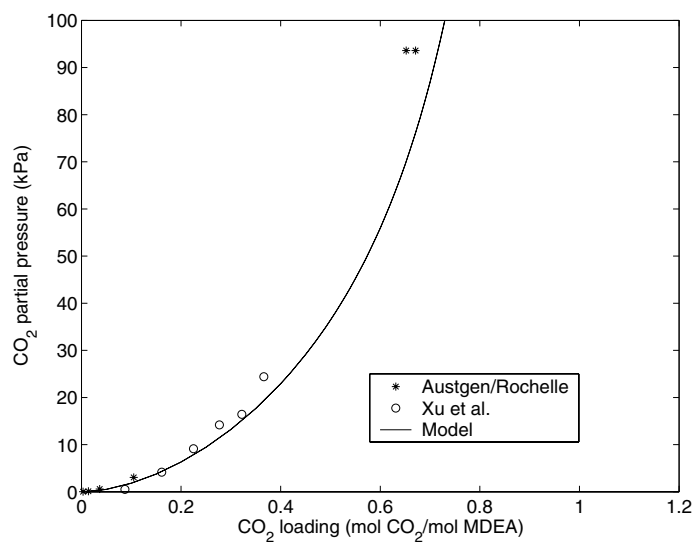


**FIGURE 4.14:** CO<sub>2</sub> equilibrium for a 48.8wt% MDEA solution at 40°C. Experimental data points from Austgen and Rochelle (1991) and Xu et al. (1992) together with the model tuned to data from Jou et al. (1982).

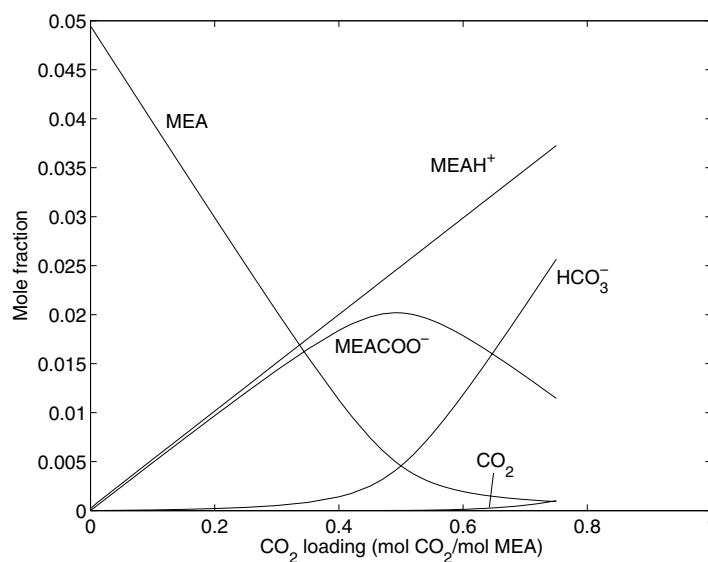


**FIGURE 4.15:** Speciation plot for a 15% MEA solution at  $T=40^{\circ}\text{C}$ , from the equilibrium model of this work.

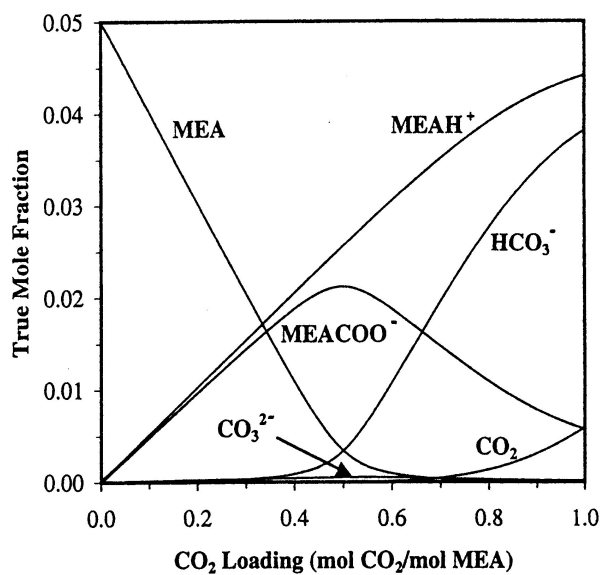


**FIGURE 4.16:** Speciation plot for a 15% MEA solution at  $T=40^{\circ}\text{C}$ , from Liu et al. (1999).

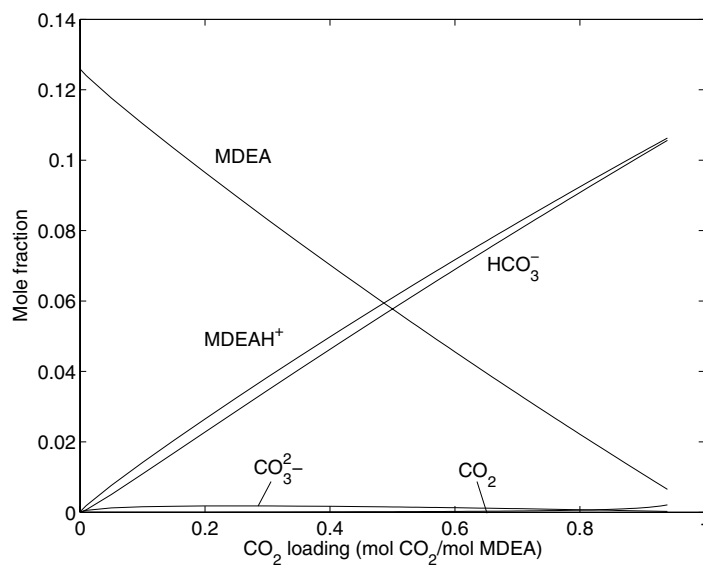


**FIGURE 4.17: Speciation plot for a 48.8% MDEA solution at 40 °C , from the equilibrium model of this work.**

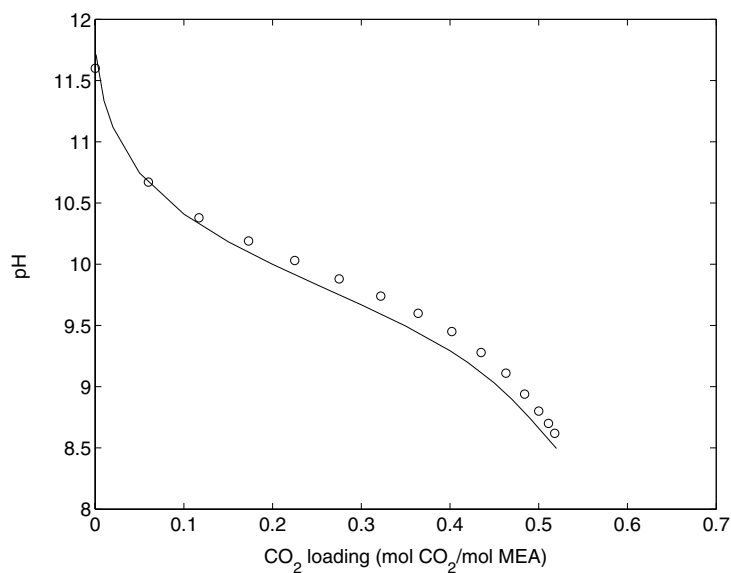


**FIGURE 4.18: pH vs. CO<sub>2</sub>-loading in a 25wt% MEA-solution at 40 °C . Model (solid line) and experimental data points from Kristiansen (1993).**

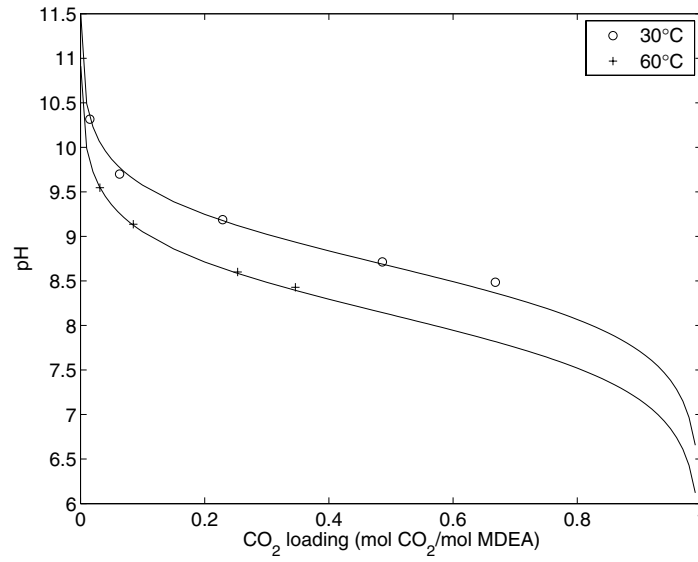


**FIGURE 4.19: pH vs. CO<sub>2</sub>-loading in a 45.6wt% MDEA-solution. Model (solid line) and experimental data points from Lidal (1992).**

---





# *Experimental study of membrane gas absorption*

---

## **5.1 Introduction**

### **5.1.1 Scale up and design of a membrane gas absorber**

The modular and discrete configuration of the membrane gas absorber principally leads to the significant advantage of a linear scale-up. This greatly enhances the value of a laboratory scale fundamental study of the process in order to capture the individual effects of operating variables like:

- Liquid velocity
- Gas velocity
- Temperature
- Amine type and strength
- CO<sub>2</sub> concentration in liquid and gas
- Membrane properties

Due to the scale-up properties, in principle a perfectly well understood industrial CO<sub>2</sub>-removal process can be designed using only data obtained on the laboratory scale. Laboratory scale here denotes an apparatus where a unique value can be given to the operating variables without significant loss of accuracy (by taking the mean of inlet and outlet properties), thus giving point measurements from a differential element of the industrial-scale unit. However, the possible presence of soot particles, hydrocarbons, nitrous oxides and other impurities in the real exhaust gas may influence the performance of the membrane modules and cause degradation of the chemical solvent. Pilot plant experiments on a real exhaust gas will thus be an important part of the design procedure.

## 5.2 Apparatus assembly

The construction and development of a lab-scale apparatus for the study of membrane gas absorption, and the establishment of experimental methods for kinetics measurements, have been major goals of this work. Two modes of operation in terms of the gas phase were implemented in the design:

1. Circulating gas phase with 0-10% CO<sub>2</sub> in N<sub>2</sub> at atmospheric total pressure. This mode resembles the conditions in an industrial process using membrane gas absorption (MGA) for the removal of CO<sub>2</sub> from exhaust gas (coal or gas fired power plant).
2. To eliminate, as far as possible, the contributions from gas bulk and membrane resistance, experiments can be performed with pure CO<sub>2</sub> in the gas phase (+solvent vapor). In this mode the gas phase is stagnant. This is the mode normally used for the assessment of rate parameters for the liquid phase reactions, as in the laminar jet and wetted wall apparatus.

A picture and a schematic diagram of the lab-scale membrane gas absorber apparatus are given in figure 5.1 and 5.2, respectively. All tubing is made of stainless steel with Swagelok connections. Dimensions are 1/4" for liquid lines and 1/2" for the gas circulation loop. The membrane module itself, delivered by W.L. Gore & Associates, is made of a polypropylene shell filled with the inter-

connected tubes, PTFE hollow fibers of 3 mm inner diameter. The flow pattern is countercurrent. This is different from the cross-flow configuration that is the most probable design of the single modules in an industrial contactor for exhaust gas CO<sub>2</sub>-removal (fig. 1.3). As will be shown later, the negligibility of the gas film resistance compared to membrane and liquid side resistance makes the mode of gas flow practically insignificant. Data for the membrane used are given in table 5–2.



**FIGURE 5.1: The lab-scale apparatus**

---

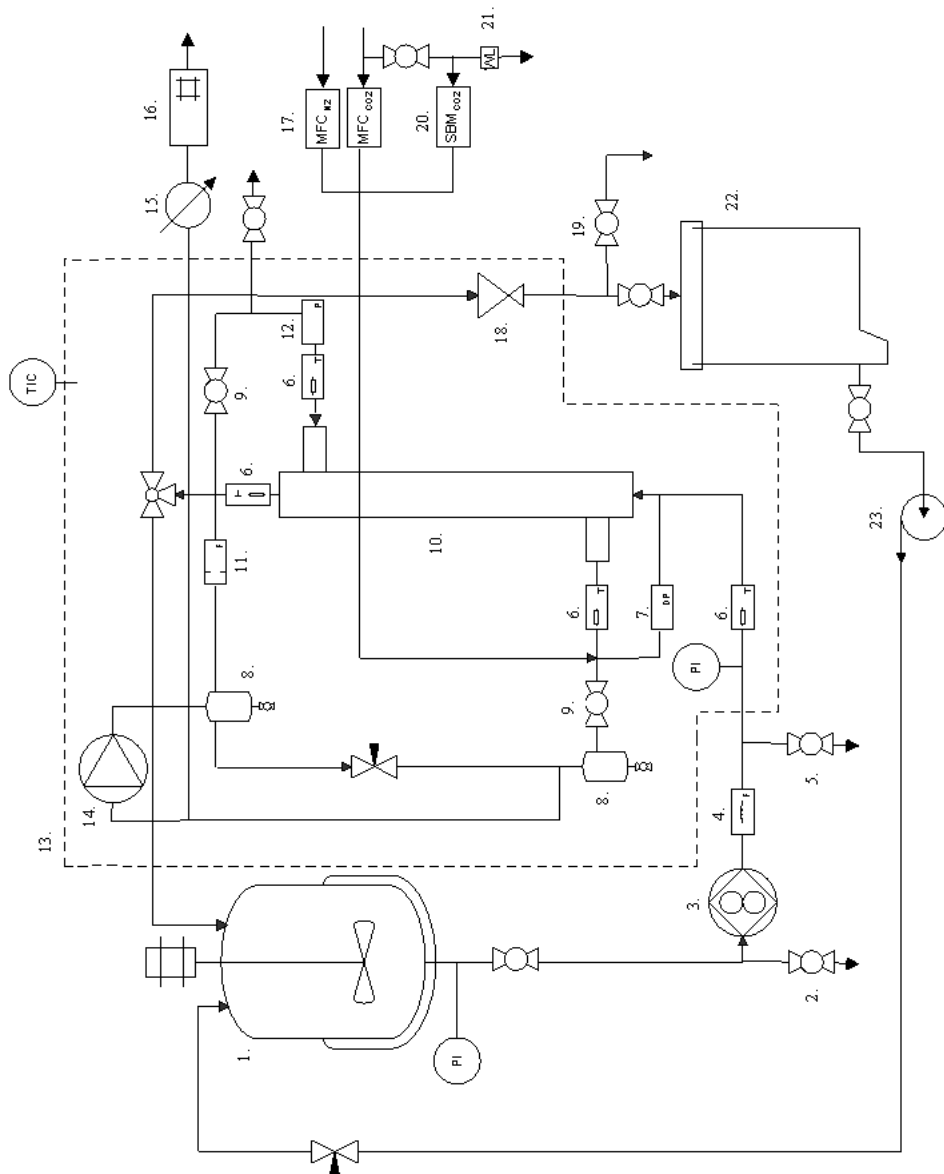


FIGURE 5.2: Diagram of the lab-scale apparatus

**TABLE 5–1: Items of figure 5.2**

1. Liquid feed tank
2. Liquid sample point (membrane inlet)
3. Liquid gear pump
4. Flow meter
5. Membrane drainage
6. Temperature RTD transmitter
7. Differential pressure transmitter
8. Condensate trap
9. Block valves for stagnant gas operation
10. Membrane module
11. Orifice meter
12. Pressure transmitter
13. Heating cabinet
14. Side channel blower
15. Condenser
16. CO <sub>2</sub> gas analyzer
17. Mass flow controllers (CO <sub>2</sub> make-up and N <sub>2</sub> )
18. Back pressure regulator
19. Liquid sample point (membrane outlet)
20. Soap bubble meter
21. Water lock (gas washing bottle)
22. Liquid collection tank
23. Centrifugal pump

**TABLE 5–2: Data of the lab-scale membrane module**

Number of tubes	28
Inner diameter of tubes	3 mm
Membrane wall thickness	240 $\mu\text{m}$
Total tube length (incl. potting)	575 mm
Active tube length	430 mm
Active inner surface area, $a_m$	0.11 $\text{m}^2$
Porosity, $\epsilon$	0.50
Tortuosity, $\tau$	1.3
Inner diameter of canister	280 mm
Specific inner surface area, $a$	416 $\text{m}^2/\text{m}^3$
Max differential pressure ( $P_{\text{liquid}}-P_{\text{gas}}$ )	0.5 bar

### 5.2.1 The liquid system

The 20 liter liquid feed storage tank is made with a jacket for circulation of heating water from a separate water bath. This serves to heat the liquid to the operation temperature of the experiment. The stirrer in the tank serves to speed up the rate of heat transfer. The liquid level is monitored by a Rosemount differential pressure transmitter. The volume of the tank above the liquid surface is continuously flushed with  $\text{N}_2$  in order to prevent contact with  $\text{O}_2/\text{CO}_2$  from air.

Liquid is pumped from the feed tank by an Ismatec gear pump with a variable speed drive and a capacity of 30 l/h. The liquid flow rate is measured by an electromagnetic sensor manufactured by Endress+Hauser. To eliminate any particles from entering the membrane module, the liquid feed passes a 60 micron in-line filter.

In order to keep the liquid side pressure in the membrane at a level 0.1-0.5 bar higher than at the gas side, a back pressure valve on the liquid outlet line is used for adjustment. The liquid/gas side pressure difference is monitored by a Rosemount differential pressure transmitter. Liquid samples can be taken from the outlet of the feed storage tank (membrane inlet) and before the liquid collection

tank (membrane outlet). After a once-through experimental series the whole batch of liquid is pumped back to the feed tank by a centrifugal pump.

### 5.2.2 The gas system

The gas, when consisting of 0-10% CO<sub>2</sub> in N<sub>2</sub> is circulated by a Rietschle side channel blower and monitored by a calibrated orifice meter with a Foxboro differential pressure transmitter. The flow is adjusted by a Siemens Micromaster frequency transmitter and has a maximum of 6 m<sup>3</sup>/h. The base case gas flow is 3 m<sup>3</sup>/h (50 l/min) which corresponds to a superficial gas velocity of approximately 1.3 m/s, based on the inner cross-section area of the module canister. The apparent real cross-section available for gas flow was measured by weighing the amount of distilled water used in filling the membrane gas side. The corresponding real gas velocity was then found to be around 5.8 m/s, or 4.5 times higher than the superficial velocity.

The CO<sub>2</sub> make-up stream is mixed with an N<sub>2</sub>-flow of 1 l/min, which corresponds to the amount required by the CO<sub>2</sub> analyzer, and introduced into the circulating gas right after the membrane module. For this purpose, digital mass flow controllers (MFC) from Bronkhorst Hi-Tec are used. Depending on the experimental conditions two different controllers for CO<sub>2</sub> are used; one with range 0-0.1 Nl/min and one with range 0-1 Nl/min. The gas sample, giving the gas composition at the membrane inlet, is taken from the blower suction line, where the system pressure is the lowest. As the CO<sub>2</sub> analyzer is operating at atmospheric pressure this serves to prevent pressures below atmospheric in any part of the circulation loop.

The flux of CO<sub>2</sub> from the gas through the membrane and into the liquid is calculated from a CO<sub>2</sub> balance on the system as a whole. It is given by the flow of CO<sub>2</sub> into the system minus the amount going out of the system to the gas analyzer. This important feature gives a high accuracy for the flux calculation, compared to making the mass balance on the membrane module itself. The CO<sub>2</sub> flux then would have to be calculated from the difference between two numbers of

similar size, as the absolute change in volume percent CO<sub>2</sub> across the membrane is very low. This would result in unacceptable uncertainty levels.

To prevent any liquid droplets from circulating with the gas, droplet collectors are placed on the blower outlet line to take out any condensate formed during the compression, and right after the membrane module to remove possible liquid permeate and condensate. The gas side pressure is monitored by a Drück pressure transmitter calibrated in the range 0-2 bar absolute. The four temperatures of gas and liquid inlet and outlet are measured by Pt-100 RTD transmitters calibrated in the range 0-100°C. The whole gas circulation loop is mounted inside a heating cabinet with circulating air providing a uniform temperature, regulated by a Shimaden temperature controller.

The analysis of CO<sub>2</sub> in the gas is done with Rosemount Binos 100 infrared CO<sub>2</sub> analyzers of different ranges depending on gas composition (0-5, 0-10 and 0-20 vol% CO<sub>2</sub>). Due to the requirement of a low humidity in the sample gas, the gas is cooled to 10°C in a condenser prior to analysis.

### 5.2.3 Control and interface

A Labview program was developed for the operation and control of the apparatus through a 12 bit Fieldpoint I/O system. Controller features implemented include shut down of the liquid pump if the gas/liquid differential pressure exceeds 0.3 bar and a PID control loop for the CO<sub>2</sub> mass flow controller in order to meet the specified gas composition. The operator interface is shown in figure 5.3.



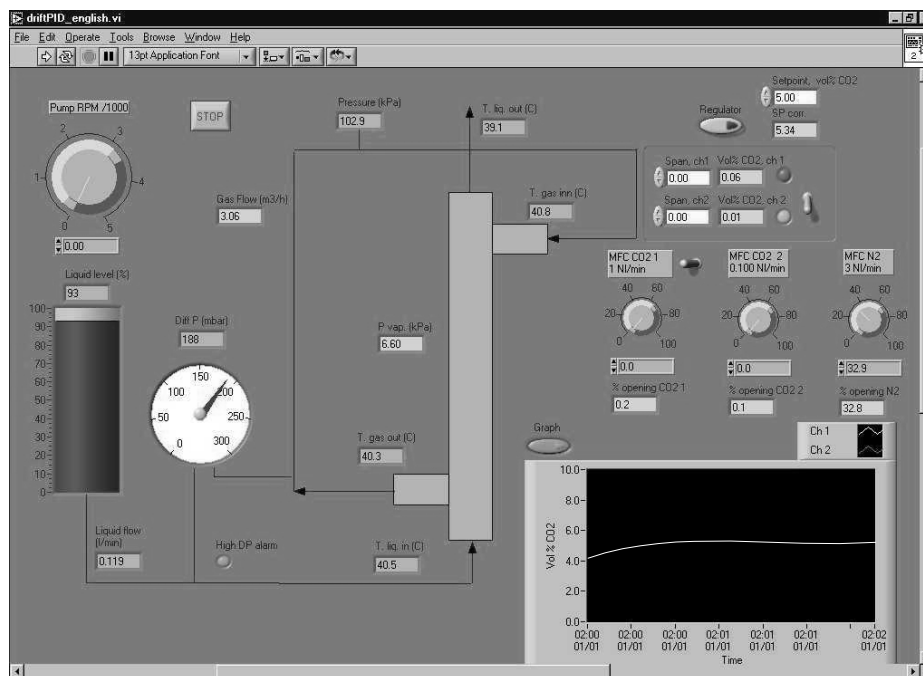


FIGURE 5.3: Operator interface of the apparatus

## 5.3 Operating procedures

### 5.3.1 Calibration

All mass flow controllers were regularly calibrated by soap-bubble meters. The mass flow controllers were used in order to generate  $\text{CO}_2/\text{N}_2$  mixtures for calibration of the infrared  $\text{CO}_2$  gas analyzers. Due to a slight sensitivity of the analyzers to atmospheric pressure this calibration was performed daily.

### 5.3.2 Chemicals

The  $\text{CO}_2$  and  $\text{N}_2$  gases used were obtained from AGA and had a purity of 99.99 and 99.999%, respectively. The MEA was obtained from Riedel-de-Haën and had a purity greater than 99.5%, and the MDEA was obtained from Acros

Organics with a purity greater than 99%. Batches of 20 l aqueous amine solution were prepared by weighing the amine and adding distilled water to the specified weight percent.

### **5.3.3 Experiments with circulating gas phase**

The set point for the temperature of the heating cabinet and the liquid feed tank was specified. The gas temperature was specified to always be at least one centigrade higher than the liquid temperature in order to, as far as possible, prevent any liquid condensate from forming in the membrane module. The residence time of the gas in the membrane module was always less than 0.1 s, and this made it possible to hold the gas temperature higher than the liquid temperature both at the inlet and the outlet. At lower gas velocities than those applied, the outlet gas temperature would equal the inlet liquid temperature due to the efficient heat exchange of the membrane module.

The gas circulation flow was adjusted to the desired level of 3 m<sup>3</sup>/h, and the apparatus was flushed with N<sub>2</sub> which was subsequently adjusted to a flow of 1 l/min. The liquid pump was started with the specified liquid flow of 0.1-0.4 l/min and the back pressure valve was adjusted to give a gas/liquid differential pressure of 0.1-0.2 bar.

The desired CO<sub>2</sub> vol% was specified and the mass flow controller for CO<sub>2</sub> was manually adjusted to approximately meet the set point before the regulator was switched on. When the system reached steady state, which normally took 10-15 minutes, all important parameters were registered and a new value of the variable under consideration was specified in order to reach a new steady state.

Experiments were done in series with 3-5 levels of a specific variable. The variables tested were gas velocity, liquid velocity, CO<sub>2</sub> partial pressure or temperature. The same liquid batch was pumped back to the feed tank for every new series, thus gradually increasing the solution loading. Extra recirculation with absorption was sometimes applied in order to make a sufficient span in the CO<sub>2</sub> loading.

Liquid samples were taken from the feed tank before each new series and analyzed for CO<sub>2</sub> loading and amine concentration as described below. Samples of the liquid outlet was generally not taken, as the outlet CO<sub>2</sub> loading was calculated from the absorption rate. The small difference between the inlet and outlet loading would not justify a mass balance test from comparing gas and liquid absorption rates separately.

The operation required the apparatus to be completely gas-tight, which was regularly tested by closing the gas outlet, applying a very low N<sub>2</sub>-flow (<0.03 NI/min) and observing the level in the water lock at the gas outlet. Before apparatus run-down the membrane was thoroughly drained and the system systematically flushed with N<sub>2</sub> to prevent any condensate from forming on the gas side. Flushing was also applied through the membrane from the gas to the liquid side.

The resulting experimental data gave the absorption rates and the dependence of the variables CO<sub>2</sub>-partial pressure, gas velocity, liquid velocity and temperature with CO<sub>2</sub>-loading as parameter. Base case values and range for the experiments are given in table 5–3.

**TABLE 5–3: Base-case values and range for the experiments with circulating gas phase**

Variable	Base Case	Range (3-4 values)
vol% CO <sub>2</sub>	5	0.5-10
Liquid flow (l/min)	0.2	0.1-0.4
Gas flow (m <sup>3</sup> /h)	3	2-5
T (°C)	40	25-70
CO <sub>2</sub> loading	Parameter	0-0.5/1 (MEA/MDEA)

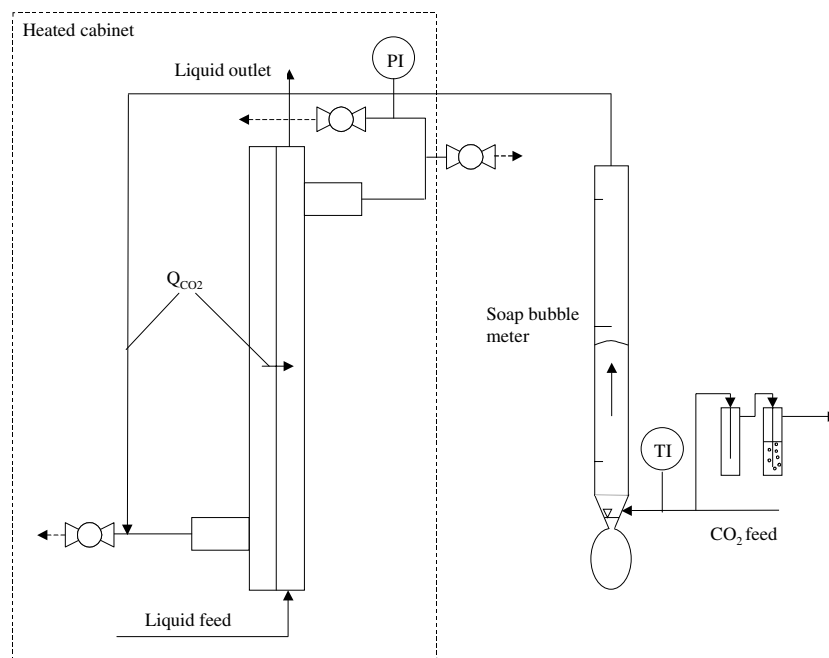


**FIGURE 5.4: Principle of operation with pure CO<sub>2</sub> stagnant gas phase**

### 5.3.4 Experiments with pure CO<sub>2</sub> and stagnant gas phase

In this mode the ball valves in the gas circulation loop before and after the membrane module were closed, defining the volume of the stagnant gas phase. A 250 ml soap bubble meter was connected to the CO<sub>2</sub> feed system. The volume including the membrane module was thoroughly flushed with CO<sub>2</sub>. This was done in a systematic manner to avoid any impurities remaining in dead volumes. The principle of operation is illustrated in figure 5.4.

Before start-up the CO<sub>2</sub> feed flow was started, with all the CO<sub>2</sub> going out through the excess line before the soap bubble meter. As the liquid flow was started, CO<sub>2</sub> flowed through the soap bubble meter and was absorbed in the liquid in the membrane module. The CO<sub>2</sub> gas feed was adjusted to always keep a small excess flow going out through the soap bubble meter. This feature assured a constant system pressure and prevented air from entering the system. The CO<sub>2</sub>

molar absorption rate was given from measuring the time required by a bubble to rise through the given volume of the soap bubble meter, using a stopwatch. The temperature of the flowing gas was measured by a thermocouple. The pressure was taken from the reading of the pressure sensor inside the apparatus. This could be done as the pressure drop from the soap bubble meter to the apparatus was found negligible from measurements with a micro-manometer.

The system was allowed 10 minutes to stabilize before measurement started. Steady state was considered when five consecutive stopwatch readings gave a difference less than 0.5 s, with a total time never less than 15 s. The average of these five readings was used in the flux calculation.

The rest of the experimental procedure was similar to that in circulating gas mode, with liquid velocity and temperature as the only variables together with CO<sub>2</sub>-loading. With temperature as variable, the CO<sub>2</sub> partial pressure would gradually decrease corresponding to the increase in solution vapor pressure, as the total pressure was fixed at atmospheric.

## 5.4 Calculation of absorption rate

From experiments with a stagnant gas phase, the molar absorption rates were calculated from the volumetric absorption rate measured by the soap bubble meter:

$$R_{CO_2} = \frac{V}{\bar{t}} \cdot \frac{P}{P^0} \cdot \frac{T^0}{T} \cdot \frac{1}{v_m^0} \quad (5.1)$$

where  $R_{CO_2}$  (mol/s) is the molar absorption rate of CO<sub>2</sub> in the membrane module.  $V$  is the volume of the soap bubble meter and  $\bar{t}$  is the mean stop-clock reading from the 5 parallels.  $P^0$  and  $T^0$  are the reference pressure and temperature at Normal conditions (101.3 kPa and 273.15 K) while  $v_m^0$  is the molar volume at Normal conditions (22.41 NI/mol). CO<sub>2</sub> is here treated as an ideal gas, a valid assumption as the compressibility at 1 bar and 25 °C is 0.9948 (VDI WärmAtlas, 1984).

The solution vapor pressure in the apparatus was calculated as described in 4.2.2. It was thus assumed that the circulating gas was saturated with vapor at the liquid temperature of the experiment, as calculated from the mean of inlet and outlet temperature readings. The partial pressure of CO<sub>2</sub> was then given from the total pressure, subtracting the solution vapor pressure:

$$p_{CO_2} = P_{tot} - p_{vap} \quad (5.2)$$

The absorption rates in circulating gas mode were calculated from a mass balance on the system, as given from the difference of inlet and outlet CO<sub>2</sub> flow:

$$R_{CO_2} = \frac{Q_{CO_2}^{in} - Q_{CO_2}^{out}}{60 \cdot v_m^0} \quad (5.3)$$

where  $R_{CO_2}$  (mol/s) is the molar absorption rate and  $v_m^0$  is the molar volume at Normal conditions. The amount of CO<sub>2</sub> entering the system is given by the mass flow controller as  $Q_{CO_2}^{in}$  (Nl/min). The amount of CO<sub>2</sub> going out of the system through the CO<sub>2</sub> analyzer is:

$$Q_{CO_2}^{out} = Q_{N_2}^{in} \frac{y_{CO_2}^{an}}{1 - \left( \frac{p_{vap}^{an}}{P} \right) - y_{CO_2}^{an}} \quad (5.4)$$

where  $Q_{N_2}^{in}$  is the amount of sweep gas given by the N<sub>2</sub> mass flow controller.  $p_{vap}^{an}$  is the vapor partial pressure in the sample gas, which is saturated at a temperature of 10°C after the cooler.  $y_{CO_2}^{an}$  is the fraction of CO<sub>2</sub> in the sample, as given by the instrument reading. The sensitivity of the calculated absorption rate to errors in  $Q_{CO_2}^{out}$  was generally low as  $Q_{CO_2}^{in}$  was always significantly larger.

The absorption rates are subject to random error propagating from the error in the individual measurements that enter into the calculation. A simple error analysis is given in appendix 3. The error in the stagnant gas experiments was found to be maximum 2.4%. For the experiments with circulating gas phase, the maxi-

mum error found was 12%, although most experiments have an error less than 5%. The difference is expected as the absorption rate in stagnant gas mode is determined more or less directly by the soap bubble meter measurement. In circulating gas mode, the absorption rate depend in a more complicated manner on the mass flow controllers and the analysis of CO<sub>2</sub>-content in the gas phase. The error is minimized by careful calibration of mass flow controllers in the desired operating range, and by minimizing the amount of CO<sub>2</sub> that leaves the system through the gas analyzer. The absorption rate is then principally determined by the feed CO<sub>2</sub> flow. In this respect an improvement of the setup was made during the course of the experimental work. A gas circulation pump was installed in the gas sampling line. This enabled the sample gas to be returned to the system instead of vented to the atmosphere. The CO<sub>2</sub> feed flow was diluted with a small N<sub>2</sub>-flow of 0.2 Nl/min to keep a small bleed flow, which served to stabilize the system and reduce the effect of possible leakage.

## 5.5 The mass transfer coefficient

The overall, gas film based mass transfer coefficient can be calculated by introducing the logarithmic mean driving force over the membrane length,  $\Delta p_{lm}$ , and the total inner membrane area of the module,  $a_m$ :

$$K_G(\text{mol/m}^2, \text{s, kPa}) = \frac{R_{CO_2}}{a_m \Delta p_{lm}} \quad (5.5)$$

with

$$\Delta p_{lm} = \frac{(p_{CO_2} - p_{CO_2}^*)_{in} - (p_{CO_2} - p_{CO_2}^*)_{out}}{\ln \frac{(p_{CO_2} - p_{CO_2}^*)_{in}}{(p_{CO_2} - p_{CO_2}^*)_{out}}} \quad (5.6)$$

The use of the logarithmic mean driving force in calculating the overall mass transfer coefficient is justified in this case by the small size of the contactor,

leading to small changes in gas and liquid composition from inlet to outlet (Kohl and Nielsen, 1997).

$p^*$  is here the partial pressure in equilibrium with the liquid “mixing-cup” CO<sub>2</sub>-loading, as calculated from the equilibrium model. The experimental conditions in this work were generally so that the gas phase was far from reaching equilibrium with the liquid bulk solution. The relation  $p_{CO_2}^*/p_{CO_2}$  was at most 0.5, corresponding to the highest loading and highest temperature (70°C) studied in the MDEA-system.

Most of the vapor in the sample gas is removed in the cooler prior to the analysis. The CO<sub>2</sub> volume fraction as given by the gas analyzer reading will thus be higher than the actual value of the gas in the membrane module, which is assumed saturated by the solvent vapor at the temperature of the experiment. The CO<sub>2</sub>-fraction of the gas phase in the apparatus was calculated by correcting the gas analyzer reading for these differences in vapor partial pressure. This gave the CO<sub>2</sub> mole fraction at the membrane *inlet* (see fig. 5.2).

$$y_{CO_2, in} = y_{CO_2}^{an} \left( 1 - \frac{P_{vap}^{app} - P_{vap}^{an}}{P_{in}} \right) \quad (5.7)$$

where  $P_{vap}^{app}$  is the solvent vapor pressure calculated at the average of the membrane inlet and outlet liquid temperatures. The membrane inlet and outlet CO<sub>2</sub> partial pressures are then given by:

$$P_{CO_2, in} = y_{CO_2, in} P_{in} \quad (5.8)$$

$$P_{CO_2, out} = \frac{y_{CO_2, in} n_{tot} - N_{CO_2} a_m}{n_{tot} - N_{CO_2} a_m} (P_{in} - \Delta P) = y_{CO_2, out} P_{out} \quad (5.9)$$

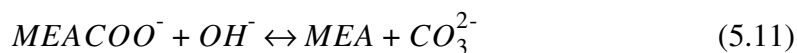
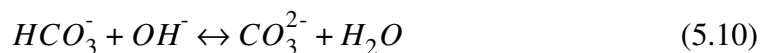
where  $n_{tot}$  is the total molar gas flow at the membrane inlet, as calculated from the orifice-meter reading. The pressure drop of the gas,  $\Delta P$ , was calculated from a correlation with gas flow, based upon measurements with an electronic micromanometer (Air Neotronics).



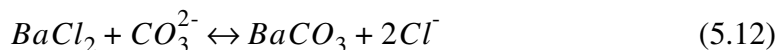
## 5.6 Liquid sample analysis

### 5.6.1 CO<sub>2</sub>-analysis

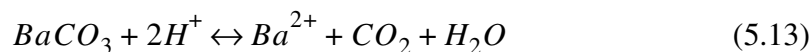
The liquid phase total CO<sub>2</sub> concentration was analyzed by a precipitation titration method. The sample was initially transferred to a flask containing 50 ml 0.1 M NaOH-solution to shift the equilibria so that all bound CO<sub>2</sub> in the form of bicarbonate and carbamate was converted to carbonate.



By subsequent addition of 25 ml 0.5 M BaCl<sub>2</sub>, the carbonate was precipitated in the form of barium carbonate:



The reaction was enhanced by heating, which also helped to agglomerate BaCO<sub>3</sub>-particles. The precipitated barium carbonate was collected by vacuum filtration through a 0.45 μm Millipore filter. The filtrate was thoroughly flushed with distilled water until the permeate had a neutral pH (100 ml was found sufficient). The filter was subsequently transferred to a graduated beaker, and dissolved with a known volume of 0.1 M HCl in excess:



This reaction was enhanced by careful boiling to remove the released CO<sub>2</sub>. After complete dissolution, distilled water was added to the 75 ml mark. Finally the remaining excess of HCl was back-titrated with a 0.1 M NaOH solution, using an automatic titrator (Metrohm 702 SM Titrino). Blind samples were analyzed to correct for CO<sub>2</sub> in NaOH/BaCl<sub>2</sub> solutions.

The total CO<sub>2</sub>-concentration in the original sample was given by:

$$c_{CO_2} = \frac{(V_{HCl} - V_t - \Delta V_b)}{2V_s} c_{NaOH} \quad (5.14)$$

where  $V_{HCl}$  is the total volume of 0.1 M HCl-solution added to dissolve the precipitate.  $V_t$  is the volume added to reach the equivalence point in the back-titration.  $\Delta V_b$  is the difference between total HCl and NaOH-titration volume for the blind sample and  $V_s$  is the sample volume.

As the total  $CO_2$  concentration normally was within an expected range, the following guidelines were followed:

- The sample volume (0.5-5 ml) was adapted to result in a minimum of 20 ml consumption of 0.1 M HCl in the dissolution of  $BaCO_3$ . This always assured a significant difference from the blind sample, normally corresponding to 0.1-0.3 ml.
- The total volume of 0.1 M HCl added was for convenience limited to 10-15 ml in excess.

The sample concentration was always calculated from the mean of two parallels. As shown in appendix 3, the error in the liquid  $CO_2$ -concentration is expected to be less than 2%.

### 5.6.2 Analysis of amine in the liquid phase

The liquid total amine analysis was done by titration of a sample on an automatic titrator, using 0.1 N  $H_2SO_4$  as titrating agent. The correct equivalence point of pH 4-5 was automatically identified by the titrator, and corresponded to the total amine initially in the unprotonated, protonated and carbamate forms.

75 ml distilled water was added to a graduated beaker, and a 0.5 ml sample added before titration. The total concentration of amine was then given by:

$$c_{am} = \frac{0.2 \cdot V_t}{V_s} \quad (5.15)$$

### *5.6 Liquid sample analysis*

---

where 0.2 is the molarity of  $\text{H}^+$  from the 0.1 N  $\text{H}_2\text{SO}_4$ .  $V_t$  is the titration volume and  $V_s$  is the sample volume. The concentration was calculated as the mean of at least two parallels, and the error was found to be less than 2% (appendix 3).



---

## *Results and discussion of the absorption experiments*

---

### 6.1 Introduction

In this chapter the results from the absorption experiments are shown and discussed qualitatively in terms of the overall mass transfer coefficients,  $K_G$ . The results in terms of the absorption rates are shown in chapter 7 and compared with the predictions of the developed model.

The overall mass transfer coefficient is an important yardstick in the traditional approach for designing gas/liquid contactors. The influence of parameters like gas velocity, liquid velocity, partial pressure and temperature on the mass transfer coefficient may serve to find the optimal operating conditions and design of an industrial scale contactor. The total membrane area required for a given separation may be estimated by (adapted from Levenspiel, 1984):

$$a_m = \frac{G}{P} \int_{P_A^{out}}^{P_A^{in}} \frac{dp_A}{K_G (P_A - P_A^*)} \quad (6.1)$$

where  $G$  is the molar gas flow of inerts. The integration is performed from the outlet to the inlet of the membrane contactor. It is seen that the higher the mass transfer coefficient, the lower is the membrane area required for separation. A lab-scale membrane module may in principle be looked upon as a differential element of the industrial scale contactor, with a membrane area  $da_m$  inflicting a change  $dp_A$  in the partial pressure. The module used in this work is however of an idealized type without the liquid mixing points that is used in the commercial Kvaerner MGA-contactor. The discussion will thus focus only on the trends that may be seen from the experimental data.

## 6.2 The individual mass transfer coefficients

The overall, gas side based mass transfer coefficient,  $K_G$  ( $\text{mol/m}^2\text{s,kPa}$ ), is a lumped parameter where the effects of the hydrodynamics of the gas and liquid phases, the chemical reaction and the presence of the membrane are combined. It may be written as a series of mass transfer resistances, of the gas film, the membrane and the liquid boundary layer:

$$K_G = \frac{1}{\frac{1}{k_g} + \frac{1}{k_m} + \frac{H}{Ek_l^0}} \quad (6.2)$$

where  $k_g$  and  $k_m$  are the mass transfer coefficients of the gas phase and the membrane with the unit ( $\text{mol/m}^2\text{s,kPa}$ ).  $k_l^0$  is the liquid side mass transfer coefficient with the unit ( $\text{m/s}$ ).  $E$  is the enhancement factor correcting the liquid phase physical mass transfer coefficient for the presence of chemical reaction. The individual terms are further discussed in the following.

### 6.2.1 Mass transfer correlations for the shell and the tube side

Convective mass transfer coefficients can generally be correlated by a relation of the form

$$Sh \propto Re^\alpha Sc^\beta f(\text{geometry}) \quad (6.3)$$

where  $Sh$ ,  $Re$  and  $Sc$  are the Sherwood number, the Reynolds number and the Schmidt number, respectively, and  $f$  is some function of geometry. The exponents  $\alpha$  and  $\beta$  and the function  $f$  must be determined from mass transfer experiments or, if available, from relations developed for the analogous heat transfer problem.

No correlation for the shell side mass transfer coefficient has been proposed that is applicable to a wide range of systems and geometries. An overview is given by Gabelman and Hwang (1999). The mass transfer coefficient may be experimentally determined from experiments with a fast reacting system like  $\text{SO}_2$  absorbing in NaOH-solution flowing inside the tubes. Alternatively a slow liquid side controlled system like  $\text{CO}_2$  absorbing in water may be utilized, with the liquid flowing on the shell side.

In contrast to the shell side, tube side mass transfer is well described and a general correlation has been established. Several authors have verified that the mass transfer coefficient for laminar flow inside straight tubes follow the Graetz-Leveque solution (Kreulen et al., 1993a; Gabelman & Hwang, 1999).

$$Sh = 1.62 \left( \frac{d_i}{L} Re Sc \right)^{1/3} \quad (6.4)$$

where  $d_i$  and  $L$  are the inner diameter and length of membrane tubes, respectively. Writing out the dimensionless groups result in the following expression for the liquid side mass transfer coefficient:

$$k_l^0 = 1.62 D_A^{2/3} \left( \frac{v_l}{L d_i} \right)^{1/3} \quad (6.5)$$

### 6.2.2 The enhancement factor

The enhancement factor  $E$ , being the relation between the chemical and the physical absorption flux at the same driving force, may be visualized as in figure 6.1. Here the enhancement factor is given as a function of two parameters, the Hatta modulus and the enhancement factor of an infinitely fast reaction. The enhancement factor may be considered a correction to the liquid side mass transfer coefficient due to the chemical reaction occurring in the concentration boundary layer.

The Hatta modulus,  $Ha$ , indicative of the rate of diffusional transport vs. chemical reaction, is given by:

$$Ha = \frac{\sqrt{D_A k_2 c_B}}{k_l^0} \quad (6.6)$$

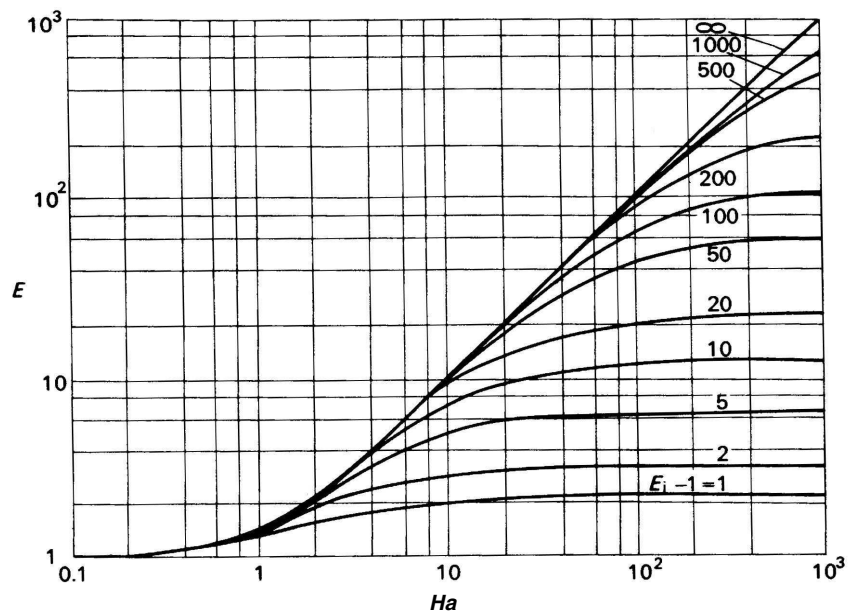


FIGURE 6.1: Enhancement factor for a second order reaction (Danckwerts, 1970)



The enhancement factor for an infinitely fast reaction,  $E_i$ , is dependent on the choice of a mass transfer model. A general expression may be written as:

$$E_i = \left( 1 + \frac{D_B c_B}{\nu D_A c_{Ai}} \right) \left( \frac{D_B}{D_A} \right)^{(n-1)} \quad (6.7)$$

with  $n = 1$  for the film model and  $n=0.5$  for the penetration model. Boundary theory, which is the basis for the Graetz-Leveque solution (eq. (6.5)) require  $n=0.66$ . Equation (6.7) then reflects the expected dependence of mass transfer coefficients on the species diffusivities as given by Cussler (1994a) for the different types of traditional mass transfer theory.

As described by Levenspiel (1984), at increasing values of the Hatta modulus the chemical reaction is approaching the liquid surface, where  $E$  is limited by the value given by  $E_i$ . Mass transfer is then limited by diffusion of all components in the liquid phase. In the increasing straight line portion of the curves in figure 6.1, where the requirement

$$2 < E \ll E_i \quad (6.8)$$

is fulfilled, the system is in the pseudo first order fast reaction regime, where  $E$  may be taken equal to  $Ha$ . In the case when the gas film and membrane resistances are negligible compared to the liquid side resistance, the following expression results for the mass transfer flux:

$$N_A = \frac{Ek_l^0}{H} (p_A - p_A^*) \quad (6.9)$$

Inserting the condition  $E = Ha$  in eq. (6.9) gives:

$$N_A = \frac{\sqrt{D_A k_2 c_B}}{H} (p_A - p_A^*) \quad (6.10)$$

In the pseudo first-order fast regime, the flux is independent of the hydrodynamic conditions (flow rates) and the sensitivity to the rate of the chemical reac-

tion is at the maximum with  $N_A \propto k_2^{0.5}$ . This defines the ultimate condition for the measurement of rate constants in CO<sub>2</sub>/alkanolamine systems (Danckwerts, 1970; Versteeg et al., 1996).

Eq. (6.7) is strictly valid only for irreversible reactions. The effect of reversibility is to lower the value of  $E_i$ , thus narrowing the range of validity for eq. (6.8) (Versteeg et al., 1996). The influence of reaction reversibility is minimized by having the CO<sub>2</sub> loading at a minimum (thus  $p^* \approx 0$ ) and reducing the gas/liquid contact time. The possibility and optimum conditions for measuring rates of reaction is further discussed in 6.4.2 and in chapter 8.

It may be noted that there are some differences in published literature regarding which form of the infinite enhancement factor is suitable for studying gas absorption in hollow fibers, although an expression similar to (6.7) was proposed by Feron and Jansen (2002). Kreulen et al. (1993b) used a form of eq. (6.7) corresponding to  $n=1.33$ , discussing the problem of using the enhancement factor on absorption in hollow fibers, as the driving forces for chemical and physical absorption cannot in general be taken equal. They, however, defined a modified enhancement factor by simply relating the chemical and physical fluxes and used it in discussing the effect of chemical reaction.

Kumar et al. (2002) discuss the validity of the penetration model for hollow fiber absorption and found it to be limited to the case where the penetration depth is significantly lower than the radius of the hollow fiber. This is normally the case, except at very large contact times. The liquid may then be considered to be of infinite depth, analogous to the original penetration model setup, where gas is absorbed in a falling liquid film with a short gas/liquid contact time. Kumar et al. (2002) calculated the Hatta modulus from eq. (6.6) and  $E_i$  from a relation similar to that resulting from penetration model (Hogendoorn et al., 1997) with the properties of the liquid defined on the axis of the fiber, thus using the value of  $c_B$  at  $r=0$  (similar to the value at the inlet). From simulation with a rigorous mass transfer model they concluded that the conventional mass transfer models can be used as a tool to describe the results from absorption in a hollow fiber contactors.

### 6.2.3 Mass transfer in the membrane

As long as the microporous membrane is operating in non-wetted mode and the liquid side pressure is lower than the breakthrough pressure, the pores may be considered totally filled with gas. The gas/liquid interface is then located at the liquid side pore opening as illustrated in fig. 1.2. The pores of the membranes used in this study have dimensions of 1-10  $\mu\text{m}$ , which is sufficient that any contribution from Knudsen diffusion can be neglected. The mass transfer inside the pores is thus governed by molecular diffusion only. The mass transfer coefficient for a stagnant gas film is given by:

$$k' = \frac{D_A}{l} \quad (6.11)$$

where  $D_A$  is the molecular diffusivity of the transferred species and  $l$  is the film thickness.  $k'$  is the mass transfer coefficient with the unit (m/s), thus corresponding to a driving force in units of molar concentration. It is converted to partial pressure driving force ( $\text{mol/m}^2\text{s,Pa}$ ) when dividing by  $RT_g$ , the product of the ideal gas constant and the gas phase temperature.

The presence of the membrane is accounted for by defining an effective diffusivity as the product of the molecular diffusivity and membrane porosity. This serves to correct for the reduced cross section available for mass transport. The diffusional distance is increased as the membrane pores are not straight. The membrane wall thickness is thus corrected by the membrane tortuosity. When the curvature of the hollow fiber wall is taken into account, the mass transfer coefficient of the membrane is given by.

$$k'_m = \frac{D_A \varepsilon}{\tau R_i \ln(R_o/R_i)} \quad (6.12)$$

where  $R_o$  and  $R_i$  are the outer and inner membrane radius.  $\varepsilon$  and  $\tau$  are the membrane porosity and tortuosity, respectively. For the membrane used in this study the resulting value of  $k'_m$  for  $\text{CO}_2$  at  $40^\circ\text{C}$  is 0.03 m/s. At this temperature, the diffusivity of  $\text{CO}_2$  is approximately  $1.8 \times 10^{-5} \text{ m}^2/\text{s}$  in the gas ( $\text{N}_2$ ) and

$1.3 \times 10^{-9} \text{ m}^2/\text{s}$  in the liquid (30% MEA). The importance of preventing any liquid from penetrating into the membrane pores is obvious as the mass transfer would then be limited by molecular diffusion through a liquid layer with diffusivities 10000 times lower than in the gas.

### 6.3 Results

CO<sub>2</sub> absorption measurements were done in the lab-scale membrane gas absorber as described in chapter 5. The results are given in figure 6.2-6.9 for the following experimental series:

- Circulating gas phase: 30% MEA/water with variable gas velocity, CO<sub>2</sub> partial pressure, liquid velocity and temperature
- Stagnant gas phase (pure CO<sub>2</sub> + vapor): 15% MEA/water with variable liquid velocity and temperature, 23.5% MDEA/water with variable liquid velocity and temperature

Base case values for each of the variables are given in table 5–3. The results are here given in terms of the overall mass transfer coefficients. Regression lines are included to show the trends clearer. In chapter 7 the corresponding absorption rates are shown and compared with the predictions of the developed model.

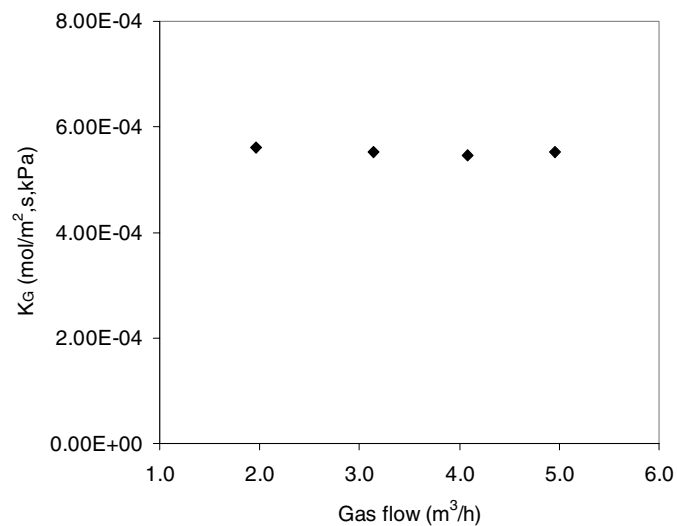


**FIGURE 6.2:** influence of gas flowrate on the mass transfer coefficient, from an experiment with 30% MEA at 40 °C ,  $p_{\text{CO}_2} = 5 \text{ kPa}$ ,  $y=0.04$ .

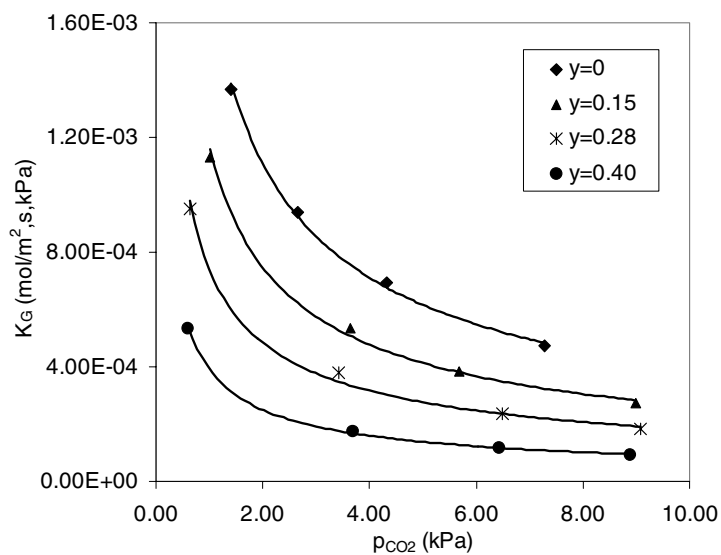


**FIGURE 6.3:** Influence of CO<sub>2</sub> partial pressure on the mass transfer coefficient. 30% MEA at 40 °C .

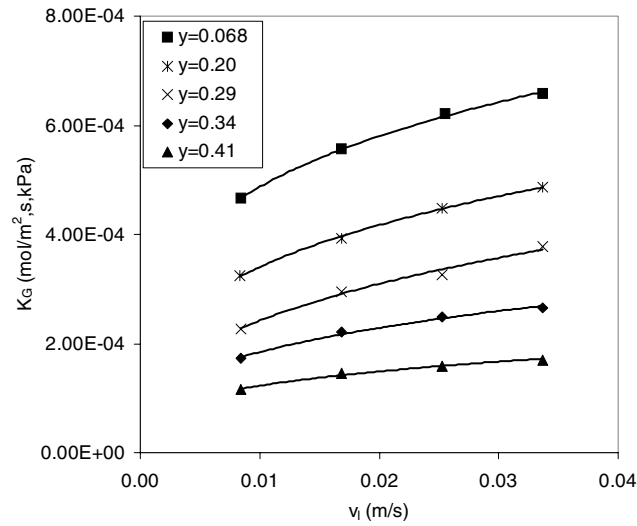


FIGURE 6.4: Influence of liquid velocity on the mass transfer coefficient. 30% MEA at 40 °C ,  $p_{CO_2}$  =5 kPa.

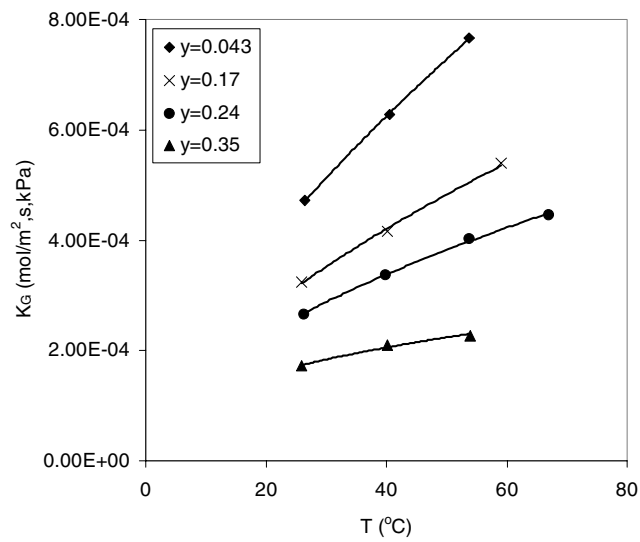


FIGURE 6.5: Influence of temperature on the mass transfer coefficient. 30% MEA,  $p_{CO_2}$  =5 kPa.

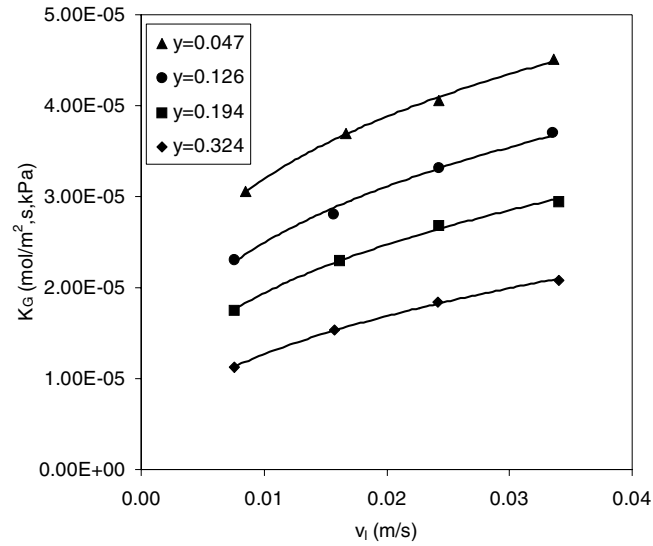


FIGURE 6.6: Influence of liquid velocity on the mass transfer coefficient. 15% MEA at  $T=40^\circ\text{C}$ ,  $p_{\text{CO}_2}=90\text{ kPa}$  (stagnant gas phase).

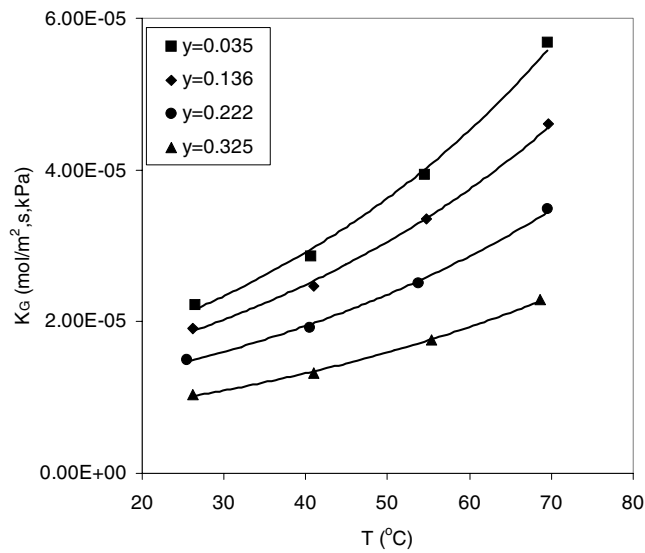
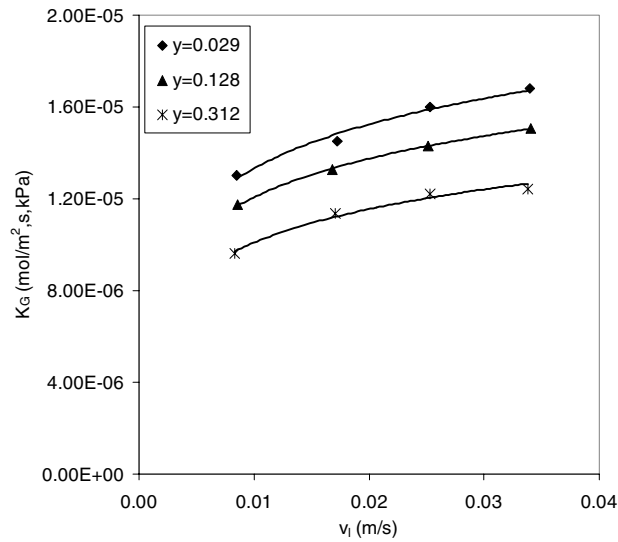
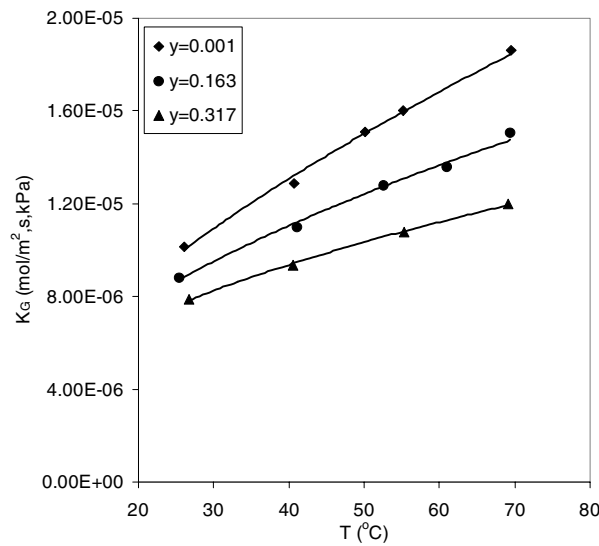


FIGURE 6.7: Influence of temperature on the mass transfer coefficient. 15% MEA,  $p_{\text{CO}_2}=98-70\text{ kPa}$  (stagnant gas phase).



**FIGURE 6.8: Influence of liquid velocity on the mass transfer coefficient. 23.5% MDEA,  $p_{CO_2} = 90$  kPa (stagnant gas phase).**

---



**FIGURE 6.9: Influence of temperature on the mass transfer coefficient. 23.5% MDEA,  $p_{CO_2} = 98-70$  kPa (stagnant gas phase).**

---



## 6.4 Discussion

### 6.4.1 Implications of the mass transfer coefficient

The measured mass transfer coefficients, given in figure 6.2-6.9, have values of similar size as those published by e.g. Nishikawa et al. (1995) and Feron and Jansen (2002), although the experimental conditions are not directly comparable. As can be seen from figure 6.2, the mass transfer coefficient is not influenced by the increasing gas velocity. From correlations of mass transfer coefficients,  $k_g \propto v_g^{0.5-1}$  would normally be expected (Gabelman and Hwang, 1999). From considering the definition of the overall mass transfer coefficient (6.2) it may then be concluded that

$$k_g \gg k_m + \frac{Ek_l^0}{H} \quad (6.13)$$

The mass transfer resistance of the gas phase is thus negligible compared to the membrane and liquid side resistances. This statement is based upon experiments with a 30% MEA solution. However, the same must be valid for the MDEA system due to the lower rate of the chemical reaction, which reduces the value of the enhancement factor. Similar conclusions was also made by Qi and Cussler (1985b), Aroonwilas et al. (1999) and Kumazawa (2000).

This is not surprising, as the CO<sub>2</sub>/alkanolamine/water systems are normally expected to have the major mass transfer resistance on the liquid side. However, a MEA/water solution would still be expected to have a significant contribution from gas side resistances at low CO<sub>2</sub> partial pressures, when considering conventional gas/liquid contacting equipment like packed towers. The physical liquid film coefficient of the idealized straight tube membrane is, however, significantly lower ( $k_l^0 \approx 5 \times 10^{-6}$  m/s) than what is achieved for liquid flowing through a tower packing ( $k_l^0 = 10^{-5} - 10^{-4}$  m/s). In addition, the membrane design, with spacers between the tube layers, combined with the high actual gas velocities of 3.8-12.5 m/s provide an efficient mixing of the gas phase.

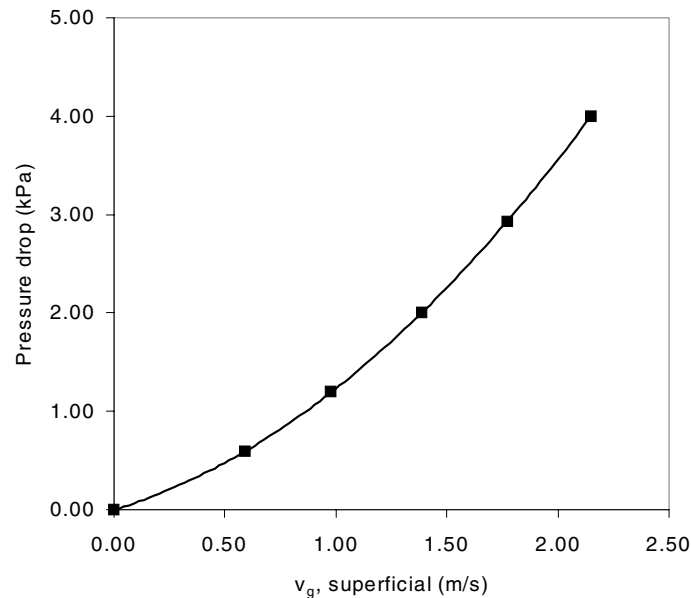


**FIGURE 6.10: Pressure drop in the lab-scale membrane module**

In figure 6.10, the result of the pressure drop measurements over the membrane gas side is shown. The increase in pressure drop with the square of gas velocity is characteristic of the turbulent flow regime, thus supporting the assumption of the presence of local shell side turbulence as discussed by Gabelman and Hwang (1999).

From figure 6.3 it can be seen that the mass transfer coefficient is a strong decreasing function of partial pressure. A similar behavior is shown by Aroonwilas et al. (1999) studying the overall mass transfer coefficient of tower packings when absorbing  $\text{CO}_2$  in an aqueous alkanolamine/water system. It is resulting from the increasing depletion of the alkanolamine at the interface, leading to a reduced rate of reaction, and the onset of diffusional limitations caused by increasing concentration gradients.

The considerable reduction of  $K_G$  with increasing liquid loading observed in all the figures is obvious as the concentration of free alkanolamine is correspondingly decreasing. Figure 6.4, 6.6 and 6.8 show the effect of increasing liquid

velocity on mass transfer coefficient for the MEA/water and MDEA/water systems. From eq. (6.5) it is seen that the physical mass transfer coefficient of the liquid phase,  $k_l^0$ , is proportional to  $v_l^{0.33}$ . A similar dependence would be expected if the instantaneous regime was realized, while practically no dependence of liquid velocity would be expected in the fast reaction regime. The curves then indicate that these experiments are closer to the instantaneous regime than the fast regime. This is further discussed below.

Figure 6.5, 6.7 and 6.9 show the effect of increasing temperature on the mass transfer coefficient. The strong increase of the mass transfer coefficient with temperature simply reflects the fact that both diffusivities and reaction rates are increasing functions of temperature. The temperature effect seen from the experiments with “pure CO<sub>2</sub>” stagnant gas phase is somewhat distorted by the fact that the liquid vapor pressure is increasing with temperature, leading to a slight decrease in the CO<sub>2</sub> partial pressure.

The fraction of membrane resistance compared to the overall resistance, given by:

$$R_m^{rel} = \frac{\frac{1}{k_m}}{\frac{1}{K_G}} = \frac{K_G}{k_m} \quad (6.14)$$

was calculated for all the experiments with diluted circulating gas phase (noting that gas and membrane resistance may be neglected in the case of stagnant gas/pure CO<sub>2</sub> gas phase). The highest value observed was  $R_m^{rel} = 0.12$ , corresponding to the lowest partial pressure and the lowest loading tested. These experiments were done in a 30% MEA-solution, with a higher rate of reaction than most other amine systems. This may thus be considered an upper limit for the relative membrane resistance, showing that the liquid side resistance is by far the dominating one.

### 6.4.2 The possibility of measuring diffusivities and rates of reaction

In order to observe in which regime the experiments have been performed, the enhancement factors were calculated by relating the experimentally observed flux to the flux that would have been observed without the presence of the chemical reaction. In case of physical absorption of CO<sub>2</sub>, the membrane resistance is negligible compared to the liquid side resistance, thus leading to:

$$E = \frac{N_{CO_2}}{\frac{k_l^0}{H} \Delta p_{lm}} \quad (6.15)$$

with  $k_l^0$  calculated by equation (6.5).

As described in 6.2.2, the regime may be characterized by relating  $E$  to  $E_i$  and  $Ha$ . This has been done for the experiments described above. The values of the relative enhancement factors,  $E/E_i$  and  $E/Ha$ , are plotted for the low loading experiments in figure 6.11-6.17. As the back-pressure of the liquid bulk is negligible for the low loadings considered here and as the change in CO<sub>2</sub> partial pressure from inlet to outlet is very small, the driving force for chemical and physical absorption is approximately similar. The penetration model equation for  $E_i$  was used, similar to Kumar et al. (2002), as this gave somewhat better results than the relation based on boundary layer theory (which gave  $E/E_i$  higher than 1 in some cases). The following conclusions may be drawn:

- The only experiments that may be placed in a specific regime is the 15% MEA/pure CO<sub>2</sub> series. From fig. 6.14 and 6.15 it can be seen that  $E$  is very close to  $E_i$ , which is characteristic of the instantaneous reaction regime, where diffusivities are rate limiting.
- The other experiments are done in a transition region where both diffusion and rate of the chemical reaction is important.

- From figure 6.11 it can be seen that the  $E$  approaches  $Ha$  at decreasing partial pressure. Thus, from performing experiments at low partial pressure, the pseudo first order regime may be realized.
- From figure 6.12 and 6.16 it can be seen that the relative importance of the chemical reaction is increasing with increasing liquid velocity, as  $E$  is approaching  $Ha$ . This is a consequence of the reduced contact time at higher liquid velocities, reducing the time available for diffusion.
- From figure 6.13 and 6.17 it can be seen that the relative importance of the chemical reaction is decreasing with temperature, as  $E/Ha$  decreases.

The sensitivity of the mass transfer to the chemical reaction is thus facilitated by low partial pressure, high liquid velocity and low temperature. Even if rate constants preferably are measured in the pseudo first order regime and diffusivities preferably are measured in the instantaneous regime, the use of a numerical mass transfer model will make these requirements less strict (Versteeg et al., 1996). This is supported by a sensitivity analysis on the model developed in this work and is further discussed in chapter 8.

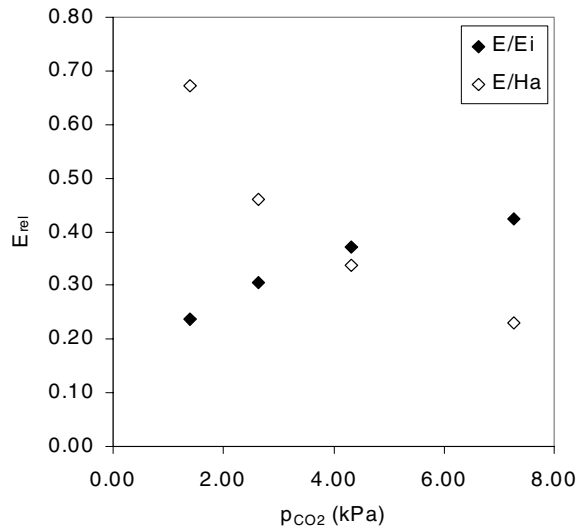


**FIGURE 6.11:** Relative enhancement factors as function of partial pressure, from experiments with 30% MEA and circulating gas phase.  $Ha=1940$ ,  $E_i=5500-1100$ .

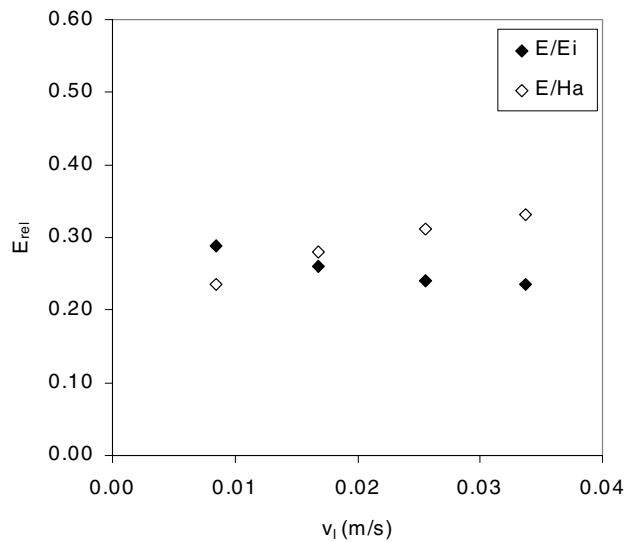


**FIGURE 6.12:** Relative enhancement factors as function of liquid velocity, from experiments with 30% MEA and circulating gas phase.  $Ha = 2100-1300$ ,  $E_i=1800$ .

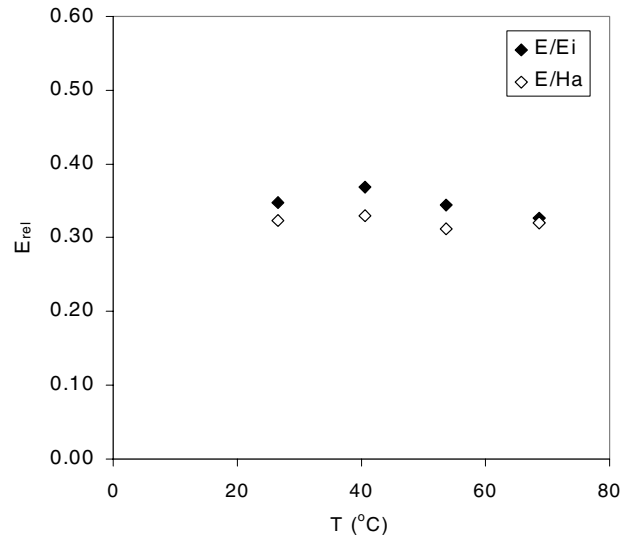


**FIGURE 6.13:** Relative enhancement factor as function of temperature,, from experiments with 30% MEA and circulating gas phase.  $Ha=1300-3300$ ,  $E_i=1200-3200$ .

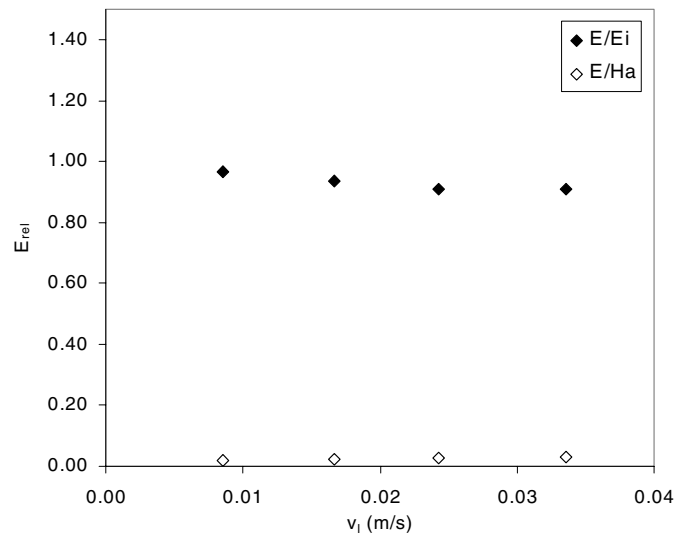


**FIGURE 6.14:** Relative enhancement factors as function of liquid velocity, from experiments with 15% MEA and stagnant gas phase.  $Ha=1000-1700$ ,  $E_i=37$ .

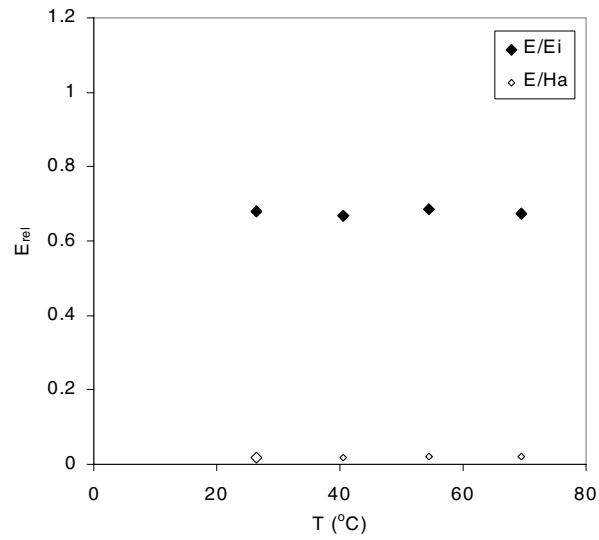


**FIGURE 6.15:** Relative enhancement factors as function of temperature, from experiments with 15% MEA and stagnant gas phase.  $Ha=900-2400$ ,  $E_i=25-74$ .

---

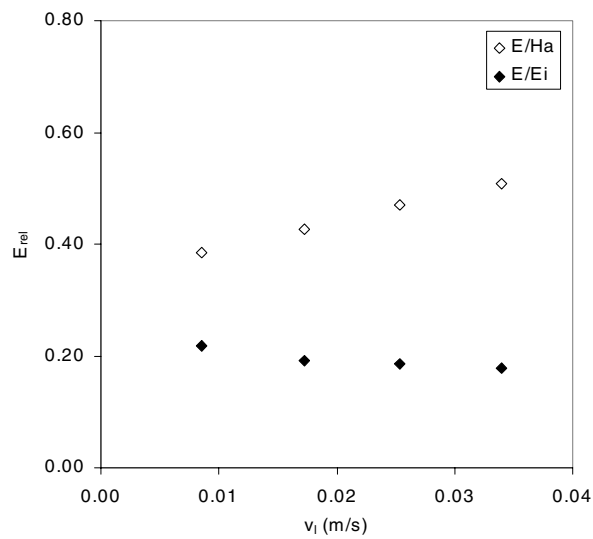


**FIGURE 6.16:** Relative enhancement factors as function of liquid velocity, from experiments with 23.5% MDEA and stagnant gas phase.  $Ha=26-43$ ,  $E_i=770$ .

---



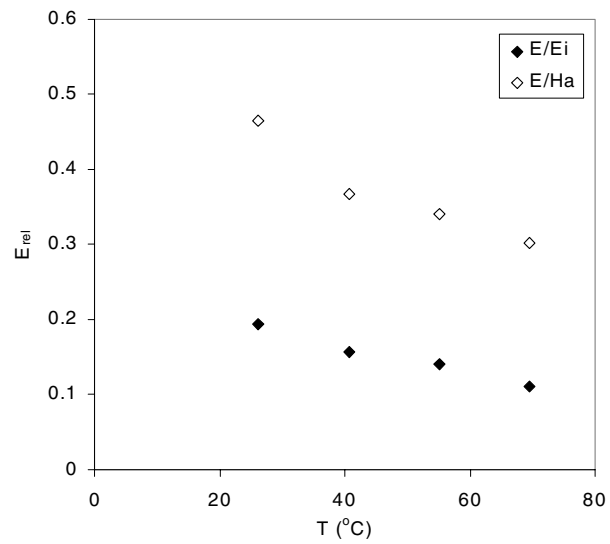


**FIGURE 6.17: Relative enhancement factors as function of temperature, from experiments with 23.5% MDEA and stagnant gas phase.  $Ha=20-63$ ,  $E_i=147-263$ .**

---



# *Modeling of the membrane gas absorber*

---

## **7.1 Introduction**

In order to simulate and predict the performance of the membrane gas absorber, a rigorous model based upon differential mass balances is needed. The results of the experiments described in chapter 5 and 6 are useful in the model development, as the model prediction of trends upon a single variable may be verified. Appropriate assumptions and simplifications may be made based upon conclusions from the experimental study. The goal has been to develop a predictive model capable of simulating the operation on an industrial scale, thus taking advantage of the linear scale-up of the membrane gas absorbers.

The model may be separated into different parts. First a model is needed to describe the gas and liquid flow and to set the limitations for the flow situations in which the model can be used. In addition, transport models for the diffusing substances are needed. Similarly, models for energy transport must be included. The chemistry of the system requires an equilibrium model and a kinetic model as described in chapter 3 and 4. Finally, a subset of routines are needed to predict the physical properties of the system.

## 7.2 Description of the model equations

### 7.2.1 The flow structure

Based upon the measurements of the overall mass transfer coefficient vs. increasing gas velocity and the pressure drop measurements, discussed in 6.4.1, the gas flow is assumed to be perfectly mixed laterally and in axial plug flow. This is facilitated by the membrane module design with interconnected tube layers separated by spacers, which contributes to enhancing the lateral mixing of the gas phase.

It is further assumed that gas flow is counter or co-current to the liquid flow. The model is thus not directly representative of the typical flow situation in a single industrial low pressure membrane module, which would be cross-current (fig. 1.3). However, normally the concentration changes in a single module are modest, thus making the difference between counter and co-current very small. This can be seen from the differences in the logarithmic mean driving force when calculated based upon counter and co-current flow. Simulations with the completed model on the countercurrent experiments performed in this work showed a negligible difference between co-current and countercurrent operation. An average of a counter and co-current calculation will in any case give a good estimate for the cross-current performance.

The diameter of the tubes in the module used for the experiments was 3.0 mm and the linear liquid velocities was in the range 0.5-4 cm/s. Industrial contactors will have even lower diameters in the range 0.5-1.5 mm. With densities and viscosities of the systems under consideration this gives liquid Reynolds numbers well below 100. In tube flow the transition to turbulence is known to occur at  $Re=2100$ , and the liquid flow is thus obviously in the laminar regime. The radial velocity profile will then be parabolic as described by Bird et al. (2002). This is known as the Hagen-Poiseuille profile.

$$v_z = 2v_{z, av} \left( 1 - \left( \frac{r}{R_i} \right)^2 \right) \quad (7.1)$$

where  $v_{z,av}$  is the average linear liquid velocity, obtained by dividing the total flow-rate by the cross-sectional area.

The velocity profile is assumed to be fully developed. This is supported by the fact that the liquid inlet region is covered by membrane fiber potting. The velocity profile of the liquid flow then has time to stabilize before the mass transfer zone is reached. The length of the entrance region,  $L_e$ , may be calculated from the following relation (Geankopolis, 1993):

$$\frac{L_e}{D} = 0.0575 Re \quad (7.2)$$

where  $D$  is the inner diameter of the tube. With a Reynolds number of 100 and a tube diameter of 3 mm this gives an entrance length of 1.7 cm, while the potting length is 7 cm for this membrane module. This justifies the assumption of a fully developed parabolic velocity profile, as illustrated in figure 7.1.

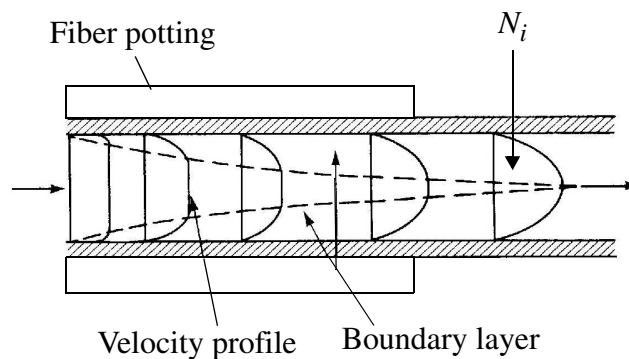


**FIGURE 7.1: Entrance region of a membrane tube. Adapted from Geankopolis (1993)**

### 7.2.2 Flux across the membrane

The flow model of the gas and liquid phase including the transfer flux is illustrated in figure 7.2. The transfer flux across the membrane is modeled using the simple resistance in series approach, including the gas film and the membrane mass transfer coefficients.

$$N_i = \frac{1}{RT_g \left( \frac{1}{k'_{i,g}} + \frac{1}{k'_{i,m}} \right)} (p_i - H_i c_{i,s}) + x_i \sum_i N_i \quad (7.3)$$

where  $c_{i,s}$  is the concentration of component  $i$  at the liquid/membrane interface. The membrane mass transfer coefficient,  $k'_{i,m}$  (m/s) is defined by equation (6.12). Following the discussion in 6.4, the gas film coefficient,  $k'_{i,g}$  is specified at a value of 1000, corresponding to a negligible mass transfer resistance of the gas phase.

This model describes the flux of water across the membrane in addition to the CO<sub>2</sub> flux. The last term on the right hand side of eq. (7.3) accounts for diffusion engendered bulk motion, which may be significant e.g. when the incoming gas is dry, resulting in a large flux of vapor countercurrent to the absorbing CO<sub>2</sub>. Multicomponent coupling effects have been neglected, using only pseudo-binary diffusivities. The alkanolamine is assumed non-volatile, following the discussion in chapter 4.

The conductive sensible heat flux is modeled in an analogous manner:

$$Q = \frac{1}{\frac{1}{h_g} + \frac{1}{h_m}} (T_g - T_{l,s}) \quad (7.4)$$

where  $h_g$  and  $h_m$  are the gas phase and membrane heat transfer coefficients, respectively.  $T_{l,s}$  is the temperature at the liquid/membrane interface.

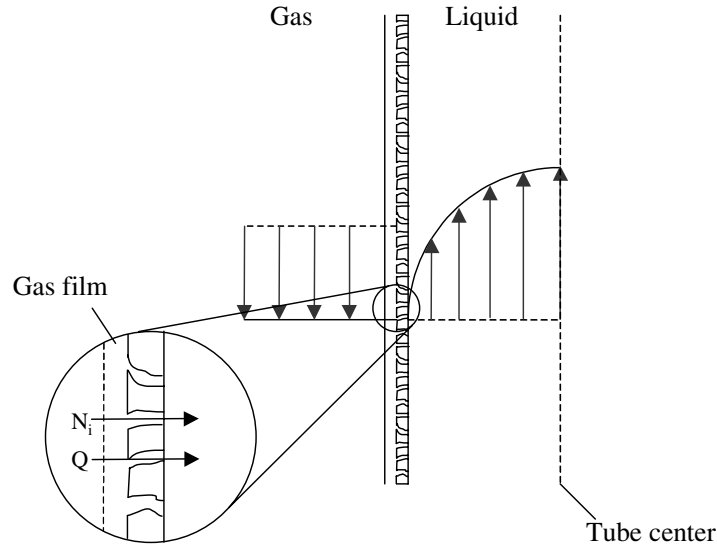


**FIGURE 7.2: The structure of the model**

Analogous to the mass transfer, the heat transfer resistance of the gas phase,  $1/h_g$  is considered negligible compared to the membrane resistance.  $h_g$  is thus specified as a large number. The membrane heat transfer coefficient is calculated from the thermal conductivities of PTFE and of the gas phase modeled as two resistances in parallel:

$$h_m = \frac{\varepsilon \lambda_g}{\tau R_i \ln(R_o/R_i)} + \frac{(1 - \varepsilon) \lambda_{PTFE}}{\tau R_i \ln(R_o/R_i)} \quad (7.5)$$

### 7.2.3 Balance equations for the gas phase

Following the plug flow assumption, the mass balance equation of the gas phase is given by:

$$-\frac{dn_{tot}}{dz} = \sum_i N_i \frac{a}{\varepsilon_g} \quad (7.6)$$

where  $n_{tot}$  (mol/m<sup>2</sup>,s) is the molar flux of the gas phase referred to the free gas cross section area.  $N_i$  (mol/m<sup>2</sup>,s) is the molar flux of component  $i$  from the gas through the membrane and into the liquid phase referred to the inner surface area of the membrane tubes.  $\epsilon_g$  is the fraction of the total area available for the gas flow, while  $a$  (m<sup>2</sup>/m<sup>3</sup>) is the specific inner surface area of the membrane module.

Introducing the ideal gas law,  $n_{tot} = Pv_g/RT_g$ , and expanding gives:

$$\frac{v_g}{RT_g} \frac{\partial P}{\partial z} + \frac{P}{RT_g} \frac{\partial v_g}{\partial z} - \frac{Pv_g}{RT_g^2} \frac{\partial T_g}{\partial z} = \sum_i N_i \frac{a}{\epsilon_g} \quad (7.7)$$

This equation can be solved for the gas velocity derivative:

$$\frac{\partial v_g}{\partial z} = -\frac{v_g}{P} \frac{\partial P}{\partial z} + \frac{v_g}{T_g} \frac{\partial T_g}{\partial z} - \frac{RT_g}{P} \sum_i N_i \frac{a}{\epsilon_g} \quad (7.8)$$

The equation describing the partial pressure of gas components is derived in an analogous manner from the balance of component  $i$ :

$$-\frac{dn_i}{dz} = N_i \frac{a}{\epsilon_g} \quad (7.9)$$

and introduction of  $n_i = p_i v_g / RT_g$ . The resulting equation is:

$$\frac{\partial p_i}{\partial z} = -\frac{p_i}{v_g} \frac{\partial v_g}{\partial z} + \frac{p_i}{T_g} \frac{\partial T_g}{\partial z} - \frac{RT_g}{v_g} N_i \frac{a}{\epsilon_g} \quad (7.10)$$

The pressure drop gradient,  $\partial P / \partial z$ , is taken from a correlation based upon the measurements shown in figure 6.10.

The thermal balance for the gas phase is straightforward when disregarding any frictional heat and heat loss to the surroundings:



$$\sum_i c_{p,i} n_i \frac{\partial T_g}{\partial z} = Q \quad (7.11)$$

where  $c_{p,i}$  is the specific heat of component  $i$ .

#### 7.2.4 Transport model for the liquid phase

Instead of using mass transfer coefficients for the liquid phase, which would be considered a lumped parameter model, a rigorous approach is chosen based upon differential mass balances for the liquid phase. The mass transport model for the liquid phase is derived from the equation of continuity for species in a reacting mixture (Bird et al., 2002). It is assumed that the transport mechanism in the liquid phase is by convection in the axial-direction and diffusion in the radial direction. The diffusional flux is described by Fick's law in cylindrical coordinates. With the parabolic velocity profile the balance for component  $i$  becomes:

$$2v_{z,av} \left(1 - \left(\frac{r}{R_i}\right)^2\right) \frac{\partial c_i}{\partial z} = \frac{1}{r} \frac{\partial}{\partial r} \left( r D_i \frac{\partial c_i}{\partial r} \right) + r_i \quad (7.12)$$

One such equation is needed for each of the components that influence the rate of absorption of CO<sub>2</sub>. This include free CO<sub>2</sub>, free alkanolamine and the bound CO<sub>2</sub> reaction products. Note that the component diffusivity can not be taken outside the derivation, as significant radial diffusivity gradients may occur. This is a result of the coupling between CO<sub>2</sub> loading and viscosity and between viscosity and diffusivity, as described in 7.3.1 and 7.3.4. Expansion of the right-hand side gives:

$$2v_{z,av} \left(1 - \left(\frac{r}{R_i}\right)^2\right) \frac{\partial c_i}{\partial z} = D_i \left( \frac{1}{r} \frac{\partial c_i}{\partial r} + \frac{\partial^2 c_i}{\partial r^2} \right) + \frac{\partial D_i}{\partial r} \frac{\partial c_i}{\partial r} + r_i \quad (7.13)$$

The thermal balance can be formulated similarly, using the thermal conductivity of the amine mixture and the heat of reaction for the CO<sub>2</sub>-alkanolamine reac-

tion. Thermal conductivity is taken outside the derivation, thus neglecting any possible effects of varying liquid viscosity, which is unknown and expected to be of minor importance.

$$2v_{z,av}\left(1 - \left(\frac{r}{R_i}\right)^2\right)c_{p,l}\rho\frac{\partial T}{\partial z} = \lambda_l\frac{1}{r}\frac{\partial}{\partial r}\left(r\frac{\partial T}{\partial r}\right) + r_i(-\Delta H_r) \quad (7.14)$$

The following boundary conditions are required:

For concentrations:

$$z = 0 \quad c_i = c_i^0 \quad (7.15)$$

$$r = 0 \quad \frac{\partial c_i}{\partial r} = 0 \quad (7.16)$$

$$r = R_i \quad \frac{\partial c_i}{\partial r} = \frac{N_i}{D_i} \quad (7.17)$$

For temperature:

$$z = 0 \quad T_l = T_l^0 \quad (7.18)$$

$$r = 0 \quad \frac{\partial T_l}{\partial r} = 0 \quad (7.19)$$

$$r = R_i \quad \frac{\partial T_l}{\partial r} = \frac{Q}{\lambda_l} + N_w \frac{\Delta H_{vap}}{\lambda_l} \quad (7.20)$$

The temperature boundary condition at the liquid/membrane interface includes the latent heat from evaporation or condensation of water at the liquid surface, which is considered a part of the total interfacial heat flux into the liquid.

## 7.3 Physical properties

An overview of the most important physical properties including functional dependence and literature sources is given in table 7–1.

**TABLE 7–1: Physical properties used in the membrane gas absorber model**

Property	Symbol	Functional dependence	Source	Comment
Specific heat of gas components	$c_{p,g}$	$f(T)$	Reid et al. (2000)	
Specific heat of alkanolamine/water solution	$c_{p,l}$	$f(T, w_{am}, y_{CO_2})$	Cheng et al. (1996)	Loading dependence from Weiland et al. (1997)
Density of alkanolamine/water solution	$\rho_l$	$f(T, w_{am}, y_{CO_2})$	Cheng et al., (1996)	CO <sub>2</sub> accounted for by adding the weight of absorbed molecules
Diffusivity of CO <sub>2</sub> and water in the gas phase	$D_{i,g}$	$f(T, P)$	Reid et al. (2000)	The Fuller equation is used
Viscosity of the loaded solution	$\mu_l$	$f(T, w_{am}, y_{CO_2})$	Weiland et al. (1998)	
Diffusivity of CO <sub>2</sub> in the loaded solution	$D_{CO_2,l}$	$f(T, \mu_l)$	Versteeg et al. (1996)	Based upon the N <sub>2</sub> O analogy and a Stoke-Einstein relation
Diffusivity of the free alkanolamine in the loaded solution	$D_{am,l}$	$f(T, c_{am}, \mu_l)$	Snijder et al. (1993)	Viscosity dependence from a Stoke-Einstein relation
Diffusivity of chemically bound CO <sub>2</sub>	$D_{cb}$	$f(T, \mu_l)$	This work	
Thermal conductivity of the gas	$\lambda_g$	$f(T, composition)$	Reid et al. (2000)	
Thermal conductivity of PTFE	$\lambda_{PTFE}$	$f(T)$	Brandrup & Immergut (1989)	
Thermal conductivity of the alkanolamine solution	$\lambda_l$	$f(T, w_{am})$	Cheng et al. (1996)	

### 7.3.1 Liquid viscosity and density

It is well known that the viscosity of amine solutions increases considerably upon absorption of CO<sub>2</sub>. Weiland et al (1998) have made an extensive experimental study to determine the viscosity of partially loaded aqueous solutions of MEA, DEA and MDEA and developed a correlation. This is implemented in the membrane absorber model. For illustration, the viscosity as a function of CO<sub>2</sub> loading is shown in fig. 7.3 for a 30% MEA-solution at 40°C.

The density of solutions was calculated by the correlation given by Cheng et al. (1996) for the binary system of alkanolamine and water. Density of loaded solutions was calculated by adding the weight of absorbed CO<sub>2</sub>-molecules. Simple density measurements have shown this to be a reasonable assumption, and it may be used as an estimate for systems where measurements are not available. Results are shown in figure 7.4 for a collection of aqueous MDEA and MEA loaded solutions. The density correlation given by Weiland et al. (1998) has a more sound theoretical basis and will be implemented in future versions.

### 7.3.2 Specific heat of liquid

The specific heat of aqueous solutions of alkanolamines are correlated by Cheng et al. (1996). Specific heat is known to decrease with increasing CO<sub>2</sub> loading, as shown by Weiland et al. (1997). The measurements published by Weiland et al. (1997) were correlated as residuals, added to the specific heat of CO<sub>2</sub>-free solution. Only measurements at 25°C are published and temperature independence was thus assumed for the loading effect.

For MEA:

$$c_{p, res} = -(2258w_{MEA} + 207.6)y \quad (7.21)$$

For MDEA:

$$c_{p, res} = -642.1y \quad (7.22)$$

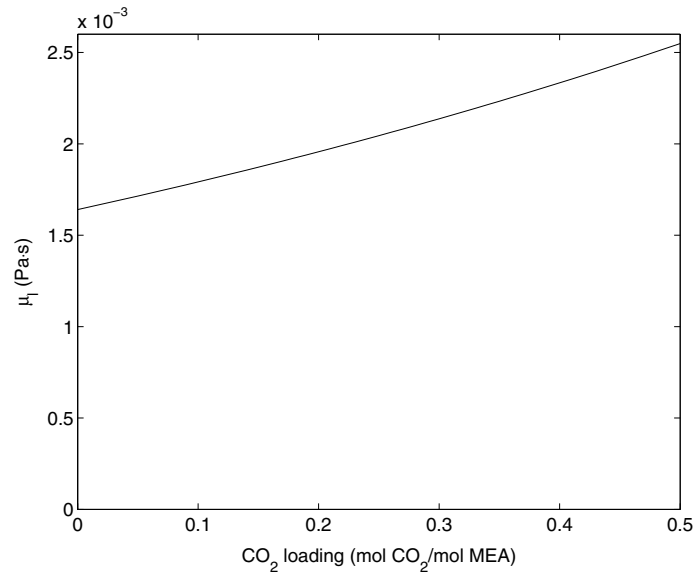


**FIGURE 7.3: Effect of CO<sub>2</sub> loading on liquid viscosity in 30% MEA/water at 40 °C , from the correlation by Weiland et al. (1998).**

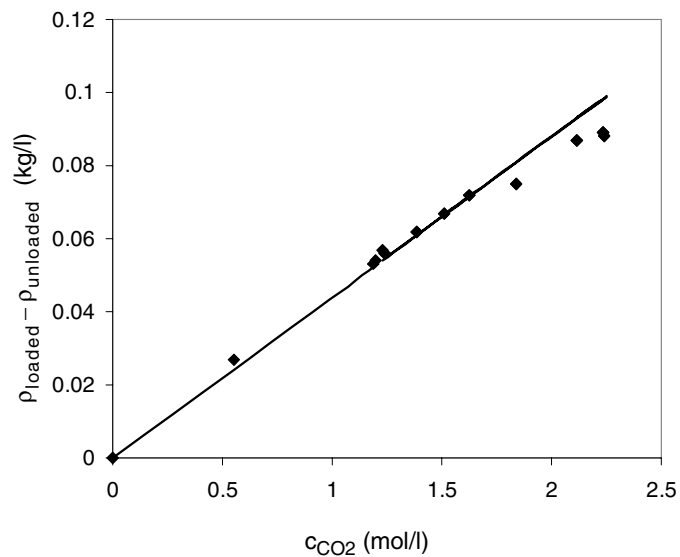


**FIGURE 7.4: Effect of total CO<sub>2</sub> concentration on the density of alkanolamine solutions. Points: Experimental data (simple measurements), Line: calculated values of the product  $c_{CO_2} M_{CO_2}$  ( $M_{CO_2} = 0.044 \text{ kg/mol}$ ).**

### 7.3.3 Diffusivities in the gas phase

The diffusivities of CO<sub>2</sub> and water in the gas phase are treated as pseudo binary diffusivities in N<sub>2</sub>. The Fuller equation (Reid et al., 2000) is used to correlate the effect of pressure and temperature:

For CO<sub>2</sub>:

$$D_{CO_2} = \frac{7.84 \times 10^{-8} T_g^{1.75}}{P} \quad (7.23)$$

For water:

$$D_{CO_2} = \frac{1.26 \times 10^{-7} T_g^{1.75}}{P} \quad (7.24)$$

### 7.3.4 Diffusivities of CO<sub>2</sub> and amine in the liquid phase

The component diffusivities in the liquid phase are of the most important parameters in modeling the mass-transfer process. The diffusivity of CO<sub>2</sub> in water is given by the following relation, compiled by Versteeg and van Swaaij (1988a):

$$D_{CO_2, w} = 2.35 \times 10^{-6} \exp\left(\frac{-2119}{T}\right) \quad (7.25)$$

It was shown by Versteeg and van Swaaij (1988a) that the diffusivity of N<sub>2</sub>O in aqueous alkanolamine solutions can be estimated according to a modified Stokes-Einstein relation.

$$(D_{N_2O} \mu^{0.8})_{am. sol.} = (D_{N_2O} \mu^{0.8})_w \quad (7.26)$$

The N<sub>2</sub>O-analogy (Al-Ghawas et al., 1989) relates the CO<sub>2</sub> and N<sub>2</sub>O diffusivities:

$$\left(\frac{D_{CO_2}}{D_{N_2O}}\right)_{am.sol.} = \left(\frac{D_{CO_2}}{D_{N_2O}}\right)_w \quad (7.27)$$

Combination of eq. (7.26) and (7.27) gives:

$$(D_{CO_2}\mu^{0.8})_{am. sol.} = (D_{CO_2}\mu^{0.8})_w \quad (7.28)$$

Equation (7.28) was used to correct the diffusivity of CO<sub>2</sub> for the increased liquid viscosity due to increasing amine concentration and CO<sub>2</sub>-loading.

The diffusivity of the free alkanolamines in water was taken from Snijder et al. (1993).

For MEA:

$$D_{MEA} = \exp\left(-13.275 - \frac{2198.3}{T} - 7.8142 \times 10^{-5} c_{MEA}\right) \quad (7.29)$$

For MDEA:

$$D_{MDEA} = \exp\left(-13.088 - \frac{2360.7}{T} - 24.727 \times 10^{-5} c_{MDEA}\right) \quad (7.30)$$

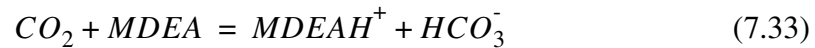
According to Snijder et al. (1993) the diffusivity can be correlated with viscosity following a modified Stokes-Einstein equation:

$$(D_{am}\mu^{0.6})_{am. sol.} = (D_{am}\mu^{0.6})_w = constant \quad (7.31)$$

Equation (7.31) was used to correct the alkanolamine diffusivity for the increased viscosity due to CO<sub>2</sub> loading at a given alkanolamine concentration.

### 7.3.5 Diffusivity of the reaction products

The main reactions in the MEA and MDEA systems are:



Other ionic species in solution in addition to these reaction products include  $H_3O^+$ ,  $OH^-$  and  $CO_3^{2-}$ . However, the concentration of these are in most situations very small compared to the main reaction products. It may thus as a simplification be assumed that the diffusion of these species does not need to be considered when modeling the "absorption-diffusion reaction-diffusion" process.

The diffusion of ionic species will be influenced by a gradient of electrical potential in addition to the concentration gradient, as described by the Nernst-Planck equation:

$$N_i = D_i \left( \nabla c_i + c_i z_i \frac{F \nabla \phi}{RT} \right) \quad (7.34)$$

where  $z_i$  is valence of ion  $i$ ,  $F$  is the Faraday constant and  $\nabla \phi$  is the gradient in electrical potential. The requirement of electrical neutrality leads to the following restrictions, as the net electrical charge ( $C$ ) will then be zero:

$$C = F \sum_i z_i c_i = 0 \quad (7.35)$$

$$\nabla C = F \sum_i z_i \nabla c_i = 0 \quad (7.36)$$

The electrical current carried by the ion  $i$  is proportional to  $z_i N_i$ . In the absence of an external electrical field the net electrical current will be zero:



$$\sum_i z_i N_i = 0 \quad (7.37)$$

Substitution of (7.37) into (7.34) leads to the following expression for the electrical potential gradient:

$$\nabla\phi = -\frac{\sum_i z_i D_i \nabla c_i}{\frac{F}{RT} \sum_i z_i^2 D_i c_i} \quad (7.38)$$

It is seen from eq. (7.38) and (7.36) that if all the ionic diffusivities are equal, the gradient of electrical potential will be zero. In general, large differences exist in the diffusivities of ionic species. The values are influenced by charge, valency and degree of solvation, which influence the effective size of the ions in solution. In this case an electric potential gradient develops in order to counteract any charge-separation so that the solution is everywhere neutral. Astarita et al. (1983) made a simplifying approximation by introducing an “apparent” diffusivity of the ionic species,  $\tilde{D}_i$ :

$$N_i = -\tilde{D}_i \nabla c_i = D_i \left( \nabla c_i + c_i z_i \frac{F \nabla \phi}{RT} \right) \quad (7.39)$$

Looking at the system CO<sub>2</sub>/MDEA/water, the ionic species to be considered are the cation MDEAH<sup>+</sup> (=C) and the anion HCO<sub>3</sub><sup>-</sup> (=A). The electroneutrality condition gives:

$$c_C = c_A \quad (7.40)$$

and the electric potential gradient is given by:

$$\nabla\phi = -\frac{RT(D_C - D_A)\nabla c_A}{F(D_C + D_A)c_A} \quad (7.41)$$

The expression for apparent diffusivities result from substitution into eq. (7.34) and rearrangement:

$$\tilde{D}_C = \tilde{D}_A = \frac{2D_C D_A}{D_C + D_A} \quad (7.42)$$

The apparent diffusivities are thus equal regardless of the difference in diffusivities between individual ions. These arguments may be used to consider the products of reaction (7.32) and (7.33) as the complexes  $\text{MEAH}^+\text{MEACOO}^-$  and  $\text{MDEAH}^+\text{HCO}_3^-$ , having similar properties as single diffusing species characterized by an apparent diffusivity.

Rowley et al. (1997, 1998) and Adams et al. (1998) studied the individual diffusivities of  $\text{CO}_2$ , alkanolamine and the reaction products as a diffusing complex, using similar assumptions as outlined above. The alkanolamines were MDEA and DEA, including mixtures of the two. Absorption of  $\text{H}_2\text{S}$  was also considered (Adams et al., 1998). A rigorous diffusion-reaction model was developed to describe their inverted tube diffusometer used in the experimental study. Following a sensitivity analysis, diffusion coefficients for the reaction products were treated as single parameters that were adjusted to give the best fit of the model to the experimental absorption rates. The authors concluded that diffusion of the reaction products could have a substantial effect on the absorption rate and may even be rate determining, as these diffusivities were found to be significantly lower than the diffusivities of the reactants.

This contradicts the traditional approach, only considering the free  $\text{CO}_2$  and free alkanolamine diffusivities when studying the absorption problem (Astarita et al., 1983; Pani et al., 1997). This actually implies that the reaction is treated as irreversible (Rowley et al., 1997). When explicitly considering the transport of ionic reaction products most authors make the assumption that ionic diffusivities have the same value for each species as required for electroneutrality. This value is then taken equal to the diffusivity of the slowest diffusing molecular component, normally the free alkanolamine (e.g. Bosch et al., 1989; Glasscock, 1990; Rinker et al., 1995). For the  $\text{CO}_2$ -MDEA system this leads to:

$$D_{HCO_3^-} = D_{MDEAH^+} = D_{MDEA} \quad (7.43)$$

From the discussion in 6.4.2 it is concluded that the experiments with pure CO<sub>2</sub> in the gas phase are performed in a regime where the rate of absorption is influenced by the diffusivities of all species in solution, especially in the MEA-system. A sensitivity analysis was performed on these experimental conditions as described in the following.

The parameters influencing the rate of absorption are the reaction rate constant ( $k_2$ ), free CO<sub>2</sub> diffusivity ( $D_{CO_2}$ ) and the apparent diffusivity of the chemically “bound CO<sub>2</sub>” reaction products (denoted by  $\tilde{D}_{cb}$ ). The sensitivity analysis was performed by multiplying each of these parameters by factor of 2 and observing the increase in the simulated absorption flux in each case. This was done in a range of temperatures covered by the experiments and with zero CO<sub>2</sub>-concentration in the inlet solution. The sensitivity factors given in table 7–2 thus represent the relation

$$\frac{R_{CO_2, 2^*p}}{R_{CO_2}} \quad (7.44)$$

where the simulated absorption rate, with the parameter  $p$  multiplied by a factor of 2, is divided by the corresponding rate from the unperturbed model. It is seen that in the MEA-system, for these experimental conditions, the absorption rate is mostly influenced by  $D_{am}$  and  $\tilde{D}_{cb}$ . The same is seen in the MDEA-system even if the sensitivity factors are lower. Since the diffusivities of the ionic complexes are significantly lower than the diffusivity of the free alkanolamine, the use of assumption (7.43) will then give an overprediction of the absorption rate.

The consequence of a difference in diffusivity between unreacted and reacted alkanolamine is that gradients in total alkanolamine concentration will occur. Total alkanolamine concentration will generally increase near the membrane wall, were the reaction products are formed. This is illustrated in figure 7.5 from a simulation on a 1910 mol/m<sup>3</sup> MDEA-solution. The slower diffusion of the

**TABLE 7–2: Sensitivity analysis on the mass transfer model. Sensitivity factors defined by eq. (7.44).**

15% MEA, $p_{CO_2} = 90$ kPa				
T (°C)	25	40	55	70
$N_{CO_2}$ (mol/s)	$3.09 \times 10^{-4}$	$3.89 \times 10^{-4}$	$4.72 \times 10^{-4}$	$5.41 \times 10^{-4}$
$2^*k_2$	1.04	1.04	1.04	1.03
$2^*D_{CO_2}$	1.05	1.05	1.04	1.02
$2^*D_{am}$	1.48	1.48	1.49	1.50
$2^*\tilde{D}_{cb}$	1.30	1.29	1.28	1.27
23.5wt% MDEA, $p_{CO_2} = 90$ kPa				
$N_{CO_2}$ (mol/s)	$1.20 \times 10^{-4}$	$1.54 \times 10^{-4}$	$1.75 \times 10^{-4}$	$1.73 \times 10^{-4}$
$2^*k_2$	1.15	1.12	1.08	1.05
$2^*D_{CO_2}$	1.20	1.17	1.13	1.10
$2^*D_{am}$	1.22	1.26	1.31	1.37
$2^*\tilde{D}_{cb}$	1.23	1.26	1.31	1.37

MDEAH<sup>+</sup>HCO<sub>3</sub><sup>-</sup>-complex compared to the free MDEA-molecules leads to a buildup of total MDEA-concentration near the wall. The equilibrium model will calculate the speciation based upon this total MDEA-concentration. Large amine concentrations may result, which are far outside the range of validity of the equilibrium model. It will thus be necessary to make the simplifying assumption that the diffusivity of the reaction products are rate limiting so that:

$$D_{MEA} = \tilde{D}_{MEA H^+ MEACOO^-} \quad (7.45)$$

$$D_{MDEA} = \tilde{D}_{MDEAH^+ HCO_3^-} \quad (7.46)$$

This will make the total alkanolamine concentration of the model a constant throughout the liquid phase. The values of the bound CO<sub>2</sub> diffusivities were

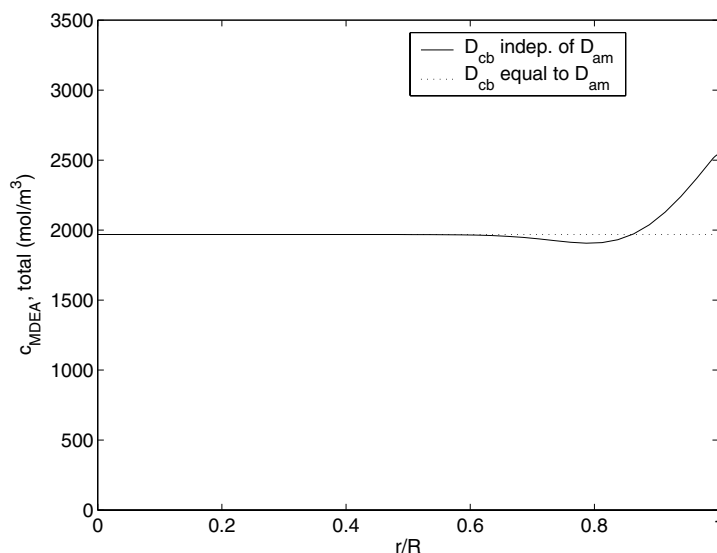


**FIGURE 7.5: Profile of total MDEA-concentration in a 23.5 wt% MDEA solution. The increase towards the membrane wall ( $r/R=1$ ) result from the low rate of diffusion of the reaction product  $\text{MDEAH}^+\text{HCO}_3^-$  compared to free MDEA.**

regressed from the experimental data with similar conditions as in table 7–2. The regression was performed both with and without assumptions (7.45) and (7.46). The functional dependence of the bound  $\text{CO}_2$  diffusivity,  $\tilde{D}_{cb}$ , was assumed similar to the correlation for free alkanolamine diffusivity presented by Snijder et al. (1993), introducing the liquid viscosity instead of the amine molarity as a variable:

$$\tilde{D}_{cb} = \exp\left(A + \frac{B}{T} + C \ln \mu\right) \quad (7.47)$$

The parameters were estimated by the Levenberg-Marquardt non-linear regression method as implemented in the in-house “Modfit” program (Hertzberg and Mejdell, 1998). Results are given in table 7–3.

**TABLE 7–3: Parameter regression results for the diffusivity of bound CO<sub>2</sub> (MDEAH<sup>+</sup>HCO<sub>3</sub><sup>-</sup> and MEAH<sup>+</sup>MEACOO<sup>-</sup>)**

		A	B	C	Std. dev. of fit
With $D_{am} = \tilde{D}_{cb}$ , assumption (7.45) and (7.46)					
(I)	MEAH <sup>+</sup> MEACOO <sup>-</sup>	-22.64	-1000	-0.70	5.84%
(II)	MDEAH <sup>+</sup> HCO <sub>3</sub> <sup>-</sup>	-21.07	-1595	-0.62	6.83%
With $D_{am}$ from literature, independent of $\tilde{D}_{cb}$					
(III)	MEAH <sup>+</sup> MEACOO <sup>-</sup>	-20.64	-1800	-0.60	4.86%
(IV)	MDEAH <sup>+</sup> HCO <sub>3</sub> <sup>-</sup>	-21.16	-1595	-0.62	4.75%

In the MEA-system the bound CO<sub>2</sub> diffusivity found was higher when introducing assumption (7.45) ( $D_{am} = \tilde{D}_{cb}$ ) than the value found when using the “real” diffusivity of the free alkanolamine. It is expected the diffusivity found when imposing the assumption  $D_{am} = \tilde{D}_{cb}$  should lie between the real diffusivities of free alkanolamine and bound CO<sub>2</sub>. It is noteworthy that almost no difference was found in the diffusivity of bound CO<sub>2</sub> in the MDEA system when fitting the parameters with and without this assumption. This reflects the fact that the sensitivity to the diffusivities was lower in the MDEA-system than in the MEA-system. The viscosity effect was relatively highly correlated with the temperature effect. This was probably caused by the lack of data with varying amine concentration, which would have given a larger span in the liquid viscosity.

In figure 7.6 the values of the bound CO<sub>2</sub> diffusivities from Rowley et al. (1997) are plotted together with corresponding values calculated from the correlation found for the MDEA system (eq.(7.47)), with parameters from table 7–3 (IV). The viscosity dependence of the correlation, basic to the recalculation in terms of weight percent dependence, is relatively uncertain. It is in any case clear that a large difference exists between the values of Rowley et al. (1997) and this work. A similar plot is given in figure 7.7, where  $\tilde{D}_{cb}$  from the MEA-system correlation is plotted together with the corresponding DEA-system data from Rowley et al. (1998). It is noteworthy that Rowley et al. found that  $\tilde{D}_{cb}$  did not

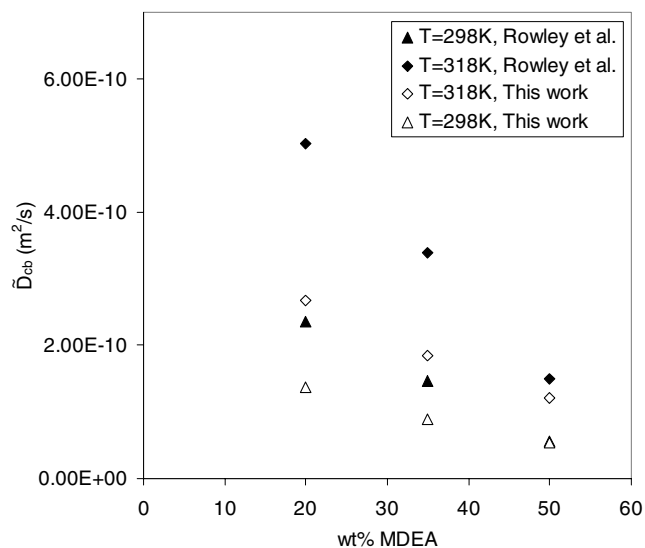


FIGURE 7.6: Diffusivity of the complex  $\text{MDEAH}^+\text{HCO}_3^-$  ( $\tilde{D}_{cb}$ ), values from this work vs. Rowley et al. (1997).

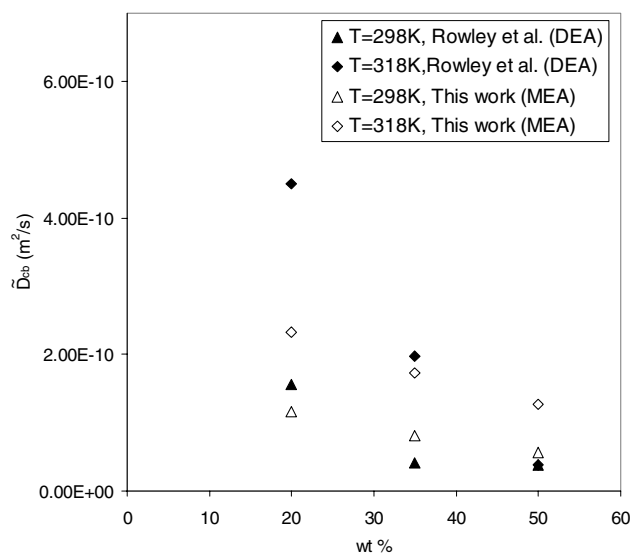


FIGURE 7.7: Diffusivity of the complex  $\text{MEAH}^+\text{MEACOO}^-$  ( $\tilde{D}_{cb}$ ) from this work vs. diffusivity of the complex  $\text{DEAH}^+\text{HCO}_3^-\text{DEACOO}^-$  from Rowley et al. (1998).

change when increasing the DEA-concentration from 35-50 wt% at 298 K, this making the diffusivity at 50 wt% and 298 K similar to the value at 318 K.

In any case it is clear that the results from this study confirm the findings from Rowley et al. that diffusion of the reaction products may be rate limiting, as these are found to be only 20-30% of the values for the corresponding free amines. More work is required in order to resolve the discrepancies. The restriction  $D_{am} = \tilde{D}_{cb}$  was imposed on the model and used in the further simulations presented in this work.

### 7.3.6 Further discussion of the problem of electrolyte diffusion

The results above show that the interdiffusion of solutes in CO<sub>2</sub>/alkanolamine systems is coupled and that multicomponent effects ideally should be accounted for in a rigorous manner. In order to calculate the electric potential gradient, the diffusion coefficient of each ionic species is required. Such data are presently not available for the protonated alkanolamines and carbamate ions. The diffusivity of ions like carbonate, bicarbonate and hydroxide are measured, with most published data at a temperature of 25 °C (Newman, 1991). This leads to the requirement of approximating values as well as the temperature dependence of ionic diffusivities, which may be considered a serious drawback by such an approach.

Littel et al. (1991) described the coupling of the diffusion of ionic species by a similar model as Glasscock and Rochelle (1989), using the Nernst-Planck equation. They compared this to the results from making an assumption similar to (7.43), for the absorption of CO<sub>2</sub> and H<sub>2</sub>S into an aqueous solution of MEA and MDEA. They found that the rate of CO<sub>2</sub> absorption was reduced and the rate of H<sub>2</sub>S absorption was increased when using the “correct” model of ionic diffusion. The effects will probably increase with increasing contact times, due to an increase in the time available for diffusion. This explains the large sensitivities to bound CO<sub>2</sub> diffusivity found in this work, as the contact times were around 20 seconds. Even if most absorption experiments published are performed in



equipment with significantly lower contact times, there should still be a need to check the consequences of the assumption that the ionic reaction products diffuse with the same rate as the free amine. This is clearly not valid.

Following Leaist et al. (1998) the CO<sub>2</sub>/alkanolamine/water system may be described by the coupled Fick equations. If a three-component system like CO<sub>2</sub> (1), alkanolamine (2) and H<sub>2</sub>O is considered, the following flux equations may be written:

$$J_1(\text{solute1}) = -D_{11}\nabla c_1 - D_{12}\nabla c_2 \quad (7.48)$$

$$J_2(\text{solute2}) = -D_{21}\nabla c_1 - D_{22}\nabla c_2 \quad (7.49)$$

where the cross-term diffusion coefficient,  $D_{12}$ , relate to the flux of CO<sub>2</sub> due to the concentration gradient of the alkanolamine and  $D_{21}$  relate the flux of alkanolamine due to the concentration gradient of CO<sub>2</sub>.

Leaist et al. (1998) studied the system TEA/oxalic acid/water and estimated ternary cross-diffusion coefficients. The process of dissolution of oxalic acid in the alkanolamine was considered analogous to the absorption of an acid gas. The rapid equilibration between oxalic acid and TEA in different chemical forms (H<sub>2</sub>L, HL<sup>-</sup> and L<sup>2-</sup> and TEA, TEAH<sup>+</sup>, respectively) and the requirement of local electroneutrality allowed for the treatment as single total solute components of oxalic acid and TEA in the ternary system. The fluxes of these solutes were found to be strongly coupled by the electric field that is generated by the diffusing ions. Leaist et al. found a large and negative cross coefficient,  $D_{21}$  leading to a significant counterdiffusion of TEA towards the surface of the solid acid. This resulted in a buildup of TEA and gave a concentration profile similar to figure 7.5, resulting from an approach using pseudo-binary diffusivities of free MDEA and MDEAH<sup>+</sup>HCO<sub>3</sub><sup>-</sup>. This qualitatively confirms the observations made in this study.

## 7.4 Model implementation

The mathematical model outlined in 7.2 is a typical marching or propagation problem. The system is steady, but the flow direction acts as a time-like coordinate enabling the governing equations for the liquid phase transport, (7.13) and (7.14), to be classified as parabolic equations. Such problems are also termed initial-boundary value problems. The “discontinuity” at  $z=0$  and  $r=R$ , which is seen from the boundary conditions (eq. (7.15) and (7.17)) makes this a problem of significant numerical stiffness.

The equations (7.3) to (7.20) were scaled by introducing the following variable transformations:

$$\alpha_i = \frac{c_i}{c_i^0} \quad \xi = \frac{z}{L} \quad \gamma = \frac{r}{R_i} \quad \theta = \frac{T}{T_l^0}$$

$$\Delta = \frac{P}{P_{in}} \quad \delta_i = \frac{p_i}{P_{in}} \quad \mu = \frac{v_g}{v_g^0} \quad d_i = \frac{D_i}{D_i^0}$$

Here,  $c_i^0$ ,  $T_l^0$  and  $v_g^0$  are the inlet values of the liquid concentration, the liquid temperature and the gas velocity, respectively.  $D_i^0$  is the diffusivity at the tube center.

The model was programmed in MATLAB, and the system of partial differential equations was solved by the Method of Lines (MoL) procedure (Schiesser, 1991). The principle of the Method of Lines is to reduce the system of partial differential equations to a system of ordinary, coupled differential equations and then integrate the system of ODE's. This is done by discretizing the spatial region in the radial dimension while the axial dimension is treated as a continuous variable leading to a vector system of ODE's to be integrated by an appropriate routine. The MoL procedure has been applied by other authors studying the similar problem (Karoor and Sirkar, 1993; Lee et al., 2001).

The  $r$ -derivatives of eq. (7.13) and (7.14) were calculated from finite difference approximations. First derivatives were calculated by fourth order finite differences, while second order finite differences were used for the second derivatives, using the routines `dss004` and `dss042` (Schiesser, 1991). In order to capture the very steep gradients close to the membrane wall, the  $r$ -domain was divided in two regions with different uniform resolutions. The two zones were typically separated at  $\gamma = 0.995$  with 40 grid points in both the “wall” zone and the bulk zone, and the model was thoroughly tested for grid independence in the whole range of conditions.

The axial direction was integrated by the MATLAB `ode15s` routine. This is a variable order (1-5) and variable step length procedure making use of the implicit Numerical Differentiation formulas. 200-400 steps were normally required for convergence, with 80% of the steps applied in the first 10% of the membrane tube length, reflecting the stiffness of the problem.

The resulting model was found to be robust and numerically stable. The solution for the cocurrent case was straightforward, while for the countercurrent case an outer iteration loop based on the Broyden method (Press et al., 1992) was used, as the integration always follows the liquid phase from inlet to outlet. In this case, the outlet gas total pressure, temperature, gas velocity and partial pressures of  $\text{CO}_2$  and water were first guessed and the iteration continued until the normalized inlet values matched within the specified tolerance of  $10^{-6}$ . A simplified block diagram of the model is shown in figure 7.8.

After integration, the overall average flux from gas to liquid was calculated by independent mass balances on the gas and the liquid phases. The liquid inlet and outlet molar flows are, respectively:

$$n_{i, in}^l = c_i^0 Q_L \quad (7.50)$$

$$n_{i, out}^l = n_{tubes} \int_0^{2\pi} \int_0^{R_i} c_i(r) v_z(r) r dr d\theta \quad (7.51)$$

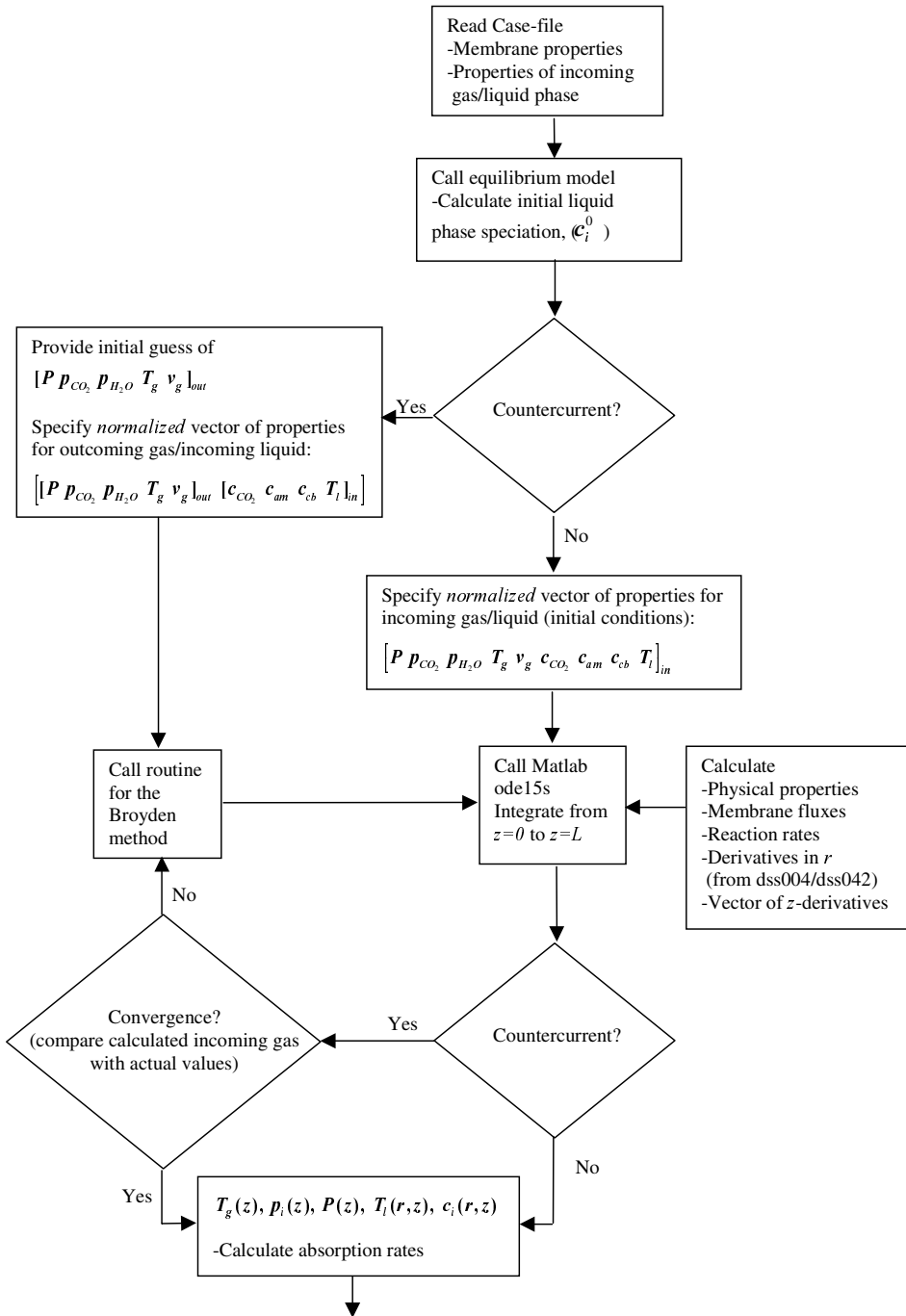


FIGURE 7.8: Simplified block diagram of the model

where  $c_i^0$  is the molar concentration of component  $i$  in the inlet liquid and  $Q_L$  is the volumetric flowrate of liquid.  $n_{tubes}$  is the number of membrane tubes in the module, while  $c_i(r)$  and  $v_z(r)$  are the radial concentration and velocity profiles. The integral in eq. (7.51) was calculated by an adaptive quadrature method (the MATLAB `quadl` routine). Because of the very steep gradients of the product  $c_i(r)v_z(r)$ , the absolute error tolerance had to be set to a low value, typically  $10^{-10}$ . The molar absorption rate of component  $i$  into the liquid phase is given by:

$$R_i^l = n_{i,out}^l - n_{i,in}^l \quad (7.52)$$

The corresponding absorption rate from the gas phase balance is given by:

$$R_i^g = \frac{A_g}{RT_g} [(p_i v_g)^{in} - (p_i v_g)^{out}] \quad (7.53)$$

The error in the global mass balances (the difference between  $R_i^g$  and  $R_i^l$ ) was typically within  $\pm 1\%$ , which reflects the fact that Finite Difference Method does not necessarily lead to conservation of the fluxes. This problem may be resolved by building a corresponding model around the Finite Volume Method, which is inherently mass conservative. The price will however be a less robust model with significantly higher computational time (Hoff et al., 2003).

## 7.5 Model verification and validation

### 7.5.1 Concentration, temperature and viscosity profiles

Three-dimensional concentration profiles of free  $\text{CO}_2$ , free alkanolamine and the bound  $\text{CO}_2$  complex are given in figures 7.9-7.10. These example diagrams are taken from simulation of an experimental point with absorption in 30% MEA. From the free  $\text{CO}_2$  concentration profile of figure 7.9 it is seen that the chemical reaction leads to an almost immediate depletion of free  $\text{CO}_2$  at the liquid surface. The peak at  $r/R=1$  and  $z/L=0$  results from the salting out effect due

to the formation of ionic reaction products, as can be seen from the corresponding rise in concentration of bound  $\text{CO}_2$  in figure 7.10. The importance of a dense computational grid close to the membrane wall is obvious from looking at the free  $\text{CO}_2$  concentration profile.

The depletion of free MEA due to the chemical reaction can be seen from figure 7.11. However, the rate of absorption is limited by the rate of diffusion of the bound  $\text{CO}_2$  reaction product,  $\text{MEAH}^+\text{MEACOO}^-$ , penetrating into the bulk of the liquid phase as seen from figure 7.10. It is also seen that the contact time is not high enough that diffusion affects the liquid bulk concentration at the tube center.

The rise in liquid temperature due to the chemical reaction can be seen from figure 7.12. The rise is somewhat higher in the reaction zone close to the membrane wall, even if the rapid thermal diffusivity of the aqueous solution considerably reduce the radial temperature gradient. The important effect of increasing viscosity upon increasing  $\text{CO}_2$ -loading is seen from the viscosity profile of figure 7.13. A similar profile results in the liquid density, although not shown.

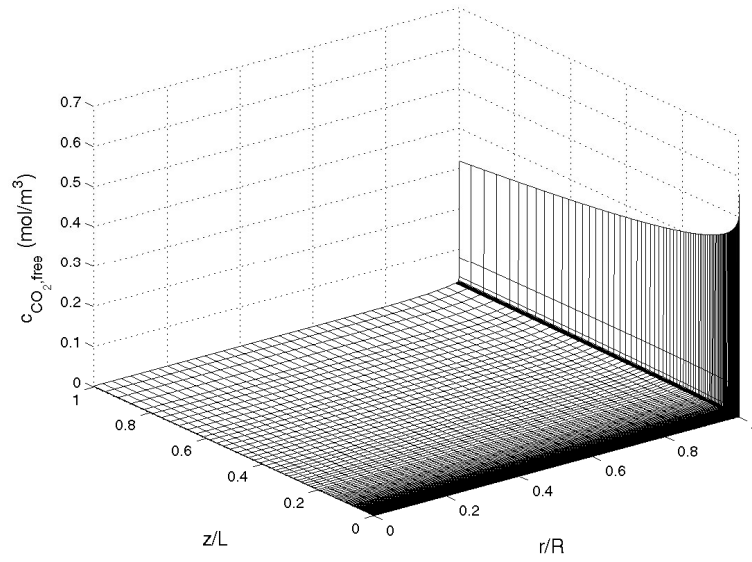


**FIGURE 7.9: Concentration profile of free CO<sub>2</sub> in a membrane tube upon absorption into a 30 wt% MEA solution**

---

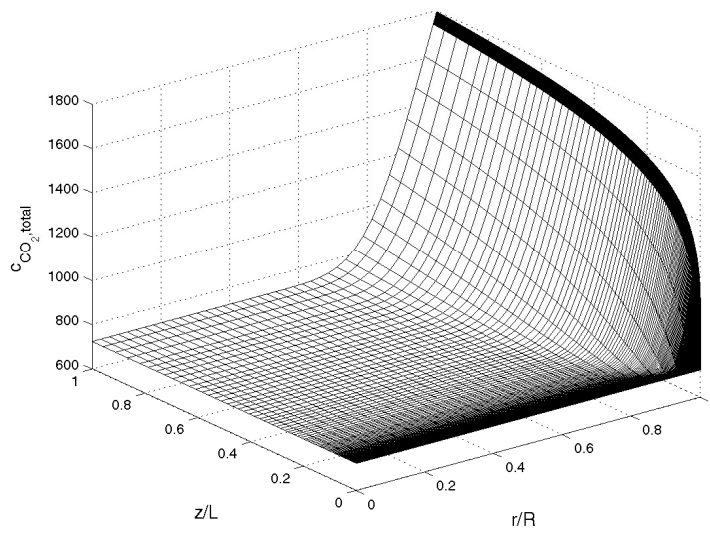


**FIGURE 7.10: Total CO<sub>2</sub> concentration profile upon absorption into a 30 wt% MEA solution**

---

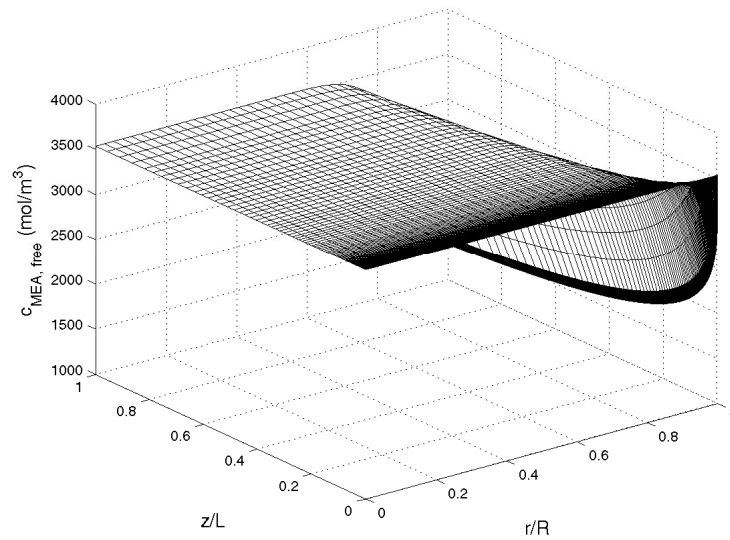


**FIGURE 7.11: Concentration profile of free MEA upon absorption of CO<sub>2</sub> into a 30 wt% solution**

---

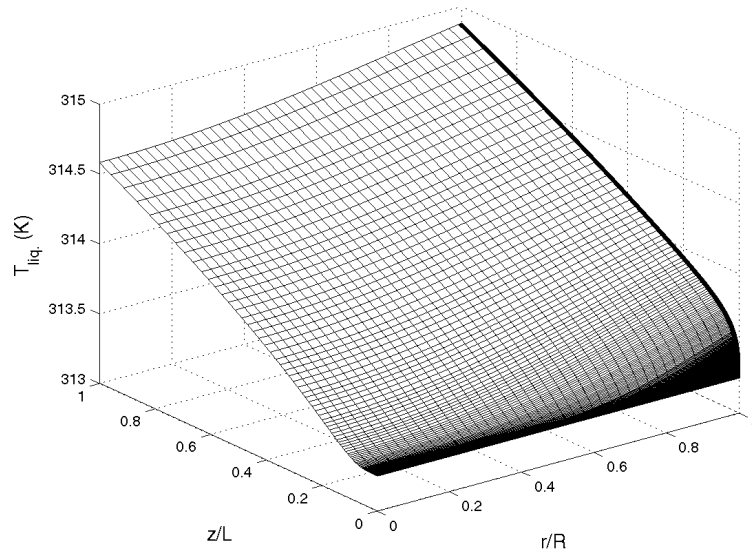


**FIGURE 7.12: Liquid temperature profile of a membrane tube upon absorption of CO<sub>2</sub> into a 30 wt% MEA solution**

---



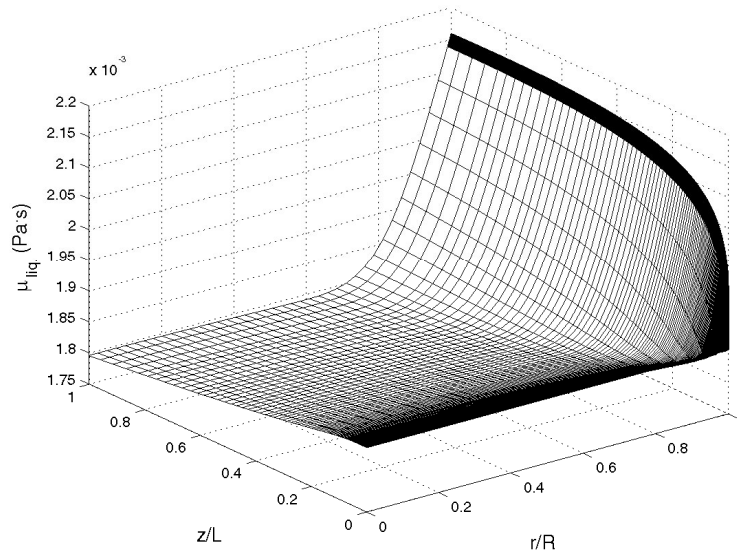


**FIGURE 7.13: Liquid viscosity profile upon absorption of CO<sub>2</sub> into a 30 wt% MEA solution**

## 7.5.2 Effect of viscosity and density gradients

The membrane absorber liquid flow model was based on the assumption of a fully developed parabolic velocity profile instead of calculating the profile from the equations of motion. The derivation of the parabolic velocity profile assumes constant viscosity and density (Bird et al., 2002). In order to test whether the observed viscosity and density gradients would lead to significant deviations from the assumed velocity profile, a CFD calculation was performed using an in-house program code (Jakobsen et al., 2002). The simulation was done twice, first with no viscosity/density gradients to check that this resulted in the parabolic profile, then the simulation was repeated with viscosity/density gradients. In figure 7.14 the resulting velocity profiles are given. The difference is so small, particularly in the wall region, that any influence from the viscosity and density gradients on the velocity profile can be disregarded.

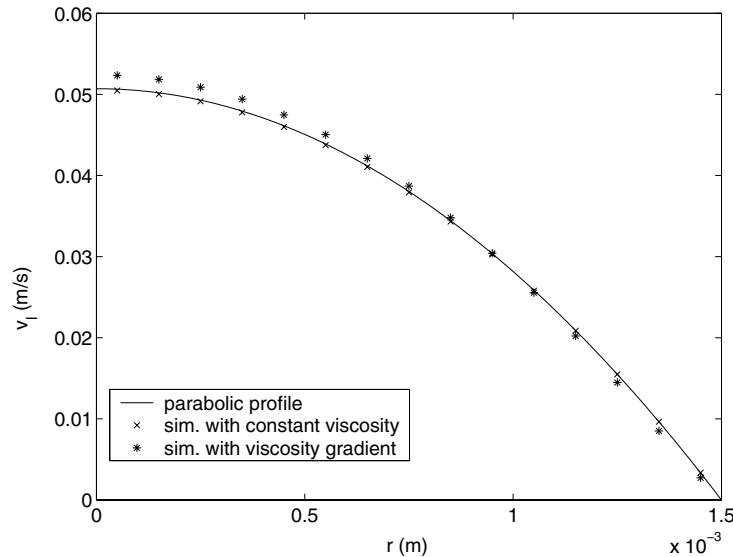


**FIGURE 7.14: Changes in velocity profile caused by the viscosity and density profiles**

### 7.5.3 The effect of partial penetration into the membrane

The model assumes that the pores are 100% gas-filled, and that an effective molecular diffusivity corrected for membrane porosity and tortuosity can be used (eq. (6.12)). The pore diameter distribution is in a range that will not give any significant contribution from Knudsen diffusion, and the only effect that may lead to deviations from the assumption is partial liquid penetration into the pores. This effect has been observed by Rangwala (1996). He calculated membrane mass transfer coefficients from experiments of CO<sub>2</sub>-absorption in a DEA-solution and found values significantly lower than expected.

These experiments were done with commercial hollow fiber membranes made of polypropylene. The diffusivity of CO<sub>2</sub> in the liquid phase is approximately 10<sup>4</sup> times lower than in the gas. Liquid that penetrates into the pores is immobilized and represents a barrier to gas/liquid mass transfer inside the tube where the absorbed components are swept away by convection. Rangwala (1996)

found that his results could be explained by liquid penetrating 0.9% of the membrane thickness and set up an equation for this, given by:

$$\frac{1}{k_m} = \left[ \frac{(1-x)}{k_m} \right]_{gas\ filled} + \left[ \frac{x}{k_m} \right]_{liquid\ filled} \quad (7.54)$$

where  $x$  is the fractional depth of liquid penetration.

Equation (7.54) was implemented in the membrane model of this work to investigate the effect of possible penetration over a range of operating conditions. A hypothetical liquid penetration of 1% was tested. The simulated results compared with experimental data showed that partial liquid penetration gives effects that are contrary to what was observed over a range of experimental conditions with varying CO<sub>2</sub> partial pressure, liquid velocity and temperature. The PTFE-membranes used in this work are known to be significantly less subject to wetting than membranes of polypropylene, as used by Rangwala (1996) and Feron and Jansen (2002).

#### 7.5.4 Porosity and effective interfacial area

The membrane porosity is accounted for in the model only in the effective diffusivity used in the calculation of the membrane mass transfer coefficient. The liquid inside the tubes is assumed not to feel the membrane porosity and to get the flux from the gas phase uniformly distributed over the inside area of the fibers.

Kreulen et al. (1993a) addressed the question of effective interfacial area investigating whether it is influenced by the membrane porosity and thereby related to the actual gas liquid contact area, i.e. at the pore mouth. They did experiments on absorption of CO<sub>2</sub> in water using polypropylene fibers with porosities of 3 and 70%. The results showed no effect of fiber porosity. This was explained by considering that the liquid is instantaneously saturated along the membrane wall compared to saturation in the radial direction.

Matsumoto et al. (1995) did similar experiments with membrane porosities ranging from 40 to 80% and found that the overall mass transfer coefficient was

independent of porosity. The results were however remarkably different when studying absorption of CO<sub>2</sub> in the chemical solvents 30% MEA and 1 mol/l NaOH. These experiments showed that the overall mass transfer coefficient was increasing with porosity. The difference observed between chemical and physical absorption was explained by comparing estimates of the distance between adjacent pores,  $l_p$  and the thickness of the concentration boundary layer,  $\delta_L$ , calculated as:

$$\delta_L = \frac{D_{CO_2} \text{ (m}^2\text{/s)}}{K_G \text{ (m/s)}} \quad (7.55)$$

It was found that in the CO<sub>2</sub>/H<sub>2</sub>O case the values of  $\delta_L$  were much larger than those of  $l_p$ , similar to Kreulen et al. (1993a). For CO<sub>2</sub>/MEA the values of  $\delta_L$  were found to be of similar size as  $l_p$ , suggesting that only the liquid closest to the pore opening is available for diffusion. If so the liquid surface may be looked upon as partially inhomogeneous with respect to mass transfer into chemical absorbents.

The membranes used by Matsumoto et al. (1995) had decreasing values of wall thickness, pore diameter and membrane tube diameter in addition to the increasing membrane porosity. This leads to an increase by a factor of 6 in the membrane mass transfer coefficient, and must be considered as part of the reported “porosity effect”. An erroneous unit conversion of mass transfer coefficients, using the Henry’s law constant instead of the product  $RT$ , must also be considered.

The absorption experiments in this work are done with aqueous MEA and MDEA, which have a significant difference in the absorption rate. This will lead to significant change in the boundary layer thickness. No principal difference in the model performance was however observed between these two systems. SEM pictures of the membrane surface used in this study reveal that the surface structure is complex, consisting of pores as slit-like voids in a three dimensional network (figure 7.15, see also Kitamura et al., 1999). The structure should

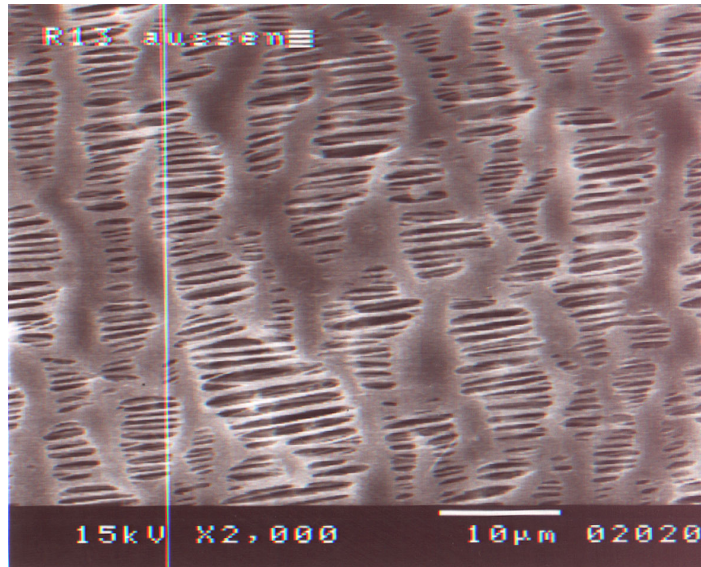


**FIGURE 7.15: SEM-picture of the microporous PTFE-membrane surface (W.L. Gore & Associates)**

---

essentially provide very good contact between gas and liquid. It is in any case concluded that the subject of effective mass transfer area requires further study in future work, both theoretically and experimentally.

## 7.6 Comparison of the model performance with experimental data

The performance of the membrane model in predicting the results of the experiments from the lab-scale membrane module, described in chapter 5, is shown in figure 7.16-7.22 in terms of the absorption rates. Regression lines for the experimental points (the solid lines of fig. 7.16-7.22) are included for convenience.

The numerical model gives a good prediction of point values and trends in the experimental data material. The deviation is generally within  $\pm 15\%$ . The model seems to give a slight overprediction of the effect of increasing  $\text{CO}_2$  partial pressure in the MEA-system, especially at low loading (fig. 7.16). The reason to this

is not clear, but it may be related to the equilibrium model through the free CO<sub>2</sub> solubility. In figure 7.22 it is seen that the absorption rate goes through a maximum with increasing temperature in the MDEA-system. The model gives a very good prediction of this trend, which is caused by a decrease in the driving force resulting from the increasing equilibrium back pressure with temperature. This effect overcomes the effect of increasing diffusivities and rates of reaction with temperature which is dominating in the MEA-system (fig. 7.18 and 7.20), also reflecting the fact that MDEA absorbs CO<sub>2</sub> more reversible than MEA.

In figure 7.23 are shown results from experimental tests performed at atmospheric pressure with the system 30% MEA/water/CO<sub>2</sub> in the pilot scale test rig erected at SINTEF/NTNU. A cross flow membrane module with hollow fibers of 1 mm inner diameter was used. The operating line of an industrial-scale membrane gas absorber was followed by systematically increasing the CO<sub>2</sub> content of the gas with increasing CO<sub>2</sub> loading of the liquid. The operating line corresponded to a process with 80% CO<sub>2</sub> removal from an exhaust gas containing 5.5 vol% CO<sub>2</sub>, thus covering the range from 1.1 to 5.5 vol% CO<sub>2</sub> with gradually increasing loading. Different values of the liquid circulation rate were also tested within this series.

The figure shows very good agreement between simulated and experimental data, with a deviation less than 10% except at loadings higher than 0.42, where the deviation is large percent-wise. The operating range of an industrial MEA-process for exhaust gas CO<sub>2</sub> removal in terms of loading will typically be 0.06-0.42 (Kohl & Nielsen, 1997). The average model deviation within this range is 2.8%.

The module used in these experiments was almost 30 times larger in terms of surface area than the one used in the lab-scale study. This verifies the ability of the model to predict the performance of larger scale units and reflects the linear scale-up of membrane gas absorbers.

7.6 Comparison of the model performance with experimental data

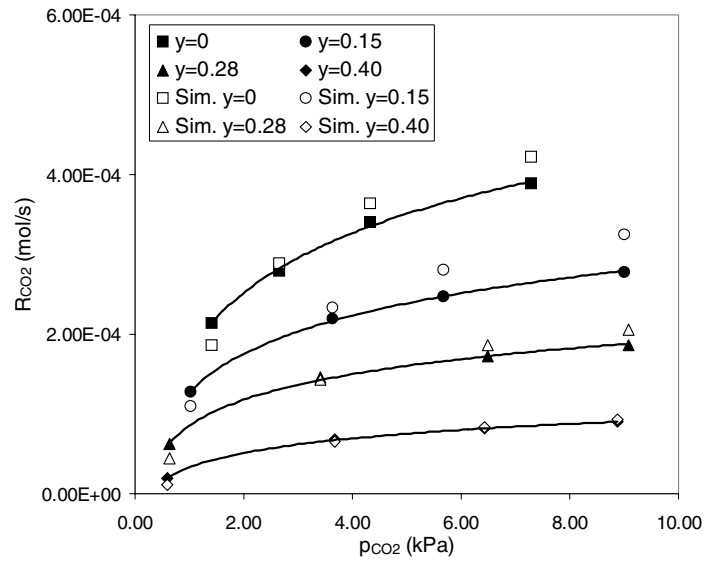


**FIGURE 7.16: 30% MEA/water with  $T=40^{\circ}\text{C}$  and variable  $\text{CO}_2$  partial pressure. Model prediction and experimental data points.**

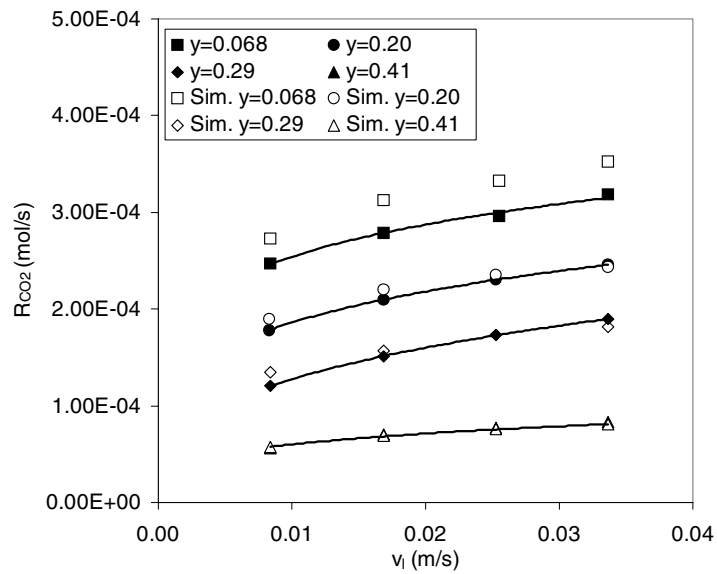


**FIGURE 7.17: 30% MEA/water with  $T=40^{\circ}\text{C}$  and  $p_{\text{CO}_2}=5\text{ kPa}$ , variable liquid velocity. Model prediction and experimental data points.**

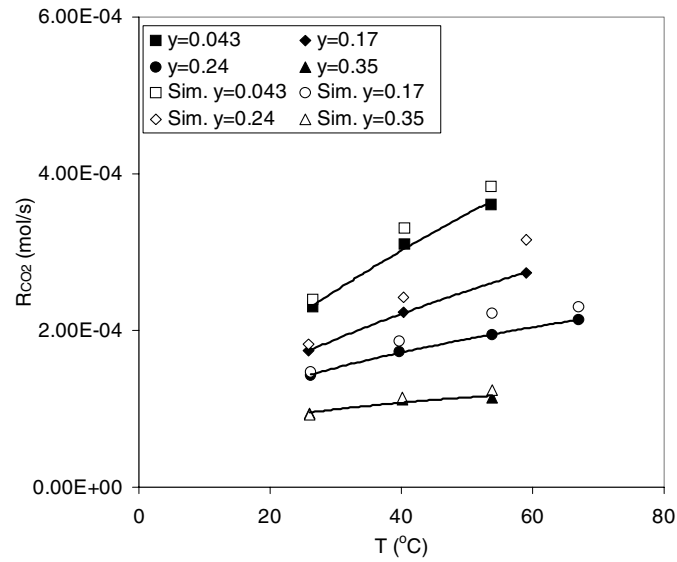


**FIGURE 7.18: 30% MEA/water with  $p_{\text{CO}_2} = 5$  kPa and variable temperature. Model prediction and experimental data points.**

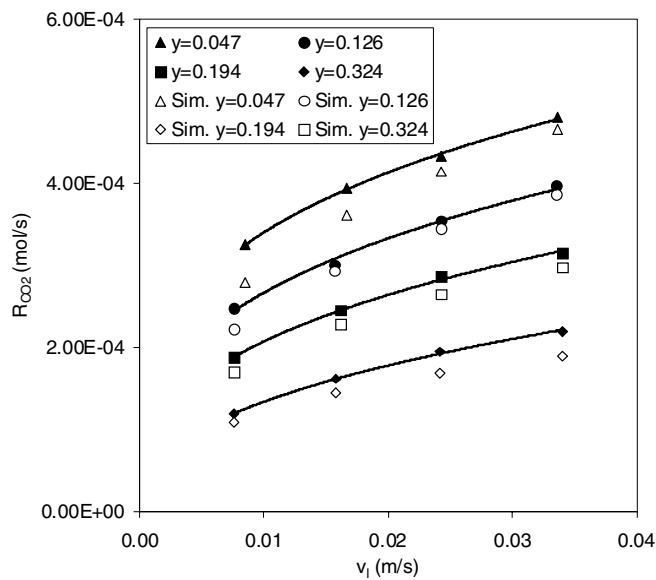


**FIGURE 7.19: 15% MEA/water with  $T=40$  °C and  $p_{\text{CO}_2} = 90$  kPa, variable liquid velocity. Model prediction and experimental data points.**



7.6 Comparison of the model performance with experimental data

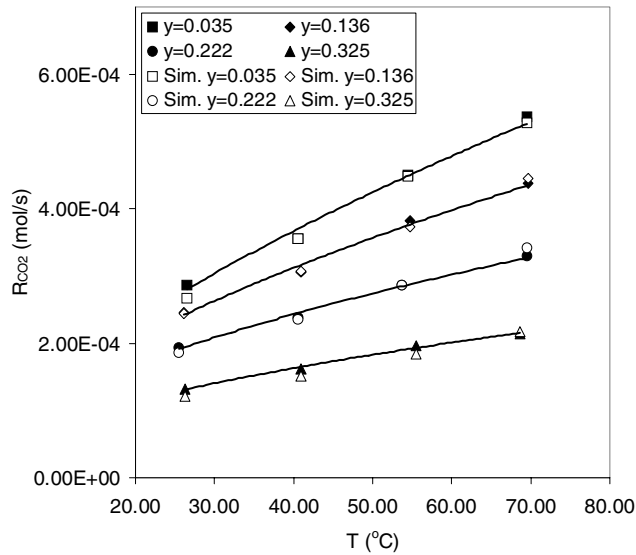


**FIGURE 7.20: 15% MEA/water with  $p_{CO_2}$  =98-70 kPa variable temperature. Model prediction and experimental data points.**

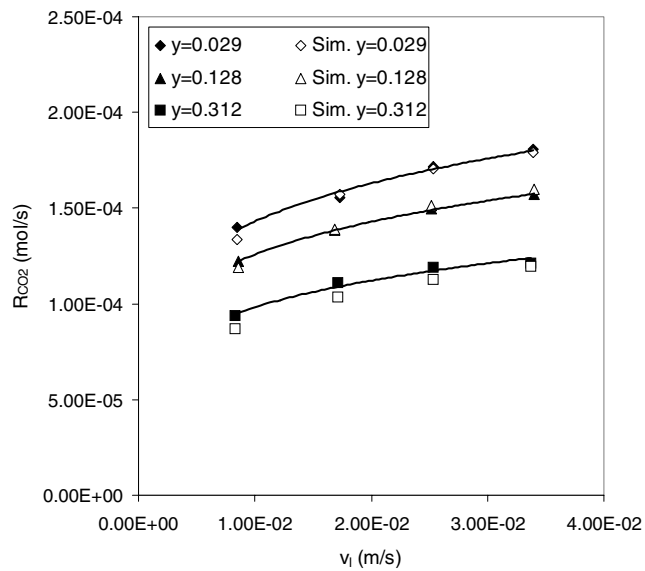


**FIGURE 7.21: 23.5% MDEA/water with T=40 °C and  $p_{CO_2}$  =90 kPa, variable liquid velocity. Model prediction and experimental data points.**

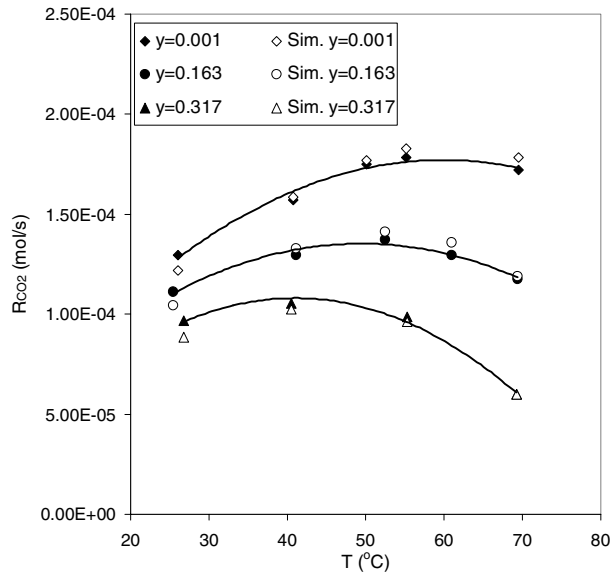


**FIGURE 7.22: 23.5% MDEA/water, variable temperature. Model predictions and experimental data points.**

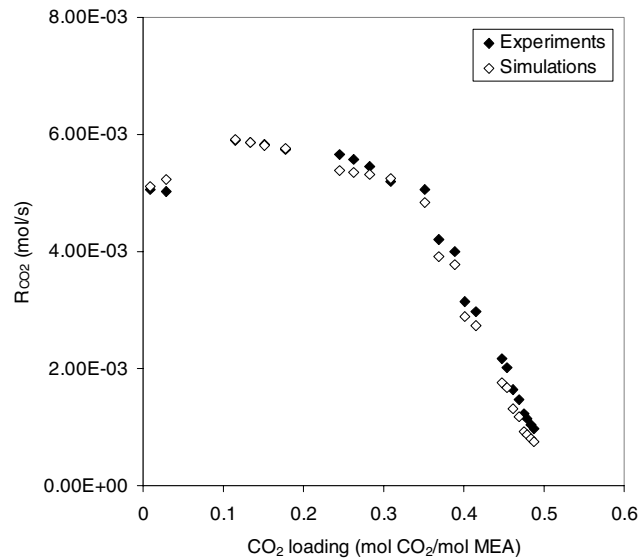


**FIGURE 7.23: Experiments from pilot scale test rig at SINTEF/NTNU, 30% MEA/water. Crossflow membrane module with 1 mm (i.d.) tubes. Model prediction and experimental data points.**

# *Measurement of kinetics for carbon dioxide absorption*

---

## **8.1 Measurement of rate constants**

Several different types of equipment have been developed for measuring the kinetics of gas/liquid reactions. The most important ones are illustrated in figure 8.1. Of these, especially the laminar jet and the wetted wall have been very popular in the measurement of CO<sub>2</sub>/alkanolamine kinetics. This is due to the fact that the hydrodynamics of these units may be easily modelled, leading to an estimate of the physical mass transfer coefficient from first principles. The mass-transfer area of these units is in principle known, and the effect of the chemical reaction may then be separated from the diffusion problem. In units like the stirred vessel and the string of discs the mass transfer area is still known, but the physical mass transfer coefficient must be measured from calibration with a non-reactive system.

The lab-scale membrane gas absorber may be classified in the same group as the laminar jet and the wetted wall column due to the properties of a fixed interfacial area and the possibility of modeling the hydrodynamics from fundamental relations. However, the membrane absorber offers significant advantages due to





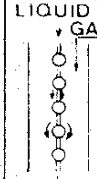
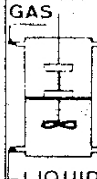

TYPE	LAMINAR JET	CYLINDRICAL WETTED WALL	CONIC WETTED WALL	SPHERICAL WETTED WALL	STRING OF DISCS OR SPHERES	STIRRED VESSEL	ROTATING DRUM
SCHEME							

FIGURE 8.1: Common equipment for the measurement of kinetics for gas/liquid reactions (Charpentier, 1982)

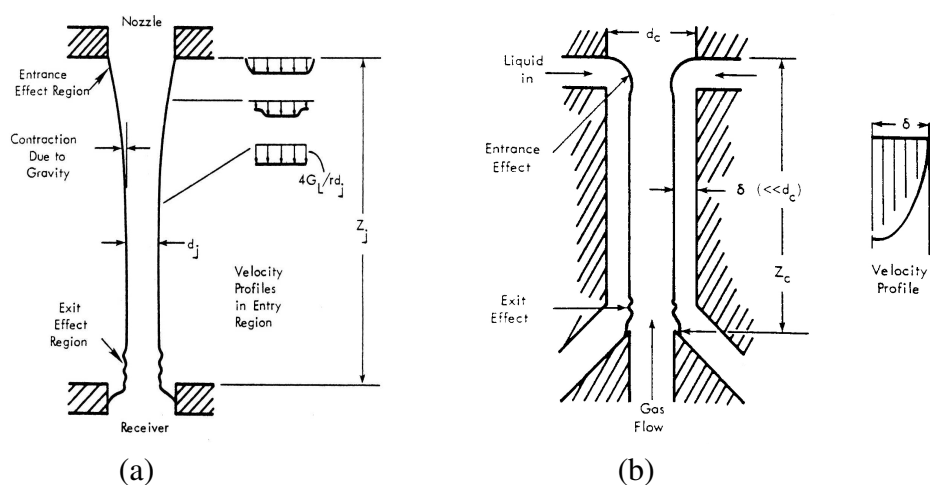


FIGURE 8.2: The laminar jet (a) and wetted wall (b) apparatus (Astarita et al. 1983)

the decoupling of the phases. In the laminar jet and the wetted wall column the mass transfer area is no longer known if the flow becomes turbulent or ripples are formed. The transition can only be visually observed and is therefore uncertain. In addition, the entrance and exit effects in traditional lab-scale mass transfer equipment lead to uncertainty and to difficulties in modeling the system (figure 8.2).

**TABLE 8–1: Mass transfer coefficients of laboratory units (Charpentier, 1982), including the membrane module used in this work, and an optimized membrane module.**

Equipment	Time of contact (s)	$k_1 \cdot 100$ (m/s)
Laminar jet	0.001-0.1	0.016-0.16
Sphere	0.1-1	0.005-0.016
Wetted wall	0.1-2	0.0036-0.016
String of discs	0.1-2	0.0036-0.016
Stirred vessel	0.06-10	0.0016-0.021
Membrane GLC S01	25	0.0005
Optimized membrane	0.025-1	0.002-0.008

In table 8–1 typical values of the mass transfer coefficient are given for the common types of equipment and for the membrane unit used in this work. The membrane unit and the liquid velocities used in this work is seen to give a significantly lower mass transfer coefficient than most other types. This is a disadvantage as the mass transfer may then be significantly influenced by diffusion phenomena. As described in 6.2.2, the rate constants should preferably be measured in the pseudo first order irreversible regime in order to get a most direct measurement, not influenced by diffusion of free alkanolamine and the ionic reaction products. In the pseudo-first order regime, the rate of absorption is given by equation (6.10), reiterated for convenience:

$$N_A = \frac{\sqrt{D_A k_2 c_B}}{H} (p_A - p_A^*) \quad (8.1)$$

From the discussion in 6.4.2 it is clear that the pseudo first order irreversible reaction regime is approached by using a low partial pressure and a high liquid velocity to lower the contact time. This implies that the membrane module used for kinetic measurements should ideally be of shorter tube length, from 1-5 cm, and with lower tube diameter of around 1 mm. This enables significantly lower contact times to be realized without increasing the liquid flow beyond what is practically possible. The reduction of tube length and diameter may be compen-

sated by increasing the number of tubes in order to maintain a suitable mass transfer area. This may be necessary in order to enable a flux measurement with significant accuracy, using conventional mass flow meters. This shows another feature of flexibility for the membrane gas absorber compared to e.g. the laminar jet. Similar compensation would require several laminar jets in parallel, which is obviously not possible. Thus, by making a membrane module of optimized design, units can be made with similar contact time and mass transfer coefficient as e.g. the laminar jet and wetted wall.

## 8.2 Sensitivity analysis on the membrane model

From the relative enhancement factors discussed in 6.4.2 it is clear that none of the initial experiments performed in the lab-scale apparatus was made in a range where the kinetic constant can be extracted from the data with a sufficient accuracy. It was however found that some experiments were close to the instantaneous reaction regime. This was especially the case for the 15% MEA/pure CO<sub>2</sub> series.

Using the membrane absorber model a sensitivity analysis was performed similar to that presented in 7.3.3, but with the restriction  $D_{am} = \tilde{D}_{cb}$ . The parameters reaction rate constant ( $k_2$ ), free CO<sub>2</sub> diffusivity ( $D_{CO_2}$ ) and the apparent diffusivity of the reaction products ( $\tilde{D}_{cb}$ ) were multiplied by a factor of 2 and the increase in the simulated absorption flux was observed in each case. In addition, the influence of reaction reversibility was tested by setting the equilibrium CO<sub>2</sub>-concentration,  $c_{CO_2, e}$  equal to zero (see eq. (3.30)).

Both the MEA and MDEA systems were tested with low partial pressures of 1/5 kPa and with partial pressures corresponding to experiments with pure CO<sub>2</sub> in the gas phase. The inlet CO<sub>2</sub> loading was set to zero and the temperature was varied from 25 to 70°C. In table 8–2 and 8–3 the results are shown in terms of the sensitivity factors, defined by eq. (7.40).

**TABLE 8–2: Results from sensitivity analysis, low  $p_{CO_2}$** 

Module GLS S01 (43 cm tube length, 3 mm i.d., 28 tubes)				
23.5wt% MDEA, $p_{CO_2} = 5$ kPa				
T (°C)	25	40	55	70
$R_{CO_2}$ (mol/s)	$1.37 \times 10^{-5}$	$1.89 \times 10^{-5}$	$2.45 \times 10^{-5}$	$2.88 \times 10^{-5}$
$2^*k_2$	1.32	1.29	1.24	1.17
$2^*D_{CO_2}$	1.36	1.36	1.33	1.26
$2^*\tilde{D}_{cb}$	1.04	1.05	1.08	1.14
Irreversible rx.	1.01	1.03	1.08	1.22
30wt% MEA, $p_{CO_2} = 1$ kPa				
$R_{CO_2}$ (mol/s)	$9.44 \times 10^{-5}$	$1.20 \times 10^{-4}$	$1.50 \times 10^{-4}$	$1.79 \times 10^{-4}$
$2^*k_2$	1.25	1.24	1.22	1.18
$2^*D_{CO_2}$	1.21	1.18	1.15	1.10
$2^*\tilde{D}_{cb}$	1.08	1.07	1.07	1.07
Irreversible rx.	1.00	1.00	1.00	1.03

From eq. (8.1) it is seen that if the pseudo first order reaction regime is achieved, the sensitivity factor of  $k_2$  will be 1.41 ( $\sqrt{2}$ ), and the sensitivity factor of free  $CO_2$  diffusivity will be in the same range. In table 8–2 it is seen that this regime is approached, but not achieved for MDEA with  $p_{CO_2} = 5$  kPa. The sensitivity to the kinetic constant is however reasonably good, but brakes down at higher temperature, where the absorption rate is more influenced by the diffusivity of bound  $CO_2$  and the reaction reversibility. It is concluded that new experiments with similar conditions may be used to regress the kinetic constant of  $CO_2$ /MDEA at temperatures below 55°C. The corresponding simulations with 30% MEA and  $p_{CO_2} = 1$  kPa, show the same trends, although the kinetics sensitivity factor is lower than in the MDEA-system. An important difference

**TABLE 8–3: Results from sensitivity analysis, high  $p_{CO_2}$** 

Module GLS S01 (43 cm tube length, 3 mm i.d., 28 tubes)				
23.5% MDEA, $p_{CO_2} = 90$ kPa				
T (°C)	25	40	55	70
$R_{CO_2}$ (mol/s)	$1.20 \times 10^{-4}$	$1.58 \times 10^{-4}$	$1.89 \times 10^{-4}$	$2.04 \times 10^{-4}$
$2*k_2$	1.14	1.12	1.09	1.05
$2*D_{CO_2}$	1.18	1.16	1.14	1.10
$2*\tilde{D}_{cb}$	1.23	1.26	1.30	1.36
Irreversible rx.	1.04	1.10	1.24	1.42
15% MEA, $p_{CO_2} = 90$ kPa				
$R_{CO_2}$ (mol/s)	$3.17 \times 10^{-4}$	$4.06 \times 10^{-4}$	$5.03 \times 10^{-4}$	$6.05 \times 10^{-4}$
$2*k_2$	1.00	1.00	1.00	1.00
$2*D_{CO_2}$	1.03	1.02	1.02	1.02
$2*\tilde{D}_{cb}$	1.54	1.54	1.54	1.52
Irreversible rx.	1.00	1.00	1.00	1.01

can be seen as there is only a minor effect from ignoring the reaction reversibility in the MEA-system, reflecting the fact that MEA absorbs  $CO_2$  almost irreversibly at low loadings.

From table 8–3 it is seen that the partial pressure has a large influence on the sensitivity factors, resulting in a large sensitivity to the bound  $CO_2$  diffusivity, and a reduced sensitivity to the kinetics. This is especially the case in the MEA-system, where bound  $CO_2$  diffusion is seen to be almost totally rate limiting with  $p_{CO_2} = 90$  kPa. The conditions are here similar to the conditions used in the experiments with 15wt% MEA and pure  $CO_2$  stagnant gas phase, and lead to the conclusion that the bound  $CO_2$  diffusivity can be regressed from these experiments, as described in 7.3.5. The corresponding simulations with the



**TABLE 8–4: Low  $p_{CO_2}$  sensitivity analysis with shorter membrane tubes**

Membrane module with tube length 5 cm, 1 mm tube diameter and 100 tubes				
48.8wt% MDEA, $p_{CO_2} = 5$ kPa				
T (°C)	25	40	55	70
$R_{CO_2}$ (mol/s)	$2.06 \times 10^{-6}$	$2.98 \times 10^{-6}$	$4.23 \times 10^{-6}$	$5.80 \times 10^{-6}$
$2*k_2$	1.39	1.36	1.32	1.26
$2*D_{CO_2}$	1.40	1.39	1.37	1.34
$2*\tilde{D}_{cb}$	1.01	1.02	1.04	1.07
Irreversible rx.	1.00	1.00	1.01	1.03
30wt% MEA, $p_{CO_2} = 1$ kPa				
$R_{CO_2}$ (mol/s)	$1.82 \times 10^{-5}$	$2.36 \times 10^{-5}$	$3.04 \times 10^{-5}$	$3.86 \times 10^{-5}$
$2*k_2$	1.31	1.30	1.29	1.27
$2*D_{CO_2}$	1.31	1.30	1.28	1.26
$2*\tilde{D}_{cb}$	1.03	1.03	1.03	1.03
Irreversible rx.	1.00	1.00	1.00	1.00

MDEA-system (90 kPa, 23.5 wt% MDEA) show the same trend, but a significant sensitivity towards the reaction kinetics is still present at the high partial pressure. In addition, the reaction reversibility is seen to have a large influence at the higher temperatures. These conditions are similar to the experiments performed with 23.5wt% MDEA with pure  $CO_2$ /stagnant gas phase. The bound  $CO_2$  diffusivity was regressed from simulations on these experiments, as described in 7.3.5, although the correlation is expected to be more uncertain than the corresponding relation for the MEA-system.

The advantage of small contact times when measuring kinetic constants is seen in table 8–4, where a sensitivity analysis is performed on a membrane module with conditions corresponding to a contact time of 1 s. The kinetic sensitivity in

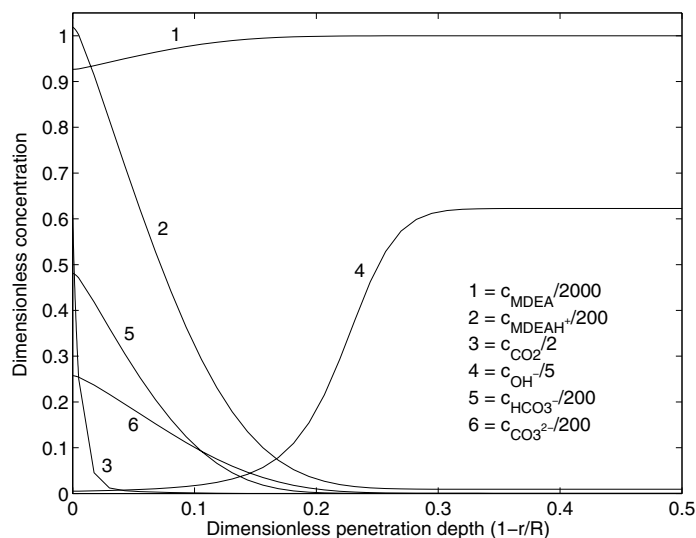


**FIGURE 8.3: Concentration profiles at the membrane tube outlet for a 23.5wt% MDEA solution.  $T=298$  K,  $Q_L=0.200$  l/min,  $p_{\text{CO}_2}=5$  kPa**

both MEA and MDEA is significantly increased, while the sensitivity to the bound  $\text{CO}_2$  diffusivity and the reverse reaction is decreased.

### 8.3 Kinetics measurement

As can be seen from table 8–2, except at the highest temperature, the sensitivity to the reaction kinetics for experiments with 23.5% MDEA with  $p_{\text{CO}_2}=5$  kPa will be significantly higher than the sensitivity to the bound  $\text{CO}_2$  diffusivity. This is because the conditions are close to what corresponds to pseudo first order reaction, as can be seen from the concentration profiles given in figure 8.3. These are liquid concentration profiles at the membrane outlet. The MDEA concentration is only moderately depleted at the liquid surface.

New absorption measurements for MDEA were performed with the same experimental conditions as in table 8–2. The membrane absorber model was used for data regression of the second order rate constant for the  $\text{CO}_2$ -MDEA reaction from the following expression:

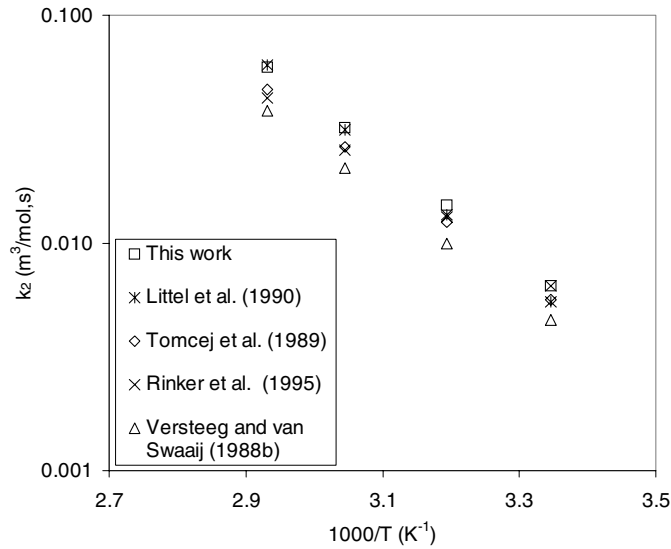


**FIGURE 8.4: Arrhenius plot of estimates for the second order rate constant for the CO<sub>2</sub>-MDEA reaction**

$$k_2 = k_{2,313} \exp\left(B\left(\frac{1}{T} - \frac{1}{313}\right)\right) \quad (8.2)$$

The Levenberg-Marquardt non-linear regression method was used, as implemented in the in-house “Modfit” program (Hertzberg and Mejdell, 1998). Due to the large sensitivity to the equilibrium model at 70°C and the reduced sensitivity to the reaction kinetics, only the experiments for 25, 40 and 55°C were used in the regression. The following Arrhenius relation resulted for the rate constant:

$$k_2 = 3.60 \times 10^5 \exp\left(\frac{-5330}{T}\right) \quad (8.3)$$

The agreement on the value of the kinetic constant for the CO<sub>2</sub>-MDEA reaction is very good between later sources as can be seen from figure 8.4, where rate constants from literature are plotted together with that resulting from eq. (8.3). It is seen that eq. (8.3) gives similar results as Littel et al. (1990) at high temper-

ature, but is more equal to Rinker et al. (1995) at lower temperature. The main subject of discussion in later literature has been related to the relative importance of the hydroxide reaction when absorbing CO<sub>2</sub> in unloaded MDEA-solutions. The overall reaction rate constant is normally expressed by:

$$k_{ov} = \frac{r_{CO_2}}{c_{CO_2}} = k_{2,OH^-} c_{OH^-} + k_{2,MDEA} c_{MDEA} \quad (8.4)$$

Early work tended to treat OH<sup>-</sup>-reaction as pseudo first order in parallel to the reaction with MDEA (Versteeg and van Swaaij, 1988b; Tomcej and Otto, 1989), then calculating  $k_{2,MDEA}$  from a combination of eq. (8.1) and (8.4). In the rigorous mass-transfer model by Glasscock and Rochelle (1989) it was however shown that OH<sup>-</sup> is significantly depleted at the liquid surface and that treating it as pseudo first order will lead to an underestimation of  $k_{2,MDEA}$ . This can be clearly seen from the OH<sup>-</sup> concentration profile in figure 8.3. The observation lead Littel et al. (1990) to re-evaluate the data from Versteeg and van Swaaij (1988b), which resulted in an increase of 30% in the reported rate-constant. Littel et al. (1990) from their mass transfer model concluded that the rate constant should be regressed from an expression neglecting the contribution from OH<sup>-</sup>. Rinker et al. (1995) discussed this subject further and showed that the kinetic constant has to be regressed from a rigorous mass-transfer model including the true concentration profile of OH<sup>-</sup>.

## 8.4 Driving force effects

The correct implementation of the contribution from the OH<sup>-</sup> reaction (eq. (3.5)) to a large extent explains the “driving force effect” observed by Glasscock and Rochelle (1989) and Rinker et al. (1995), as the relative contribution from the OH<sup>-</sup> reaction is decreasing with increasing CO<sub>2</sub> partial pressure. This is due to the increased interfacial concentration of CO<sub>2</sub>, which leads to faster depletion of OH<sup>-</sup> at higher partial pressures.

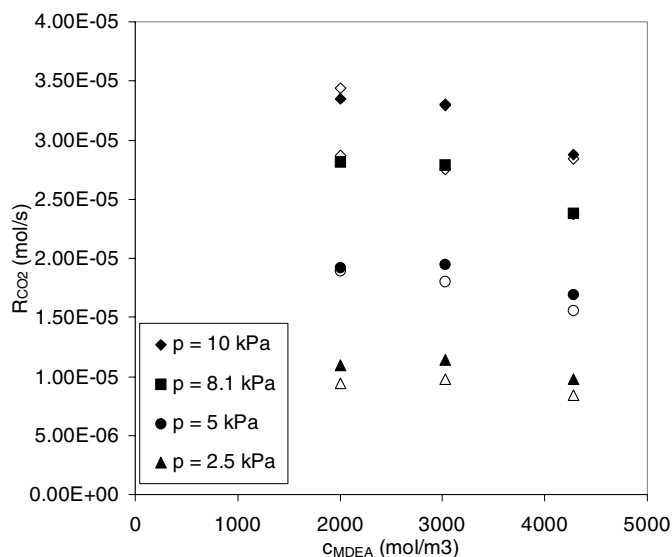


**FIGURE 8.5: Absorption rates from experiments with varying  $p_{CO_2}$  and MDEA-concentration at 40°C (closed points). Model prediction in open data points.**

To further study the absorption under these conditions, new experiments were performed in the MDEA system with variable  $CO_2$  partial pressure from 2.5 to 10 kPa and concentrations of 23.5, 35 and 48.8 wt% MDEA at a fixed temperature of 40°C.

The results from these experiments are plotted in figure 8.5, including the model prediction, using eq. (8.3) for the rate constant. The average model deviation in predicting these experiments was -4.7% with a maximum of -14.6%. It is seen that the model tends to underpredict the absorption rate at lower partial pressure. The effect is a similar as would have been expected if the contribution from  $OH^-$  was not included in the model. This suggested that a chemical reaction not accounted for in the model contributed to the absorption in this regime. Versteeg et al. (1986, 1996) suggested that similar effects can be caused by primary and secondary amine contaminants in commercial MDEA. This hypothesis was investigated by Glasscock (1990) by analyzing the MDEA for impurities using a similar commercial grade MDEA as in this work. Only traces of the secondary amines methyl-monoethanolamine and N-methyl-diglycolamine were

found (<0.1% in total) and it was concluded that this effect was not able to account for the high absorption rates at low partial pressure.

One option that has not been considered in the literature in this context is the contribution from the monoalkylcarbonate-reaction, discussed in 3.3.3. As this is a reaction involving  $\text{OH}^-$  its contribution will show a similar driving force dependence as the direct reaction with  $\text{OH}^-$ . The Arrhenius expression for the kinetic constant of this third order reaction was estimated from the TEA data at 273 and 291 K from Jørgensen and Faurholt (1954) and Jørgensen (1956), leading to:

$$k_3 = 1662 \exp\left(\frac{-3456}{T}\right) \quad (8.5)$$

The rate of reaction was assumed similar in the MDEA-case, which is expected to be a reasonable estimate, and the rate expression was included in the absorber model. The reaction was treated as irreversible due to the relatively high equilibrium constant of reaction (3.28) and the observation by Jørgensen (1956) that the monoalkylcarbonate quickly decomposes to bicarbonate. A new parameter regression was performed for the second order rate constant for the  $\text{CO}_2$ -MDEA reaction, leading to an expression slightly different from eq. (8.3) but very close to Littel et al. (1990).

$$k_2 = 1.22 \times 10^6 \exp\left(\frac{-5749}{T}\right) \quad (8.6)$$

When simulating the experiments with the model consistently accounting for the monoalkylcarbonate reaction the resulting average and maximum deviation was reduced to -4.3 and -11.2%, respectively. It may thus be concluded that the effect of monoalkylcarbonate formation is noticeable but still of minor importance. In apparatus with lower contact times than used for these experiments, the contribution may be more important due to the lower degree of  $\text{OH}^-$  depletion. As opposed to the direct reaction with  $\text{OH}^-$  the contribution from the alky-

Ikarbonate reaction may still be present at higher MDEA-concentration, since MDEA enters in the rate expression of this reaction.

From figure 8.5 it is seen that the absorption rates are nearly constant when MDEA-concentration increases from 2000-3000 mol/m<sup>3</sup> and is reduced when MDEA-concentration increases from 3000-4280 mol/m<sup>3</sup>. A similar trend was observed by Pani et al. (1997). This behavior results from the fact that viscosity is strongly increasing with MDEA-concentration and that the physical solubility is correspondingly decreasing. These effects overcome the effect of the increasing pseudo first order rate constant  $k_2 c_{MDEA}$ . The trend is very well predicted by the model.





## **9.1 Summary**

This dissertation has presented a rigorous model for the simulation of CO<sub>2</sub> absorption in a membrane contactor with aqueous alkanolamines. The model explicitly accounts for diffusion and chemical reaction including thermal effects and the effects of radial viscosity gradients on the molecular transport. An equilibrium model is developed solving for CO<sub>2</sub> partial pressure and concentrations of all molecular and ionic species at given CO<sub>2</sub>-loading in solution.

A new lab-scale test rig for the study of membrane gas absorption has been constructed and established. Experiments are done with absorption of CO<sub>2</sub> in aqueous solution of monoethanolamine (MEA) and methyldiethanolamine (MDEA) respectively. The effects of varying CO<sub>2</sub> partial pressure, liquid velocity and temperature are systematically investigated with conditions covering the range of interest for the industrial application in exhaust gas CO<sub>2</sub>-removal.

New correlations are developed for the diffusivities of the ionic products of the CO<sub>2</sub>-alkanolamine reactions and the possibility of measuring reaction kinetics in a lab-scale membrane contactor is discussed and investigated. Experiments

are performed and used in regression of the rate constant for the CO<sub>2</sub>-MDEA reaction.

## 9.2 Conclusions

The review of membrane gas absorption in the literature shows that many approaches to the problem have not been investigated in earlier literature. This especially includes rigorous modeling of the diffusion/reaction problem including thermal effects and an equilibrium speciation model. Little work has been done in experimentally investigating the operation of membrane gas absorbers covering industrially relevant conditions.

The generally accepted “zwitterion mechanism”, used in explaining the observed orders of reaction in primary and secondary amines, requires a proton transfer reaction, the zwitterion deprotonation, to be considered rate limiting in special cases. This contradicts the general conception that reactions only involving a proton transfer are considered instantaneous. From using *ab initio* calculations, it is possible to show that the actual reaction mechanism probably consists of a set of parallel third order reactions. The reactions involve carbon dioxide, alkanolamine and the set of species capable of acting as a base in extracting a proton from the alkanolamine. It is suggested that the fractional reaction orders observed in several systems result from the extent of which the amphiprotic solvent may act as a base compared to the other bases in solution.

A speciation model based upon apparent equilibrium constants is shown to give similar results in terms of liquid speciation as other rigorous activity based models, which are considerably more computer intensive. The implementation of activity based models in absorber simulators is presently still limited by the lack of kinetic and mass transfer data based upon a similar approach.

The experimental study of membrane gas absorption, with a module of straight tube hollow fibers of microporous PTFE, clearly shows the effects of varying partial pressure, liquid velocity and temperature in a wide range of operation. It is shown that the contribution from the gas phase in the overall mass transfer

resistance is negligible for the conditions studied. Membrane mass transfer resistance corresponds to less than 12% of the total, leaving the liquid side as the totally dominating resistance term. The liquid side mass transfer is dominated by diffusion of the ionic reaction products into the bulk of the liquid for all conditions except at very low partial pressures, where the sensitivity to reaction kinetics is larger. New correlations are developed for the diffusivities of the reaction products modeled as a bound CO<sub>2</sub> chemical species.

The effect of increasing liquid viscosity with increasing CO<sub>2</sub>-loading is important in modeling of the diffusion problem. The radial viscosity and density gradients are however not large enough to significantly influence the liquid velocity profiles in the membrane tubes. This allows the use of the parabolic velocity profile derived with the constant viscosity and density assumption.

The developed membrane gas absorber model gives a good prediction of experimental data including the observed trends. The deviation is generally less than  $\pm 15\%$ . Within the range of operation for an industrial contactor with CO<sub>2</sub> absorbing in aqueous MEA, the average model deviation is 2.8%.

A lab-scale membrane gas absorber is considered an excellent unit for the measurement of kinetics of CO<sub>2</sub>-alkanolamine reactions. The accuracy of measurement can be improved by using a membrane module of optimized design with a shorter tube length than the one used in this work.

### 9.3 Future work

There is a number of subjects encountered that have been considered outside the scope of this work, but should still receive further attention in future work. All computer models are “dynamic models” in the sense that they can continuously evolve and improve as a result of increased knowledge, increased computational power and access to new data material. The most important points of improvement, both in terms of modeling and general understanding of membrane gas absorbers are summarized below:

- A more rigorous equilibrium model should be included, which is more easily extended to other conditions (temperatures/pressures/chemical systems) than those studied in this work. This is made topical through the observation that the diffusion of bound CO<sub>2</sub> reaction products have a rate limiting contribution to the mass transfer. Large gradients result in the total amine concentration, which may increase far outside the range of experimental equilibrium data.
- The equilibrium speciation model developed in this work is non-iterative and has a minimum effect on the computation time. A rigorous model will be iterative in terms of both composition and activity/fugacity coefficients and lead to larger computation time. The possibility of a more efficient numerical solution of the governing equations should be considered, especially in terms of discretization in the radial direction. This may be improved by using an adaptive non-uniform grid and a different method of calculating spatial derivatives.
- The effects from diffusion of ionic reaction products should be studied more, both theoretically and experimentally.
- Even if the contribution from gas side mass transfer resistance has been found negligible for the conditions studied in this work, new experiments should be performed aimed at correlating the mass transfer coefficient of the gas. This will be particularly important when modeling a high pressure application of the membrane gas absorbers, as the gas diffusivities are significantly decreased upon increasing pressure. The contribution from gas side mass transfer may then be more significant.
- The model should be checked against experiments with physical absorption, like CO<sub>2</sub> in water and chemical absorption of CO<sub>2</sub> in NaOH.
- The effect of membrane porosity on the effective mass transfer area is not completely understood. This should be investigated further through measurements on membranes with different values of porosity.

### *9.3 Future work*

---

- A new membrane module of significantly shorter tube length should be tested for the purpose of measuring reaction kinetics.



---

## References

---

Adams, M.E. and Marshall, T.L. (1998), Diffusion Coefficients Significant in Modeling the Absorption Rate of Carbon Dioxide into Aqueous Blends of N-Methyldiethanolamine and Diethanolamine and of Hydrogen Sulfide into Aqueous N-Methyldiethanolamine, *J. Chem. Eng. Data*, **43**:605-610.

Al-Ghawas, H.A., Hagewiesche, D.P., Ruiz-Ibanez, G. and Sandall, O.C. (1989), Physicochemical Properties Important for Carbon Dioxide Absorption in Aqueous Methyldiethanolamine, *J. Chem. Eng. Data.*, **34**:385-391.

Alvarez, E., Rendo, R., Sanjurjo, B., Sánchez-Vilas, M. and Nazava, J.M. (1998), Surface Tension of Binary Mixtures of Water + N-Methyldiethanolamine and Ternary Mixtures of This Amine and Water with Monoethanolamine, Diethanolamine, and 2-Amino-2-methyl-1-propanol from 25 to 50°C, *J. Chem. Eng. Data*, **43**:1027-1029.

Aroonwilas, A., Veawab, A. and Tontiwachwuthikul, P. (1999), Behaviour of the Mass-Transfer Coefficient of Structured Packings in CO<sub>2</sub> Absorbers with Chemical Reactions, *Ind. Eng. Chem. Res.*, **38**:2044-2050.

Astarita, G., Savage, D.W. and Bisio, A. (1983), Gas Treating with Chemical Solvents, New York:John Wiley & Sons.

Atwood, K., Arnold, M.R. and Kindrick, R.C. (1957), Equilibria For The System Ethanolamine-Hydrogen Sulfide-Water, *Ind. Eng. Chem.*, **49**:1439.

Austgen, D.M. (1989), A Model of Vapor-Liquid Equilibrium for Acid Gas-Alkanolamine-Water Systems, Ph.D. dissertation, University of Texas at Austin.

Austgen, D.M., Rochelle, G.T. and Chem, C-C. (1991), Model of Vapor-Liquid Equilibria for Aqueous Acid Gas-Alkanolamine Systems. 2. Representation of H<sub>2</sub>S and CO<sub>2</sub> Solubility in Aqueous MDEA and CO<sub>2</sub> Solubility in Aqueous Mixtures of MDEA with MEA or DEA, *Ind. Eng. Chem. Res.*, **30**:543-585.

---

Austgen, D.M., Rochelle, G.T., Peng, X. and Chen, C-C. (1989), Model of Vapor-Liquid Equilibria for Aqueous Acid Gas-Alkanolamine Systems Using the Electrolyte-NRTL Equation, *Ind. Eng. Chem. Res.*, **28**:1060-1073.

Barth, D., Tondre, C., Lappal, G. and Delpuech, J.J. (1981), Kinetic Study of Carbon Dioxide Reaction with Tertiary Amines in Aqueous Solution, *Am. Chem. Soc.*, **85**:3660-3667.

Bates, R.G. and Pinching, G.D. (1951), Acidic Dissociation Constant and Related Thermodynamic Quantities for Monoethanolammonium Ion in Water From 0 to 50° C, *J. Res. Nat. Bur. Stand.*, **46**:349-352.

Bird, R.B., Stewart, W.E. and Lightfoot, E.N. (2002), *Transport Phenomena*, 2nd ed., New York:John Wiley & Sons.

Bishnoi, S. (2000), Carbon Dioxide Absorption and Solution Equilibrium in Piperazine Activated Methyldiethanolamine, Ph.D. dissertation, University of Texas at Austin.

Blauwhoff, P.M.M., Versteeg, G.F. and van Swaaij, W.P.M. (1984), A Study on the Reaction between CO<sub>2</sub> and Alkanolamines in Aqueous Solutions, *Chem. Eng. Sci.*, **39**:207-225.

Bolland, O. and Undrum, H. (2002), A novel methodology for comparing CO<sub>2</sub> capture options for natural gas-fired combined cycle plants., *Adv. Environ. Res.*, In press.

Bosch, H., Kuipers, J.A.M., van Swaaij, W.P.M. and Versteeg, G.F. (1989), Mass transfer with complex chemical reactions, *Gas Sep. & Purif.*, **3**:75-83.

Bottoms, R.R. (1930), U.S. Patent No. 1,783,901.

Brandrup, J. and Immergut, E.H. (1989), *Polymer Handbook*, 3rd ed., New York:John Wiley & Sons.

Browning, G.J. and Weiland, R.H. (1994), Physical Solubility of Carbon Dioxide in Aqueous Alkanolamines via Nitrous Oxide Analogy, *J. Chem. Eng. Data*, **38**:817-822.



---

Button, J.K. and Gubbins, K.E. (1999), SAFT prediction of vapour-liquid equilibria of mixtures containing carbon dioxide and aqueous monoethanolamine or diethanolamine, *Fluid Phase Equilibria*, **158-160**:175-181.

Caplow, M. (1968), Kinetics of Carbamate Formation and Breakdown, *J. Am. Chem. Soc.*, **90**: 6795-6803.

Charpentier, J.C. (1982), What's new in absorption with chemical reaction?, *Trans. IChemE*, **60**:131-156.

Chen, C.-C. and Evans, L.B. (1986), A Local Composition Model for the Excess Gibbs Energy of Aqueous Electrolyte systems, *AIChE J.*, **32**:444-454.

Cheng, S., Meisen, A. and Chakma, A. (1996), Predict amine solution properties accurately, *Hydrocarb. Process*, **75**:81-84.

Chun, M.-S. and Lee, K.-H. (1997), Analysis on a Hydrophobic Hollow-Fiber Membrane Absorber and Experimental Observations of CO<sub>2</sub> Removal by Enhanced Absorption, *Sep. Purif. Technol.*, **32**:2445-2466.

Chunxi, L. and Fürst, W. (2000), Representation of CO<sub>2</sub> and H<sub>2</sub>S Solubility in Aqueous MDEA Solutions using an Electrolyte Equation of State, *Chem. Eng. Sci.*, **55**:2975-2988.

Crooks, J.E. and Donnelan, J.P. (1989), Kinetics and Mechanism of the Reaction between Carbon Dioxide and Amines in Aqueous Solution, *J. Chem. Soc. Perkin. Trans.*, II:331-333.

Cussler, E.L. (1994a), Diffusion - Mass Transfer in Engineering Practice, Cambridge University Press.

Cussler, E.L. (1994b), Hollow Fiber Contactors, in: J.G. Crespo and K.W. Bödiker (Eds.), Membrane Processes in Separation and Purification, Kluwer Academic Publishers, The Netherlands, 375-394.

Danckwerts, P.V. (1970), Gas-Liquid Reactions, McGraw-Hill Book Co.

Danckwerts, P.V. and McNeil, K.M. (1967), The absorption of Carbon Dioxide Into Aqueous Amine Solutions and The Effects of Catalysis, *Trans. Inst. Chem. Eng.*, **45**:T32-T4.

---

Desmukh, R.D. and Mather, A.E. (1981), A mathematical Model For Equilibrium Solubility of Hydrogen Sulfide and Carbon Dioxide in Aqueous Alkanolamine Solutions, *Chem. Eng. Sci.*, **36**:355-362.

Doebelin, E.O. (1990), *Measurement Systems - Application and Design*, McGraw Hill Publishing Company.

Donaldson, T.L. and Nguyen, Y.N. (1980), Carbon Dioxide Reaction Kinetics and Transport in Aqueous Amine Membranes, *Ind. Eng. Chem. Fundam.*, **19**:260-266.

Edwards, T.J. and Maurer, G., Newman, J. and Prausnitz, J.M. (1978), Vapor-Liquid Equilibria in Multicomponent Aqueous Solutions of Volatile Weak Electrolytes, *AIChE J.*, **24**:966-976.

Edwards, T.J., Newman, J. and Prausnitz, J.M. (1975), Thermodynamics of Aqueous Solutions Containing Volatile Weak Electrolytes, *AIChE J.*, **21**:248-259.

Eimer, D. (1994), *Simultaneous Removal of Water and Hydrogen Sulphide From Natural Gas*, Ph.D. dissertation, Norwegian Institute of Technology.

Emmert, R.E. and Pigford, R.L. (1962), Gas Absorption Accompanied by Chemical Reaction: A Study of the Absorption of Carbon Dioxide in Aqueous Solutions of Monoethanolamine, *AIChE J.*, **8**:171-175.

Esato, K. and Eiseman, B. (1975), Experimental evaluation of Gore-Tex membrane oxygenator, *J. Thorac. Cardiovascular Surg.*, **69**:690-697.

Falk-Pedersen, O., Dannstrøm, H., Grønvold, M., Stuksrud, D-B. and Rønning, O. (2000), *Gas Treatment using Membrane Gas/Liquid Contactors, GHGT-5*, Cairns, Australia.

Feron, P.H.M. and Jansen, A.E. (2002), CO<sub>2</sub> Separation with Polyolefin Membrane Contactors and Dedicated Absorption Liquids: Performances and Prospects, *Sep. Purif. Technol.*, **27**:231-242.

Feron, P.H.M., Jansen, A.E. and Klaassen, R. (1992), Membrane Technology in Carbon Dioxide Removal, *Energy Convers. Mgmt.*, **33**:421-428.

- 
- Fürst, W. and Renon, H. (1959), Representation of Excess Properties of Electrolyte Solutions using a new Equation of State, *AIChE J.*, **39**:335-343.
- Gabelman, A. and Hwang, S-T. (1999), Hollow Fiber Membrane Contactors, *J. Memb. Sci.*, **159**:61-106.
- Geankopolis, C.J. (1993), Transport Processes and Unit Operations, Prentice-Hall, Inc.
- Glasscock, D.A. (1990), Modelling and Experimental Study of Carbon Dioxide Absorption in to Aqueous Alkanolamines, Ph.D. dissertation, University of Texas at Austin.
- Glasscock, D.A. and Rochelle, G.T. (1989), Numerical Simulation of Theories for Gas Absorption with Chemical Reaction, *AIChE J.*, **35**:1271-1281.
- Guggenheim, E.A. (1935), The Specific Thermodynamic Properties of Aqueous Solutions of Strong Electrolytes, *Phil. Mag.*, **19**:588.
- Haimour, N. and Sandall, O.C. (1984), Absorption of Carbon Dioxide into Aqueous Methyl-diethanolamine, *Chem. Eng. Sci.*, **39**:1791-1796.
- Hertzberg, T. and Mejdell, T. (1998), MODFIT for MatLab; Parameter Estimation in a General Nonlinear Multiresponse Model.
- Hoff, K.A., Poplsteinova, J., Jakobsen, H.A., Falk-Pedersen, O., Juliussen, O. and Svendsen, H.F. (2003), Modeling of Membrane Reactor, *Int. J. Chem. React. Eng.*, **1**:A9/1-12.
- Hogendoorn, J.A., Vas Bhat, R.D., Kuipers, J.A.M., van Swaaij, W.P.M. and Versteeg, G.F. (1997), Approximation for the enhancement factor applicable to reversible reactions of finite rate in chemically loaded solutions, *Chem. Eng. Sci.*, **52**:4547-4559.
- Hu, W. and Chakma, A. (1990), Modelling of Equilibrium Solubility of CO<sub>2</sub> and H<sub>2</sub>S in Aqueous Amino Methyl Propanol (AMP) Solutions, *Chem. Eng. Comm.*, **94**:53-61.
- Jakobsen, H.A., Lindborg, H., and Handeland, V. (2002). A Numerical Study of the Interactions Between Viscous Flow, Transport and Kinetics in Fixed Bed Reactors. *Computers & Chemical Engineering*, **26**:333-357.

- 
- Jansen, A.E. and Feron, P.H.M. (1998), Method for Gas Absorption Across a Membrane, US Patent 5,749.941.
- Johnson, S.L. and Morrison, R.L. (1971), Kinetics and Mechanism of Decarboxylation of N-Arylcarbamates. Evidence of Kinetically Important Zwitterionic Carbamic Acid Species of Short Lifetime, *J. Am. Chem. Soc.*, **94**:1323-1334.
- Jørgensen, E. (1956), Reactions between Carbon Dioxide and Amino-alcohols III. Diethanolamine, *Acta. Chim. Scand.*, **10**:747-755.
- Jørgensen, E. and Faurholt, C. (1954), Reactions between Carbon Dioxide and Amino-alcohols II. Triethanolamine, *Acta. Chim. Scand.*, **8**:1141-1144.
- Jou, F.-Y., Mather, A.E. and Otto, F.D. (1982), Solubility of Acidic Gases in Aqueous Methyldiethanolamine Solutions, *Ind. Eng. Chem. Proc. Des. Dev.*, **21**:539-544.
- Jou, F.-Y., Mather, A.E. and Otto, F.D. (1995), The Solubility of CO<sub>2</sub> in a 30 Mass Percent Monoethanolamine Solution, *Can J. Chem. Eng.*, **73**:140-147.
- Kaewsichan, L., Al-Bofersen, O., Yesavage, V.F. and Sami Selim, M. (2001), Predictions of the solubility of acid gases in monoethanolamine (MEA) and methyldiethanolamine (MDEA) solutions using the electrolyte-Uniquac model, *Fluid Phase Equilibria*, **183**:159-171.
- Kamps, Á.P., Balaban, A., Jödecke, M., Kuranov, G., Smirnova, N. and Maurer, G. (2001), Solubility of Single Gases Carbon Dioxide and Hydrogen Sulfide in Aqueous Solutions of N-methyldiethanolamine at Temperatures from 313 to 393 K and Pressures up to 7.6 MPa: New experimental Data and Model Extension, *Ind. Eng. Chem. Res.*, **40**:696-706.
- Kamps, Á.P-S. and Maurer, G. (1996), Dissociation Constant of N-Methyldiethanolamine in Aqueous Solution at Temperatures from 378 to 368K, *J. Chem. Eng. Data*, **41**:1505-1513.
- Karoor, S. and Sirkar, K.K. (1993), Gas Absorption Studies in Microporous Hollow Fiber Membrane Modules, *Ind. Eng. Chem. Res.*, **32**:674-684.
- Kent, R.L. and Eisenberg, B. (1976), Better Data for Amine Treating, *Hydrocarbon Proc.*, **55**:87-90.

---

Kim, Y.-S. and Yang, S.-M. (2000), Absorption of Carbon Dioxide through Hollow Fiber Membranes Using Various Aqueous Absorbents, *Sep. Purif. Technol.*, **21**:101-109.

King, S.I., Falk-Pedersen, O., Stuksrud D-B., Grønvold, M.S., Svendsen, H.F., Palla, R., Meyer, H.S. and Leppin, D. (2002), Membrane Gas/Liquid Contactors for Natural Gas Dehydration, The 52nd Annual Laurance Reid Gas Conditioning Conference.

Kitamura, T., Kuramada, K-I., Tanigaki, M., Ohshima, M. and Kanazawa, S-I. (1999), Formation mechanism of Porous Structure in Polytetrafluorethylene (PTFE) Porous Membrane Through Mechanical Operations, *Polym. Eng. Sci.*, **39**:2256-2263.

Klyamer, S.D. and Kolesnikova, T.L. (1972), General Mathematical Description of Experimental Data for the Thermodynamic Equilibrium in Carbon Dioxide-Monethanolamine (Diethanolamine)-Water Systems, *Russian. J. Phys. Chem.*, **46**:620.

Klyamer, S.D., Kolesnikova, T.L. and Rodin, Y.A. (1973), *Gazov. Prom.*, **18**:44.

Kohl, A. and Nielsen, R. (1997), Gas Purification, Gulf Publishing Company, Houston, Texas.

Kreulen, H., Smolders, C.A., Versteeg, G.F. and van Swaaij, W.P.M. (1993a), Microporous Hollow Fibre Membrane Modules as Gas-Liquid Contactors. Part I. Physical Mass Transfer Processes, *J. Membr. Sci.*, **78**:197-216.

Kreulen, H., Smolders, C.A., Versteeg, G.F. and van Swaaij, W.P.M. (1993b), Microporous Hollow Fibre Membrane Modules as Gas-Liquid Contactors. Part II. Mass Transfer with Chemical Reaction, *J. Membr. Sci.*, **78**:217-238.

Kristiansen, R.A. (1993), Absorpsjon av CO<sub>2</sub> i aminer, Diploma thesis, Norwegian Institute of Technology.

Kritpiphat, W. and Tontiwachwuthikul, P. (1996), New Modified Kent-Eisenberg Model for Predicting Carbon Dioxide Solubility in Aqueous 2-Amino-2-Methyl-1-Propanol (AMP) Solutions, *Chem. Eng. Comm*, **144**:73-83.

---

Kumar, P.S., Hogendoorn, J.A., Feron, P.H.M. and Versteeg, G.F. (2002), New Absorption Liquids for the Removal of CO<sub>2</sub> From Dilute Gas Streams Using Membrane Contactors, *Chem. Eng. Sci.*, **57**:1639-1651.

Kumazawa, H. (2000), Absorption and Desorption of CO<sub>2</sub> by Aqueous Solutions of Sterically Hindered 2-Amino-2-Methyl-1-Propanol in Hydrophobic Microporous Hollow Fiber Contained Contactors, *Chem. Eng. Comm.*, **182**:163-179.

Kuranov, G., Rumpf, B., Maurer, G. and Smirnova, N. (1997), VLE modelling for aqueous systems containing methyldiethanolamine, carbon dioxide and hydrogen sulfide, *Fluid Phase Equilibria*, **136**:147-162.

Leaist, D.G., Li, Y. and Poissant, R. (1998), Coupled Diffusion in Aqueous Weak Acid + Alkanolamine Absorbents, *J. Chem. Eng. Data*, **43**:1048-1055.

Lee, J.L., Otto, F.D. and Mather, A.E. (1976), Equilibrium Between Carbon Dioxide and Aqueous Monoethanolamine Solutions., *J. Appl. Chem. Biotechnol.*, **26**:541-549.

Lee, L.L. (1996), Thermodynamic Models For Natural Gas Sweetening Fluids, Gas Research Institute, Chicago.

Lee, Y., Noble, R.D., Yeom, B.-Y., Park, Y.-I. and Lee, K.-H. (2001) Analysis of CO<sub>2</sub> Removal by Hollow Fiber Membrane Contactors, *J. Membr. Sci.*, **194**:57-67.

Levenspiel, O. (1984), The Chemical Reactor Omnibook, OSU Bookstores, Inc., Oregon.

Li, K. and Teo, W.K. (1998), Use of Permeation and Absorption Methods for CO<sub>2</sub> Removal in Hollow Fibre Membrane Modules, *Sep. and Purif. Technol.*, **13**:79-88.

Li, M.-H. and Shen, K.-P. (1993), Calculation of Equilibrium Solubility of Carbon Dioxide in Aqueous Mixtures of Monoethanolamine with Methyldiethanolamine, *Fluid Phase Equilibria*, **85**:129-140.

Li, Y.-G. and Mather, A.M. (1994), Correlation and Prediction of the Solubility of Carbon Dioxide in a Mixed Alkanolamine Solution, *Ind. Eng. Chem. Res.*, **33**:2006-2015.

---

Lidal, H. (1992), Carbon Dioxide Removal in Gas Treating Processes, Dr.Ing. dissertation, Norwegian Institute of Technology.

Lide, D.R. (1991), Handbook of Chemistry and Physics, CRC Press, Inc.

Littel, R.J., Filmer, B., Versteeg, G.F. and van Swaaij, W.P.M. (1991), Modeling of Simultaneous Absorption of H<sub>2</sub>S and CO<sub>2</sub> in Alkanolamine solutions: The Influence of Parallel and Consecutive Reversible Reactions and the Coupled Diffusion of Ionic Species, *Chem. Eng. Sci.*, **46**:2303-2313.

Littel, R.J., van Swaaij, W.P.M. and Versteeg, G.F. (1990), Kinetics of Carbon Dioxide with Tertiary Amines in Aqueous Solution, *AIChE J.*, **36**:1633-1640.

Liu, Y., Zhang, L. and Watanisiri, S. (1999), Representing Vapor-Liquid Equilibrium for an Aqueous MEA-CO<sub>2</sub> System Using the Electrolyte Nonrandom-Two-Liquid Model, *Ind. Eng. Chem. Res.*, **38**:2080-2090.

Matsumoto, H., Kitamura, H., Kamata, T., Ishibashi, M., Ota, H. and Akutsu, N. (1995), Effect of Membrane Properties of Microporous Hollow-Fiber Gas-Liquid Contactor on CO<sub>2</sub> Removal From Thermal Power Plant Flue Gas, *J. Chem. Eng. Japan*, **28**:125-128.

Morimoto, S., Taki, K. and Maruyama, T. (2002), Current Review of CO<sub>2</sub> Separation and Recovery Technologies, International Test Network for CO<sub>2</sub> Capture, 4<sup>th</sup> Workshop, Kyoto, Japan.

Mulder, M. (1991), Basic Principles of Membrane Technology, Kluwer Academic Publishers, Dordrecht, The Netherlands.

Newman, J.S. (1991), Electrochemical Systems, 2nd Ed., Englewood Cliffs: Prentice-Hall.

Nii, S. and Takeuchi, H. (1994), Gas Absorption with Membrane Permeation-Acid Gas Removal From Flue Gases By a Permabsorption Method, *Trans IChemE*, **72**: 21-26.

Nishikawa, N., Ishibashi, M., Ohta, H., Akutsu, N., Matsumoto, H., Kamata, T. and Kitamura, H. (1995), CO<sub>2</sub> Removal by Hollow-Fiber Gas-Liquid Contactor, *Energy Convers. Mgmt.*, **36**:415-418.

---

Ohno, K., Inoue, Y., Yoshida, H. and Matsuura, H. (1999), Reaction of Aqueous 1-(N-Methylamino)ethanol Solutions with Carbon Dioxide. Chemical Species and Their Conformation Studied by Vibrational Spectroscopy and ab initio Theories, *J. Phys. Chem.*, **10**:4283-4292.

Oscarson, J.L., Wu, G., Faux, P.W., Izatt, R.M. and Christensen, J.J. (1989), Thermodynamics of Protonation of Alkanolamines in Aqueous Solution to 325 °C, *Thermochimica Acta*, **154**:119-127.

Pani, F., Gaunand, A., Richon, D., Cadours, R. and Bouallou, D. (1997), Absorption of H<sub>2</sub>S by an Aqueous Methyldiethanolamine Solution at 296 and 343K, *J. Chem. Eng. Data*, **42**:865-870.

Pinsent, B.R.W., Pearson, L. and Roughton, F.J.W. (1956), The Kinetics of Combination of Carbon Dioxide with Hydroxide Ions, *Trans. Faraday Soc.*, **52**:1512-1520.

Pitzer, K.S. (1973), Thermodynamics of Electrolytes. I. Theoretical Basis and General Equations, *J. Phys. Chem.*, **77**:268-277.

Pohorecki, R. and Moniuk, W. (1988), Kinetics of Reaction between Carbon Dioxide and Hydroxyl Ions in Aqueous Electrolyte Solutions, *Chem. Eng. Sci.*, **43**:1677-1684.

Poplsteinova, J., Svendsen, H.F. and Lee, L.L. (2002), Modeling Vapor-Liquid Equilibrium for Systems H<sub>2</sub>O-MEA-CO<sub>2</sub> and H<sub>2</sub>O-MDEA-CO<sub>2</sub>, *Chisa-2002*, Prague, Czech Republic.

Prausnitz, J.M., Lichtenthaler, R.N. and Gomez de Azevedo, E. (1999), Molecular Thermodynamics of Fluid-Phase Equilibria, 3rd. ed., Prentice Hall, New Jersey.

Press, W.H., Teukolsky, S.A., Vetterling, W.T. and Flannery, B.P. (1992), Numerical Recipes in Fortran 77. The Art of Scientific Computing, Vol. 1, 2<sup>nd</sup> ed., Cambridge University Press.

Qi, Z. and Cussler, E.L. (1985a), Microporous Hollow Fibers for Gas Absorption. I: Mass Transfer In the Liquid, *J. Membr. Sci.*, **23**:321-332.

Qi, Z. and Cussler, E.L. (1985b), Microporous Hollow Fibers for Gas Absorption. II: Mass Transfer Across the Membrane, *J. Membr. Sci.*, **23**:333-345.



---

Rangwala, H.A. (1996), Absorption of Carbon Dioxide into Aqueous Solutions Using Hollow Fiber Membrane Contactors, *J. Membr. Sci.*, **112**:229-240.

Reid, R.C., Prausnitz, J.M. and Poling, B.E. (1986), The Properties of Gases and Liquids, 4th Ed., McGraw-Hill Book Co.

Rinker, E.B., Ashour, S.S. and Sandall, O.C. (1995), Kinetics and Modelling of Carbon Dioxide Absorption into Aqueous Solutions of N-Methyldiethanolamine, *Chem. Eng. Sci.*, **50**:755-768.

Rowley, R.L., Adams, M.E., Marshall, T.L., Oscarson, J.L., Wilding, W.V. and Anderson, D.J. (1997), Measurement of Diffusion Coefficients Important in Modeling the Absorption Rate of Carbon Dioxide into Aqueous N-Methyldiethanolamine, *J. Chem. Eng. Data*, **42**:310-317.

Rowley, R.L., Adams, M.E., Marshall, T.L., Oscarson, J.L., Wilding, W.V. and Anderson, D.J. (1998), Measurement of the Absorption Rate of Carbon Dioxide into Aqueous Diethanolamine, *J. Chem. Eng. Data*, **43**:427-432.

Sander, B., Fredenslund, Aa and Rasmussen, P. (1986), Calculation of Vapour-Liquid Equilibria in Mixed Solvent/Salt Systems using an Extended UNIQUAC Equation, *Chem. Eng. Sci.*, **41**:1171-1183.

Sartori, G. and Savage, D.W. (1983), Sterically Hindered Amines for CO<sub>2</sub> Removal Gases, *Ind. Eng. Chem. Fundam.*, **22**:239-249.

Schiesser, W.E. (1991). The Numerical Method of Lines, Academic Press, Inc., San Diego.

Shen, K.-P. and Li, M.-L. (1992), Solubility of Carbon Dioxide in Aqueous Mixtures of Monoethanolamine with Methyldiethanolamine, *J. Chem. Eng. Data*, **37**:96-100.

Sieder, E.N. and Tate, G.E. (1936), Heat transfer and pressure drop of liquids in tubes, *Ind. Eng. Chem.*, **28**:1429.

Silkenbäumer, D., Rumpf, B. and Lichtentaler, R.N. (1998), Solubility of Carbon Dioxide in Aqueous Solutions of 2-Amino-2-methyl-1-propanol and N-methyldiethanolamine and Their mixtures in the Temperature Range from 313 to 353 K and Pressures up to 2.7 MPa, *Ind. Eng. Chem. Res.*, **37**:3133-3141.

---

Silva, E.F.da (2003), On the Kinetics between CO<sub>2</sub> and Alkanolamines, a Review by ab initio Methods, *To be published*.

Sirkar, K.K. (1992), Other New Membrane Processes, in W.S.W Ho, K.K. Sirkar (Eds.), *Membrane Handbook*, Chapman & Hall, New York, 885-899.

Snijder, E.D., te Riele, M.J.M., Versteeg, G.F. and van Swaaij, W.P.M (1993), Diffusion Coefficients of Several Aqueous Alkanolamine Solutions. *J. Chem. Eng. Data*, **38**:475-480.

Thomas, W.J. (1966), The Absorption of Carbon Dioxide in Aqueous Monoethanolamine in a Laminar Jet, *AIChE J.*, **12**:1051-1057.

Tomcej, R.A. and Otto, F.D. (1989), Absorption of CO<sub>2</sub> and N<sub>2</sub>O into Aqueous Solutions of Methyldiethanolamine. *AIChE J.*, **35**:861-864.

Vallée, G., Mougin, P., Jullian, S. and Fürst, W. (1999), Representation of CO<sub>2</sub> and H<sub>2</sub>S Absorption by Aqueous Solutions of Diethanolamine using an Electrolyte Equation of State, *Ind. Eng. Chem. Res.*, **38**:3473-3480.

Van Krevelen, D.W, Hoftijzer, P.J. and Huntjens, F.J. (1949), Composition and Vapor Pressures of Aqueous Solutions of Ammonia, Carbon Dioxide and Hydrogen Sulfide, *Recueil*, **68**:191-216.

Vásquez, G., Alvarez, E., Navaza, J.M., Rendo, R. and Romero, E. (1997), Surface Tension of Binary Mixtures of Water + Monoethanolamine and Water + 2-Amino-2-methyl-1-propanol and Tertiary Mixtures of These amines with Water from 25-50°C, *J. Chem. Eng. Data.*, **42**:57-59.

VDI Wärmeatlas 1984, Berechnungsblätter for den Wärmeübergang, VDI Verlag, GmbH.

Versteeg, G.F. and van Swaaij, W.P.M. (1988a), Solubility and Diffusivity of Acid Gases (CO<sub>2</sub>,N<sub>2</sub>O) in Aqueous Alkanolamine Solutions, *J. Chem. Eng. Data*, **33**:29-34.

Versteeg, G.F. (2000), *Personal Communication*.

Versteeg, G.F. and van Swaaij, W.P.M. (1988b), On the Kinetics Between CO<sub>2</sub> and Alkanolamines Both in Aqueous and Non-Aqueous Solutions-II. Tertiary Amines, *Chem. Eng. Sci.*, **43**:587-591.

- 
- Versteeg, G.F., van Dijck, L.A.J. and van Swaaij, W.P.M. (1996), On the Kinetics between CO<sub>2</sub> and Alkanolamines both in Aqueous and Non-Aqueous Solutions. An Overview, *Chem. Eng. Comm.*, **144**:113-158.
- Wakeham, W.A. and Mason, E.A. (1979), Diffusion through Multiperforate Lamellae, *Ind. Eng. Chem. Fundam.*, **18**:301-305.
- Wang, K.L. and Cussler, E.L. (1993), Baffled Membrane Modules made with Hollow Fiber Fabric, *J. Membr. Sci.*, **85**:265-278.
- Weiland, R.H., Chakravarty, T. and Mather, A.E. (1993), Solubility of Carbon Dioxide and Hydrogen Sulfide in Aqueous Alkanolamines, *Ind. Eng. Chem. Res.*, **32**:1419-1430.
- Weiland, R.H., Dingman, J.C. and Cronin, D.B. (1997), Heat Capacity of Aqueous Monoethanolamine, Diethanolamine, N-Methyldiethanolamine, and N-Methyldiethanolamine-Based Blends with Carbon Dioxide, *J. Chem. Eng. Data*, **42**:1004-1006.
- Weiland, R.H., Dingman, J.C., Cronin, D.B. and Browning, G.J. (1998), Density and Viscosity of Some Partially Carbonated Aqueous Alkanolamine Solutions and Their Blends, *J. Chem. Eng. Data*, **43**:378-382.
- Weiland, R. H., Rawal, M. and Rice, R.G. (1982), Stripping of Carbon Dioxide from Monoethanolamine Solutions in a Packed Column, *AIChE J.*, **28**:963-973.
- Wu, H.S. and Sandler, S.I. (1991), Use of ab Initio Quantum Mechanics Calculations in Group Contribution Methods, 1. Theory and the Basis for Group Identifications, *Ind. Eng. Chem. Res.*, **30**:881.
- Wu, R.S. and Lee, L.L. (1992), Vapor-Liquid Equilibria of Mixed-Solvent Electrolyte Solutions; Ion-size Effects Based on the MSA Theory, *Fluid Phase Equilibria*, **78**:1.
- Xu, G.W., Zhang, C.F., Qin, S.J. and Wang, Y.W. (1992), Kinetics Study on Absorption of Carbon Dioxide into Solutions of Activated Methyldiethanolamine, *Ind. Eng. Chem. Res.*, **31**:921-927.

---

Yang, M.C. and Cussler, E.L. (1986), Designing Hollow-Fiber Contactors. *AIChE J.*, **32**:1910-1916.

Yu, W.C., Astarita, G. and Savage, D.W. (1985), Kinetics of Carbon Dioxide Absorption in Solutions of Methyldiethanolamine, *Chem. Eng. Sci.*, **40**:1585-1590.

---

## *Solution in terms of the extent of reaction*

---

In 4.4.2 the chemical equilibrium speciation is expressed as a set of equations in terms of the unknown extents of reaction,  $\xi_1$  and  $\xi_2$ . Equations (4.62) and (4.63) are here repeated:

$$K_{c1} = \frac{(my + \xi_1)\xi_1}{[m(1-y) - \xi_1 - \xi_2](my - \xi_1 - \xi_2)} \quad (\text{A1.1})$$

$$K_{c2} = \frac{\xi_2}{[m(1-y) - \xi_1 - \xi_2](my - \xi_1 - \xi_2)} \quad (\text{A1.2})$$

The solution in terms of  $\xi_1$  and  $\xi_2$  may be expressed as the roots of a fourth order polynomial in the dummy variable  $z$ .

$$\xi_1 = \text{roots}(Az^4 + Bz^3 + Cz^2 + Dz + E) \quad (\text{A1.3})$$

$$\xi_2 = \frac{K_{c2}\xi_1(\xi_1 + my)}{K_{c1}} \quad (\text{A1.4})$$

$$\begin{aligned}
 A &= K_{c2}^2 \\
 B &= 2K_{c2}^2my + 2K_{c1}K_{c2} \\
 C &= K_{c1}^2 - K_{c1} + 2K_{c2}myK_{c1} + K_{c2}^2m^2y^2 - K_{c2}K_{c1}m \\
 D &= -K_{c1}^2m - K_{c1}my - K_{c2}m^2yK_{c1} \\
 E &= K_{c1}^2m^2y - K_{c1}m^2y^2
 \end{aligned} \tag{A1.5}$$

For MDEA, not capable of forming carbamate,  $\xi_2 = 0$  and a polynomial of second order results. The solution satisfying the constraints (4.64)-(4.67) is:

$$\xi_1 = \frac{K_{c1} + y - m\sqrt{K_{c1}^2 + 6K_{c1}y + y^2 - 4K_{c1}^2y + 4K_{c1}y^2 - 4K_{c1}y^2}}{2(K_{c1} - 1)} \tag{A1.6}$$

As discussed in 3.2, except for loadings approaching zero, the carbonate formation reaction can often be neglected as a first approximation. In this case  $\xi_1 = 0$  and the MEA solution reduces to a polynomial of second order. The root satisfying the constraints (4.64)-(4.67) is given as:

$$\xi_2 = \frac{m + 1/K_{c2} - \sqrt{(m + 1/K_{c2})^2 - 4m^2y(1 - y)}}{2} \tag{A1.7}$$

---

## *Correlations for the equilibrium model*

---

### **A2.1 Equilibrium Constants**

The equilibrium constants are taken from literature as the following temperature dependent correlations. These may be considered the infinite dilute solution limit and are thus equal to the true thermodynamic equilibrium constants. From the original sources, equilibrium constants are based on the mole fraction or molality scale. In this work the molar concentration ( $\text{mol/m}^3$ ) is used, thus some of the equilibrium constants are corrected by the molar density of water,  $c_w^0$ .

#### *Dissociation of water*

Originally with mole fraction scale (Austgen et al., 1989):

$$K_1 = K_1^{orig} = \exp(132.899 - 13445.9/T - 22.4773 \ln T) \quad (\text{A1.8})$$

#### *First dissociation of $\text{CO}_2$*

Originally with mole fraction scale (Austgen et al., 1989):

$$K_2 = \frac{K_2^{orig}}{c_w^0} = \frac{1}{c_w^0} \exp(231.465 - 12092.10/T - 36.7816 \ln T) \quad (A1.9)$$

*Second dissociation of CO<sub>2</sub>*

Originally with mole fraction scale (Austgen et al., 1989):

$$K_3 = K_3^{orig} = \exp(216.049 - 12431.70/T - 35.4819 \ln T) \quad (A1.10)$$

*Dissociation of protonated MDEA*

Originally with molality scale (Oscarson et al., 1989, correlation from Kamps and Maurer, 1996). Water originally included in the constant:

$$K_4 = \frac{K_4^{orig}}{c_w^0} = \frac{1}{c_w^0} \exp(-64.506 - 1609.2/T + 8.8096 \ln T) \quad (A1.11)$$

*Dissociation of protonated MEA*

Originally with molality scale (Bates and Pinching, 1951). Water originally included in the constant:

$$K_5 = \frac{K_5^{orig}}{c_w^0} = \frac{1}{c_w^0} 10^{(0.3869 + 2677.99/T + 0.0004277T)} \quad (A1.12)$$

*MEA carbamate reversion*

The only source of a temperature correlation is Austgen et al. (1989). This is referred to pure MEA as standard state for alkanolamine, and must be corrected by the infinite dilution activity coefficient,  $\hat{\gamma}_{MEA}^\infty$ . This is correlated by relating



the deprotonation constant of Austgen et al. (1989) to that from Bates and Pinching (1951).

$$K_6 = \frac{K_6^{orig}}{\hat{\gamma}_{MEA}^\infty} = \frac{1}{\hat{\gamma}_{MEA}^\infty} \exp(2.8898 - 3635.09/T) \quad (A1.13)$$

with

$$\hat{\gamma}_{MEA}^\infty = 4.162 \times 10^{-6} T^2 + 5.781 \times 10^{-4} T - 0.3561 \quad (A1.14)$$

Austgen et al. (1989) made the correlation by tuning in their equilibrium model. The resulting value is lower by a factor of 2 compared to the experimentally determined value at 40°C given by Sartori and Savage (1983), and this factor is introduced in the model, thus keeping only the temperature dependence from Austgen et al.

## A2.2 The Henry's law constants

The Henry's law constant for CO<sub>2</sub> in an unloaded MDEA solution is correlated by the model from Al-Ghawas et al. (1989) as a function of weight percent amine and temperature, as follows:

$$K_{10} = 2.01874 - 23.7638w_{MDEA} + 290.092w_{MDEA}^2 - 480.196w_{MDEA}^3 \quad (A1.15)$$

$$K_{11} = 3135.49 + 15493.1w_{MDEA} - 183987w_{MDEA}^2 + 300562w_{MDEA}^3 \quad (A1.16)$$

$$K_{12} = -813702 - 2480810w_{MDEA} - 29201300w_{MDEA}^2 + 4.7085200w_{MDEA}^3 \quad (A1.17)$$

$$H_{CO_2}^s \left( \frac{\text{m}^3}{\text{mol} \cdot \text{kPa}} \right) = 0.01013 \exp \left( K_{10} + \frac{K_{11}}{T} + \frac{K_{12}}{T^2} \right) \quad (A1.18)$$

The Henry's law constant for CO<sub>2</sub> in an unloaded MEA solution is calculated from the value for the pure components according to the mole fraction based mixing rule recommended by Reid et al. (1986).

$$H_{mix} = x_w H_w + x_{MEA} H_{MEA} \quad (A1.19)$$

The pure component values are taken from Austgen et al. (1989):

$$H_w(\text{kPa}) = 0.001 \exp\left(170.7126 - \frac{8477.771}{T} - 21.95743 \ln T + 0.005781 T\right) \quad (A1.20)$$

$$H_{MEA}(\text{kPa}) = 0.001 \exp\left(89.452 - \frac{2934.6}{T} - 11.592 \ln T + 0.01644 T\right) \quad (A1.21)$$

### A2.3 Salting-out coefficients

The salting-out coefficients, as applied in the van Krevelen correlation (4.5.1), are given by Browning and Weiland (1994):

$h_{MEA H^+}$	0.055
$h_{MDEA H^+}$	0.041
$h_{MEA COO^-}$	0.043
$h_{HCO_3^-}$	0.073
$h_{CO_3^{2-}}$	0.021
$h_{CO_2}$	-0.019

## A2.4 Solvent vapor pressure

The MEA/water mixed solvent vapor pressure is calculated by Raoult's law for water, neglecting the contribution from the alkanolamine, as discussed in 4.2.2. The pure water pressure is calculated by the correlation given by Austgen (1989):

$$P_{H_2O}^0(\text{kPa}) = 0.001 \exp\left(72.55 - \frac{7206.7}{T} - 7.1385 \ln T + 4.0460 \times 10^{-6} T^2\right)$$

where  $T$  is the temperature in Kelvin.



---

### **A3.1 Error analysis**

The errors in a measurement process may be separated in two parts; the bias, or systematic error and the imprecision or random error. Systematic errors arise from making incorrect assumptions or from improper experimental measuring techniques. These may be minimized by making valid or reasonable assumptions and from careful design of the experimental apparatus, operating procedures and from regular calibration of measuring devices. This is believed to be the case for the experiments performed in this work, as described in chapter 5. The random error is a purely statistical term and result from the nonrepeatability of any measurement. It can not be prevented but it can be minimized by using accurate measuring devices and techniques. The concept of error analysis deals with the quantification of random errors.

In an experiment that uses the values of parameters from several different measurements to compute some quantity, the inaccuracy of the final result will be influenced by the errors associated with each of the independent variables. This is termed error propagation. If the resulting quantity,  $N$ , is defined as a function

of  $n$  independent measured quantities,  $N = f(u_1, u_2, u_3, \dots, u_n)$ , the error in  $N$ , denoted  $\Delta N$ , may be related to the error in the independent variables  $u_1, u_2, u_3, \dots, u_n$  by:

$$\Delta N = \left| \Delta u_1 \frac{\partial f}{\partial u_1} \right| + \left| \Delta u_2 \frac{\partial f}{\partial u_2} \right| + \left| \Delta u_3 \frac{\partial f}{\partial u_3} \right| + \dots + \left| \Delta u_n \frac{\partial f}{\partial u_n} \right| \quad (\text{A1.22})$$

where the  $\Delta u_i$ 's are statistical bounds on the error in the measured quantities, which will cause an error  $\Delta N$  in the computed result  $N$  (Doebelin, 1990). The use of equation (A1.22) requires an explicit function for  $N$  in terms of the measured quantities in order to calculate the partial derivatives. The random error in the calculated absorption rates and the measured liquid concentrations are evaluated in the following.

### A3.2 Accuracy of the absorption rates

The absorption rate of  $\text{CO}_2$  from experiments with stagnant gas mode is given by equation (5.1), where the measured quantities are the volume of the soap bubble meter ( $V$ ), the average stopwatch reading ( $\bar{t}$ ), the system pressure ( $P$ ) and the room temperature ( $T$ ). The estimated errors are as follows:

- $\Delta V = 1$  ml
- $\Delta t = 0.2$  s, the average standard deviation in the stopwatch readings.
- $\Delta P = 0.3$  kPa, 0.15% of full scale, as given by manufacturer.
- $\Delta T = 0.5^\circ\text{C}$ , for the thermocouple used.

The error in the absorption rate was calculated for each of the experimental points, making use of eq. (A1.22). The maximum error found was 2.4%.

In the stagnant gas mode, the absorption flux was more or less directly measured. The most important point was to adapt the measuring volume of the soap bubble meter to the absorption rate in order to minimize the effect of error in the average stopwatch reading.

The accurate measurement of absorption rates in circulating gas mode, was considered more difficult, as the final result rely on several measured parameters, as can be seen from eq. (5.3) and (5.4). The measured quantities were the feed CO<sub>2</sub>-flow,  $Q_{CO_2}$ , the sweep N<sub>2</sub>-flow,  $Q_{N_2}$ , the total pressure,  $P$ , and the mole-fraction of CO<sub>2</sub> in the sample gas,  $y_{CO_2}^{an}$ . The estimated errors are as follows:

- $\Delta Q_{CO_2} = 0.006/0.0006$  NI/min from the calibration of the 1 NI/min or 0.1 Nml/min mass flow controllers.
- $\Delta Q_{N_2} = 0.016$  NI/min from the calibration of the 3 NI/min mass flow controller.
- $\Delta P = 0.3$  kPa, 0.15% of full scale, as given by manufacturer.
- $\Delta y_{CO_2}^{an} = 0.002/0.001/0.0005$  NI/min for the CO<sub>2</sub> gas analyzers, according to manufacturer (maximum error equal to 1% of full scale).

The error in the absorption rate was calculated for each of the experimental points, making use of eq. (A1.22). The maximum error found was 12%, corresponding to the points with the lowest absorption rates (high loading, low temperature, low  $p_{CO_2}$ ). For loadings lower than 0.25 (MEA), the maximum error found was 5%. The most important factor in the error was the accuracy of the CO<sub>2</sub> mass-flow controllers.

### A3.3 Accuracy of the liquid sample analysis

The liquid CO<sub>2</sub> concentration was calculated from eq. (5.14), made up of HCl-volume,  $V_{HCl}$ , titration volume,  $V_t$ , blind sample correction,  $\Delta V_b$ , sample volume,  $V_s$  and NaOH-concentration,  $c_{NaOH}$ . The following errors were estimated:

- $\Delta V_{HCl} = 0.05$  ml
- $\Delta V_t = 0.1$  ml
- $\Delta(\Delta V_b) = 0.1$  ml
- $\Delta V_s = 0.005$  ml

- $\Delta c_{NaOH} = 0.0001 \text{ mol/l}$

From eq. (A1.22) the error in the calculated concentration of  $CO_2$  is  $\Delta c_{CO_2} = 0.02 \text{ mol/l}$  or 2%, using typical values of the quantities ( $V_{HCl}=30 \text{ ml}$ ,  $V_t=10 \text{ ml}$ ,  $\Delta V_b = 0.3 \text{ ml}$ ,  $V_s=1 \text{ ml}$  and  $c_{NaOH}=0.1 \text{ mol/l}$ ).

The liquid amine concentration was calculated from eq. (5.15), made up of the concentration of sulfuric acid,  $c_{H_2SO_4}$ , the titration volume,  $V_t$  and the sample volume,  $V_s$ . The estimated errors are:

- $\Delta c_{H_2SO_4} = 0.0001 \text{ mol/l}$
- $\Delta V_t = 0.1 \text{ ml}$
- $\Delta V_s = 0.005 \text{ ml}$

From eq. (A1.22) the error in the calculated concentration of amine is  $\Delta c_{am} = 0.1 \text{ mol/l}$  or 2%. This corresponds to the standard deviation found from a test with 10 parallels of one sample.